

AD-A008 662

A DIFFERENTIAL THRUST CONTROLLER FOR
AIR CUSHION LANDING SYSTEM AIRCRAFT

Matthew A. Husson

Air Force Institute of Technology
Wright-Patterson Air Force Base, Ohio

December 1974

DISTRIBUTED BY:

NTIS

National Technical Information Service
U. S. DEPARTMENT OF COMMERCE

UNCLASSIFIED

SECURITY CLASSIFICATION OF THIS PAGE (When Data Entered)

REPORT DOCUMENTATION PAGE		READ INSTRUCTIONS BEFORE COMPLETING FORM
1. REPORT NUMBER GR/ED/74-51	2. GOVT ACCESSION NO.	3. RECIPIENT'S CATALOG NUMBER AD-A008 662
4. TITLE (and Subtitle) A DIFFERENTIAL THRUST CONTROLLER FOR AIR CUSHION LANDING SYSTEM AIRCRAFT		5. TYPE OF REPORT & PERIOD COVERED M S Thesis
7. AUTHOR(s) Matthew A. Huzson Capt, USAF		6. PERFORMING ORG. REPORT NUMBER
9. PERFORMING ORGANIZATION NAME AND ADDRESS Air Force Institute of Technology (AFIT-EN) Wright-Patterson AFB, Ohio 45433		8. CONTRACT OR GRANT NUMBER(s)
11. CONTROLLING OFFICE NAME AND ADDRESS Systems Dynamics Branch (FGD) Air Force Flight Dynamics Laboratory Wright-Patterson AFB, Ohio 45433		10. PROGRAM ELEMENT, PROJECT, TASK AREA & WORK UNIT NUMBERS
14. MONITORING AGENCY NAME & ADDRESS (if different from Controlling Office)		12. REPORT DATE December 1974
		13. NUMBER OF PAGES 108
		15. SECURITY CLASS. (of this report) Unclassified
		16a. DECLASSIFICATION/DOWNGRADING SCHEDULE
16. DISTRIBUTION STATEMENT (of this Report) Approved for public release; distribution unlimited.		
17. DISTRIBUTION STATEMENT (of the abstract entered in Block 20, if different from Report)		
18. SUPPLEMENTARY NOTES Approved for public release IAW AFR 190-17 PRICES SUBJECT TO CHANGE JERRY C. HIX, Captain, USAF Director of Information		
19. KEY WORDS (Continue on reverse side if necessary and identify by block number) Air Cushion Landing System Feedback Control Aircraft Control Pilot Modeling Control System Time-Lag System Differential Thrust Control Reproduced by NATIONAL TECHNICAL INFORMATION SERVICE US Department of Commerce Springfield, VA 22151		
20. ABSTRACT (Continue on reverse side if necessary and identify by block number) A control system was designed to improve the heading response of the Air Cushion Landing System aircraft to differential thrust input. The aircraft equations of motion and low speed stability derivatives were obtained from work done at the Air Force Flight Dynamics Laboratory at Wright-Patterson Air Force Base, Ohio. Five different values of engine response time-delay were selected for the design study. These time-delay values were 0.2, 0.4, 0.6, 0.8, and 1.0 seconds. The principle used for the design was to compensate the system		

DD FORM 1 JAN 73 1473

EDITION OF 1 NOV 65 IS OBSOLETE,

UNCLASSIFIED

SECURITY CLASSIFICATION OF THIS PAGE (When Data Entered)

UNCLASSIFIED

SECURITY CLASSIFICATION OF THIS PAGE(When Data Entered)

20. Abstract (Cont)

ignoring the time-delay and then to compensate for the time-delay. A two stage lead network was used to reduce the effect of the engine time-delay. The system was simulated by using a digital computer program called MIMIC, which simulates the functions of an analog computer. The average mean square error was computed for the system with and without the control installed, for each of the five time-delay values. In all cases, the average mean square error was reduced approximately 70% by the addition of the compensator. The design procedure was based on the Crossover Model for the human pilot as developed by Systems Technology Incorporated of Hawthorne, California.

1a
UNCLASSIFIED

SECURITY CLASSIFICATION OF THIS PAGE(When Data Entered)

A DIFFERENTIAL THRUST CONTROLLER
FOR
AIR CUSHION LANDING SYSTEM AIRCRAFT

THESIS

Presented to the Faculty of the School of Engineering
of the Air Force Institute of Technology
Air University
in Partial Fulfillment of the
Requirements for the Degree of
Master of Science

by

Matthew A. Husson III, B.S.E.E.
Captain USAF

Graduate Guidance and Control

December 1974

Approved for public release; distribution unlimited.

18

Preface

The topic for this thesis was suggested by Captain Randall Gressang of the Air Force Flight Dynamics Laboratory (AFFDL). A control system was designed by the author to improve the heading response of the Air Cushion Landing System (ACLS) aircraft to differential thrust commanded by the pilot.

I wish to express my appreciation to Captain Thomas Moriarty, my thesis advisor, for his untiring assistance during the course of this project. I would also like to thank Captain Randall Gressang and Mr. George Kurylowich of AFFDL for their assistance with explanations of the ACLS. Credit should also be given to Lieutenant John Pinnel, a classmate at the Air Force Institute of Technology, who helped me with the computer programming. Finally, I wish to thank my family for their patience with me during the study.

Contents

	Page
Preface	ii
List of Figures	v
List of Tables	viii
List of Symbols	ix
Abstract	xii
I. Introduction	1
Background	1
Problem	2
Objectives	3
Approach	3
II. The Plant Model	5
Engines	8
Aircraft	9
III. The Wind Model	18
IV. The Pilot Model	20
Background	20
The Crossover Model	21
The ACLS Pilot Model	25
V. Control System Design	27
Design Philosophy	27
Design Method	29
VI. Simulation and Results	42
Simulation	42
Wind Gust Simulation	43
Pilot Simulation	43
Error Analysis	44
Simulation Results	45
VII. Conclusions and Recommendations	57
Conclusions	57
Recommendations	58

	Page
Bibliography	60
Appendix A: Root Locus Plots for Systems with Time-Lag	62
Appendix B: Root Locus Plots Used for the Design	64
Appendix C: MIMIC Simulation Program	80
Appendix D: Pulse Representation of Band Limited White Noise .	90
Vita	93

List of Figures

Figure		Page
1	Block Diagram of the Multiloop Taxi Task	6
2	Block Diagram of the Heading Control Loop as a Regulator Problem	7
3	Block Diagram of the Heading Control Loop as a Compensatory Tracking Task	7
4	Thrust Response of the XC-3A Engines Fitted with a Beta Control System	10
5	Wind Effect on the Taxiing ACLS Aircraft	13
6	Relevant Data for the XC-8A Model	17
7	Block Diagram of the Plant Model	17
8	Power Spectral Density of the Wind Model	19
9	The Compensatory Tracking Task	22
10	Cooper-Harper Handling Qualities Rating Scale	24
11	Rating Decrement Due to Pilot Lead as Inferred from Handling Qualities Tests	27
12	Block Diagram of the Heading Control Loop with Compensator Added	30
13	Closed Loop Bode Plot of CCL, $\tau_a = 0.2$ Second	34
14	Closed Loop Bode Plot of CCL, $\tau_a = 0.4$ Second	36
15	Closed Loop Bode Plot of CCL, $\tau_a = 0.6$ Second	37
16	Closed Loop Bode Plot of CCL, $\tau_a = 0.8$ Second	38
17	Closed Loop Bode Plot of CCL, $\tau_a = 1.0$ Second	40
18	Input and Output of Uncompensated System, $\tau_a = 0.2$ Second	46
19	Input and Output of Compensated System, $\tau_a = 0.2$ Second	47
20	Input and Output of Uncompensated System, $\tau_a = 0.4$ Second	48

Figure		Page
21	Input and Output of Compensated System, $\tau_a = 0.4$ Second	49
22	Input and Output of Uncompensated System, $\tau_a = 0.6$ Second	50
23	Input and Output of Compensated System, $\tau_a = 0.6$ Second	51
24	Input and Output of Uncompensated System, $\tau_a = 0.8$ Second	52
25	Input and Output of Compensated System, $\tau_a = 0.8$ Second	53
26	Input and Output of Uncompensated System, $\tau_a = 1.0$ Second	54
27	Input and Output of Compensated System, $\tau_a = 1.0$ Second	55
B.1	Root Locus Plot for Yaw Rate Feedback, $\tau_a = 0.2$ Second	65
B.2	Root Locus Plot for Yaw Rate Feedback, $\tau_a = 0.4$ Second	66
B.3	Root Locus Plot for Yaw Rate Feedback, $\tau_a = 0.6$ Second	67
B.4	Root Locus Plot for Yaw Rate Feedback, $\tau_a = 0.8$ Second	68
B.5	Root Locus Plot for Yaw Rate Feedback, $\tau_a = 1.0$ Second	69
D.6	Root Locus Plot for Lead Compensator, $\tau_a = 0.2$ Second	70
B.7	Root Locus Plot for Lead Compensator, $\tau_a = 0.4$ Second	71
B.8	Root Locus Plot for Lead Compensator, $\tau_a = 0.6$ Second	72
B.9	Root Locus Plot for Lead Compensator, $\tau_a = 0.8$ Second	73
B.10	Root Locus Plot for Lead Compensator, $\tau_a = 1.0$ Second	74

Figure		Page
B.11	Root Locus Plot for Time-Delay Compensator, $\tau_a = 0.2$ Second	75
B.12	Root Locus Plot for Time-Delay Compensator, $\tau_a = 0.4$ Second	76
B.13	Root Locus Plot for Time-Delay Compensator, $\tau_a = 0.6$ Second	77
B.14	Root Locus Plot for Time-Delay Compensator, $\tau_a = 0.8$ Second	78
B.15	Root Locus Plot for Time-Delay Compensator, $\tau_a = 1.0$ Second	79
D.1	Power Spectral Density of Band Limited White Noise . .	90
D.2	Pulse Train	91
D.3	Autocorrelation of a Pulse Train	91
D.4	Power Spectral Density of a Pulse Train	92

List of Tables

Table		Page
I	Time Delay Compensator Parameter Values	33
II	Required Pilot Parameters for the Compensated Systems .	41
III	Average Mean Square Error Results	56

List of Symbols

b	- Wing span, ft.
C_{N_R}	- Stability derivative of yaw moment due to yaw rate
C_{N_β}	- Stability derivative of yaw moment due to sideslip
e	- Error in a feedback control system (output-input)
$\overline{e^2}$	- Mean square error
G_C	- Lead compensator transfer function
G_{TDC}	- Time delay compensator transfer function
$H(j\omega)$	- System Fourier transform
I_{zz}	- Moment of inertia of aircraft about z-axis, slugs-ft ²
j	- Imaginary component
K	- Open loop sensitivity or gain
K_A	- Gain of lead compensator transfer function
K_C	- Gain of compensation control loop transfer function
K_{TDC}	- Gain of time delay compensator transfer function
K_P	- Gain of pilot model transfer function
n	- Order of lead, time-delay compensator
N_E	- Yaw moment due to engine differential thrust, foot-pounds
N_W	- Yaw moment due to wind, foot-pounds
p	- Position of pole on s-plane
PLA	- Power Lever Angle, degrees
R	- Yaw rate, radians per second
s	- Laplace operator
S	- Wing area, ft ²
$S(\omega)$	- Power spectral density

T	- Elapsed time, seconds
T_I	- Lag time constant in pilot model transfer function
T_L	- Lead time constant in pilot model transfer function
V	- Relative wind acting on aircraft, feet/second
V_g	- Wind gust velocity, feet/second
V_X	- Component of relative wind along aircraft x-axis, ft/sec
V_Y	- Component of relative wind along aircraft y-axis, ft/sec
y	- Distance of aircraft from taxiway centerline, feet
y_C	- Commanded distance from taxiway centerline, feet
Y_C	- Controlled element transfer function
Y_{CCL}	- Compensation control loop transfer function
Y_P	- Pilot model transfer function
z	- Position of zero on s-plane
β	- Aircraft sideslip angle, radians
ρ	- Atmospheric density, slugs/ft
σ	- Standard deviation
τ	- Time-delay, seconds
τ_a	- Time-delay of aircraft engines, seconds
τ_e	- Time-delay of pilot model, seconds
τ_o	- Time-delay of pilot model with zero input, seconds
ψ	- Aircraft heading, radians
ψ_C	- Commanded aircraft heading, radians
ψ_D	- Input heading disturbance, radians
ψ_E	- Heading due to engine differential thrust yaw moment, radians
ψ_W	- Heading due to wind, radians

- ω - Frequency, radians per second
- ω_b - Bandwidth, radians per second
- ω_c - Crossover frequency, radians per second
- ω_{co} - Crossover frequency with zero input, radians per second

Special Notation

- $(.)$ - Derivative with respect to time
- \approx - Approximately equal to
- exp - The quantity e (2.7183) raised to the following power
- Δ - Change in following quantity

Abstract

A control system was designed to improve the heading response of the Air Cushion Landing System aircraft to differential thrust input. The pilot can then control the aircraft in a more effective manner while taxiing in gusting crosswinds. The aircraft equations of motion and low speed stability derivatives were obtained from work done at the Air Force Flight Dynamics Laboratory at Wright-Patterson Air Force Base, Ohio. Five different values of engine response time-delay were selected for the design study. These time-delay values were 0.2, 0.4, 0.6, 0.8, and 1.0 seconds. The principle used for the design was to compensate the system ignoring the time-delay and then to compensate for the time-delay. A two stage lead network was used to reduce the effect of the engine time-delay. The system was simulated by using a digital computer program called MIMIC, which simulates the functions of an analog computer. The average mean square error was computed for the system with and without the control installed, for each of the five time-delay values. In all cases, the average mean square error was reduced approximately 70% by the addition of the compensator. The design procedure was based on the Crossover Model for the human pilot as developed by Systems Technology Incorporated of Hawthorne, California.

A DIFFERENTIAL THRUST CONTROLLER
FOR
AIR CUSHION LANDING SYSTEM AIRCRAFT

I. Introduction

Background

Aircraft dependence upon the wheel for ground operation has often presented great problems, especially with heavy aircraft. The surface used for taking-off, landing, and taxiing has to be strong enough to accept the large force exerted by the small area of tire contact. This causes considerable expense in airfield construction and reduces the mobility of air forces. Also, the wheels have to be attached to the aircraft with strong structures, adding considerable weight.

A solution to this problem has been sought for the past five or six years, in the form of the Air Cushion Landing System (ACLS). This apparatus is a replacement for the conventional landing gear. The main piece of equipment is an oval tube, called the trunk, which is attached to the bottom of the aircraft fuselage. An auxiliary engine on the aircraft fills the trunk with air and forces the air out through holes, located on the bottom and inside of the trunk. As a result, an air cushion is created between the trunk and the surface of the ground. In this way, the weight of the aircraft is evenly distributed over the total area of the air cushion, resulting in a lower ground contact pressure than is possible with tires in the same amount of ground area. The aircraft is then able to taxi over very soft surfaces, such as dirt and mud. The idea for this system came from the hovercraft, a water vessel designed in the 1950's in England.

GE/100/14-21

The Bell Aerospace Company of Buffalo, New York has designed and flown an ACLS on a single-engine aircraft. Tests with this system revealed that it was possible to go over mud, ditches, small tree stumps, and other objects that would have stopped a wheeled vehicle. Also, taking-off and landing on unimproved strips was possible. The successful use of an ACLS on a small aircraft has paved the way for further development.

The Air Force Flight Dynamics Laboratory at Wright-Patterson Air Force Base is presently involved in the testing of a twin-engine aircraft, equipped with an ACLS. This aircraft is a Canadian "Buffalo" and is designated the XC-8A by the U.S. Air Force. Through scale model testing, and computer runs with a mathematical model, the design has been accepted for flight, and the aircraft is presently undergoing an extensive flight testing program. The XC-8A is an important step in the development of the ACLS for use on other and larger military aircraft.

Problem

A problem that has been discovered in the testing is the susceptibility of the aircraft to movement in crosswinds while taxiing. Since there is no tire contact to give directional stability, the aircraft can easily be blown about by light to moderate winds. The initial solution attempted was to install exhaust ports on the outer sides of the trunk. These exhaust holes, also called puff ports, can be individually controlled by the pilot, to push the aircraft in one way or another. However, the forces from the puff ports are only adequate in a very light wind.

As a result of the directional control problem, attention was turned to a powerful source of yaw control, differential thrust. The potential difference in thrust between the two engines is the greatest source of low speed yaw moment in the XC-8A (Ref. 5:150). The engine thrust can be changed, or even reversed, by changing the pitch of the propellers and/or the throttle setting. Since many aircraft are steered on the ground by movement of the rudder pedals, it would be natural to control the differential thrust by movement of the rudder pedals. However, the time-lags associated with the engines and the pilot, and the large inertia of the taxiing aircraft, dictate the need for a compensation system in the differential thrust controller.

Objectives

It was desired to design a control system that would improve the aircraft heading response to the pilot's input, with a random heading disturbance due to the wind. It was also desired to test the system with and without the controller to determine the improvement obtained.

Approach

Developing an adequate model for the engines and the aircraft was the first important part of the project. Then the design portion was accomplished using classical control theory and the well known Crossover Model for the pilot. It was assumed that future application of the ACLS will be on jet-powered aircraft, where the engine time-lags are higher than on the conventional-powered XC-8A. Therefore, larger lags than the one associated with the XC-8A engines were considered for further design purposes. The simulations of the controlled and

original system were performed on a digital computer, using the MIMIC simulation language, which is a means of performing analog type simulations by digital techniques. MIMIC was used because the program was easier to set up than an analog program, and the time-lags were more accurately simulated on a digital computer than on an analog, where a Padé approximation would have to be used. Finally, a mean square error analysis of the system was performed.

II. The Plant Model

As a preliminary to modeling the aircraft and its engines, it was necessary to determine how the pilot interacted with the aircraft in the taxi problem. Much thought and research was dedicated to this fundamental task and the resulting block diagram can be seen in Fig. 1.

While the pilot is taxiing the aircraft, he is involved in a multiloop task. There are two loops, one in which the pilot is controlling the heading of the aircraft (ψ), which is referenced to the direction of the taxiway, and a second, outer loop in which he is controlling the aircraft distance from the taxiway centerline (y).

Each loop has a random input disturbance caused by the wind. The theme for this multiloop approach came from two sources, References 19 and 21, in which the pilot controls the pitch of an aircraft and the distance off the glide slope while on an instrument approach.

An analysis of the complete multiloop task was beyond the scope of this thesis; however, it was believed that when control of heading in the inner loop is optimized, the outer loop response will be satisfactory. Therefore, the inner loop was investigated and a controller designed to improve its characteristics.

The block diagram of the heading control loop can be seen in Fig. 2, where the task appears as a regulator control problem and the commanded heading (ψ_c) will be zero. This block diagram is topologically equivalent to the block diagram shown in Fig. 3. If the portion of the block diagram inside the broken line in Fig. 3 is considered, the problem becomes a compensatory tracking task and can be analyzed by the Crossover Model theory presented in Chapter IV.

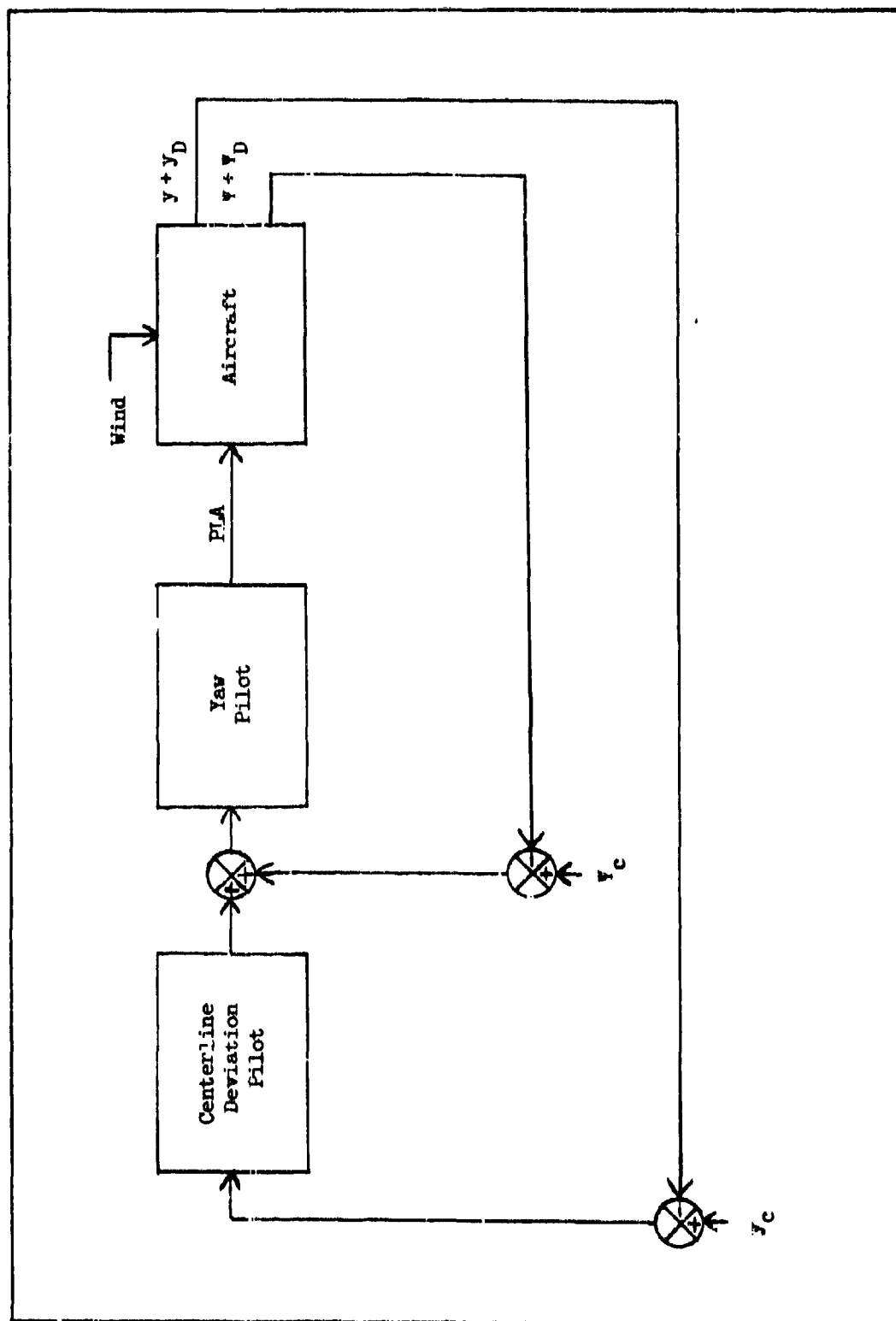


Fig. 1 Block Diagram of the Multiloop Taxi Task

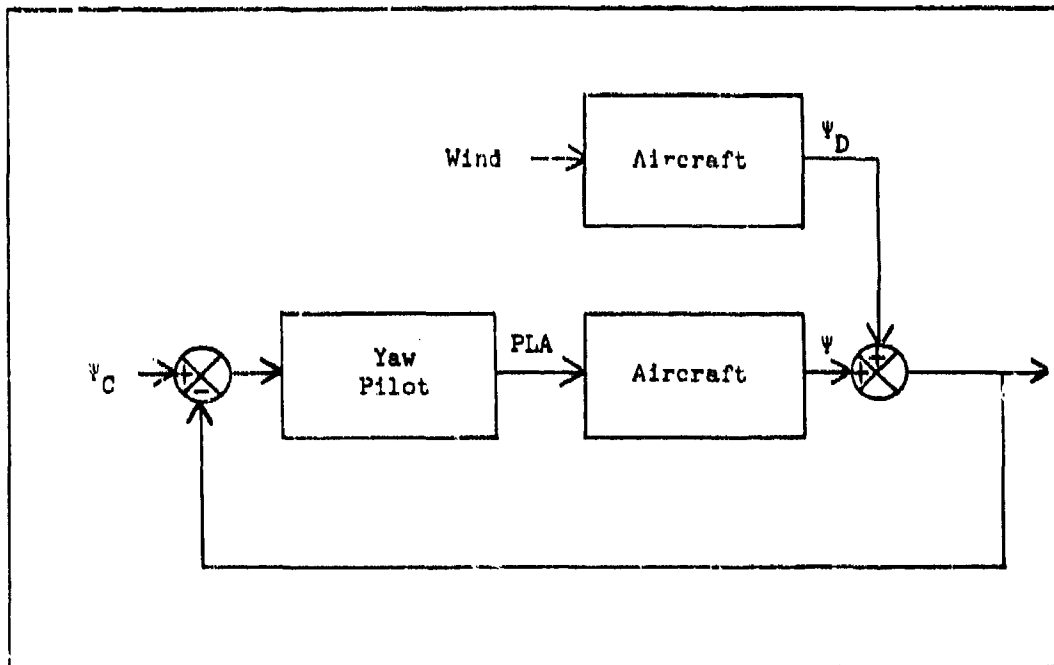


Fig. 2 Block Diagram of the Heading Control Loop as a Regulator Problem

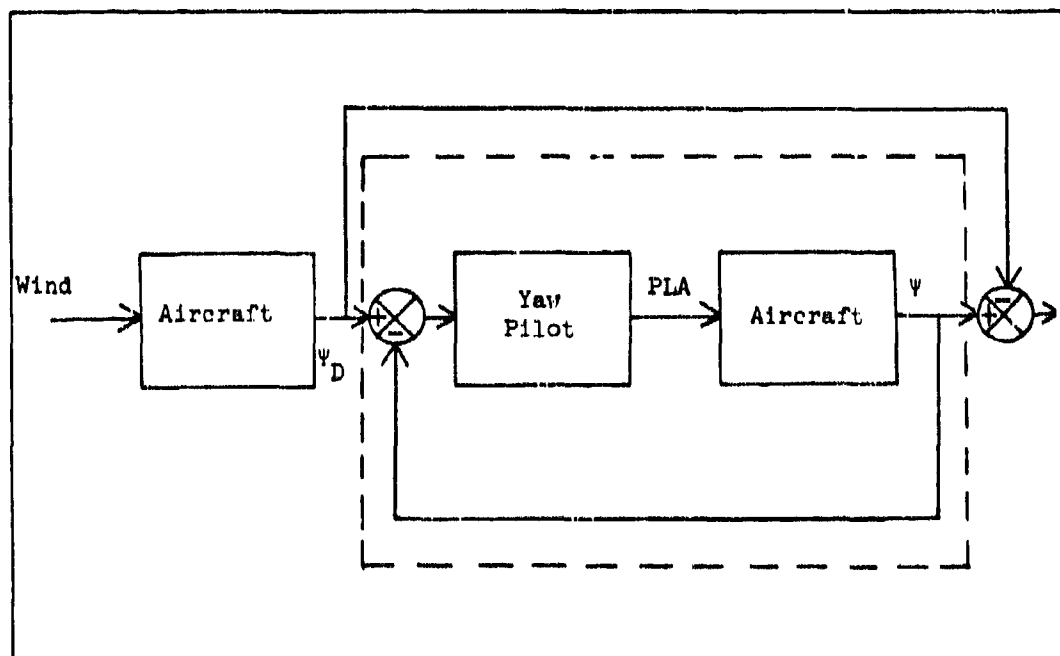


Fig. 3 Block Diagram of the Heading Control Loop as a Compensatory Tracking Task

Engines

The first part of the plant to be studied was the engines. The engines receive their input, called the power lever angle (PLA), from the power levers, which control thrust. In the lower thrust ranges, used while taxiing, the thrust is changed by a combination of changing both power and the blade angle of the propellers. The blade angle of the propellers is changed by the beta control system, which is a modification of the original engine control. The engine output is thrust, which converts directly to yawing moment (N_E) by multiplying thrust times the distance of the engine from the aircraft center. Therefore, the transfer function needed for the engines is N_E/PLA .

As mentioned, the engines on the XC-8A have a beta (propeller blade incidence angle) control system. This is a modification of the original engine control and was incorporated because the original control gave only a gross, stepped variation of thrust at the lower power setting. The installation of the ACLS on the aircraft dictated the need for a vernier adjustment of thrust while taxiing. One result of adding the beta control system was the reduction of the pure time-delay of the engine response to about 0.2 second. This is considered to be a very low delay time, as the delay times for turbojet and turbofan engines are on the order of one second. (This time-lag information was obtained from discussions with Dr. George Kurylowich and with Mr. Elisha Rachovitsky of the Air Force Flight Dynamics Laboratory, Wright-Patterson Air Force Base). Since larger delay times may be encountered in future ACLS aircraft, it was decided to perform the design study for values of engine response pure time-delay of 0.2,

0.4, 0.6, 0.8, and 1.0 seconds. In the ground-based simulation of the XC-8A with Air Force test pilots, the differential thrust control was simulated by a direct mechanical hookup from the rudder pedals to the power levers. The engine response time-delay was varied, and when it was increased to one second, the pilots could not effectively control the simulator while taxiing (Ref. 10).

The remainder of the engine dynamics were simulated, in this report, as a first order lag. From the thrust-versus-time response curve of Fig. 4, it appears that the thrust response to a step input of PLA is well approximated by a first order lag with a time constant of 0.9 second. Both the thrust response and the ideal first order lag curves are drawn for comparison. The maximum steady-state thrust of 2000 pounds is used because this is the limit of the beta control system and is considered sufficient for taxi purposes. The maximum amount of yawing moment that can be obtained from ± 2000 pounds of thrust is 65,000 foot-pounds (Ref. 5:151). Therefore, the complete engine transfer function is

$$\frac{N_E}{PLA} = \frac{1969.697 e^{-st_d}}{1 + 0.9s} \quad (1)$$

where N_E is in foot-pounds, PLA is in degrees, and t_d is the engine response pure time-delay.

Aircraft

The aircraft model required the use of many engineering approximations. The effect of the vertical stabilizer on the yaw moment,

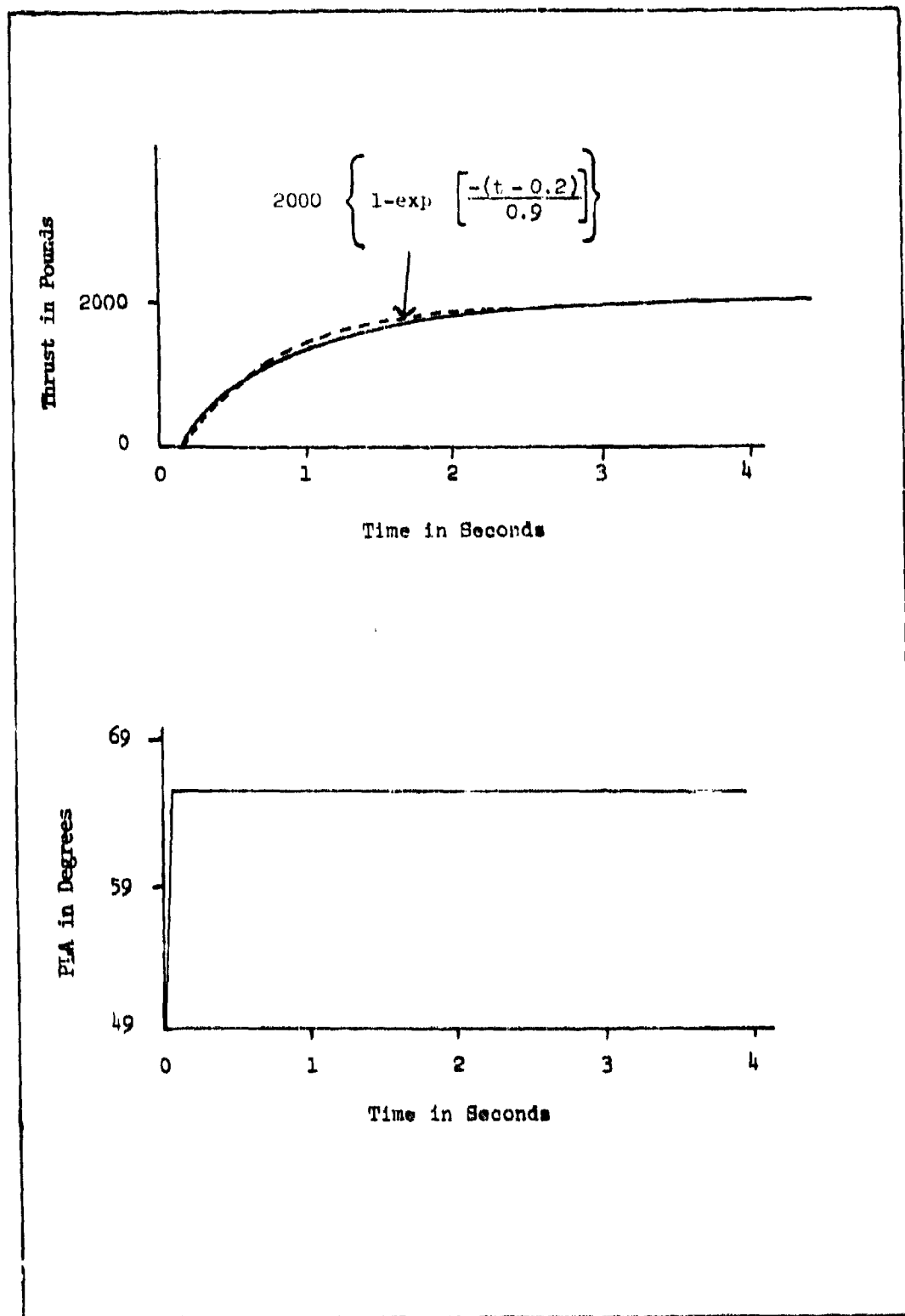


Fig. 4 Thrust Response Curve of the XC-8A Engine Fitted with Beta Control System (Ref. 6)

due to the C_{N_R} and C_{N_β} stability derivatives, was the only aerodynamic effect considered. This assumption is justified by the low taxi speed. The aerodynamic effect considered was necessary because it accounts for the heading input disturbance. There is one aerodynamic effect neglected which may have some significance, the rolling moment caused by propeller wash over the wings. It was assumed that this can be eliminated, if undesirable, by means of automatic spoiler or aileron control. It was also assumed that the pilot keeps the forward speed of the aircraft constant at twenty knots (33.78 feet/second) by controlling power and brakes. (The brakes are expandable pillows on the bottom of the trunk, with attached skid pads). Finally, the yaw moments due to the brakes and the puff ports were neglected.

With the necessary assumptions made, the model for the aircraft can be derived. The model must account for two inputs and two outputs, so each input/output pair will be discussed separately. The engines deliver a yaw moment input to the aircraft, which is converted into aircraft heading. The model for this conversion process is a simple inertia transfer function:

$$\frac{\psi_E}{N_E} = \frac{1}{I_{zz}s^2} \quad (2)$$

where ψ_E is the heading due to the engines and I_{zz} is the moment of inertia about the aircraft z-axis.

The other input to the aircraft is the wind disturbance, and the aerodynamic effect of the wind on the heading of the aircraft is mainly due to the vertical stabilizer. The geometry of the wind effect problem can be seen in Fig. 5. The following equation accounts for the yaw due to wind:

$$N_W = \frac{1}{2} \rho V^2 S b \left(C_{N_\beta} \beta + C_{N_R} \frac{R}{2} \frac{b}{V} \right) \quad (3)$$

where ρ is the atmospheric density, S is the wing area, b is the wing-span, and R is the yaw rate. The relative wind velocity is found from the relationship

$$V = \sqrt{V_X^2 + V_Y^2} \quad (4)$$

where V_X and V_Y are the relative wind velocities along the X and Y aircraft axes, and the sideslip angle is defined as

$$\beta = \frac{V_Y}{V} \quad (5)$$

Substituting equations (4) and (5) into (3) yields

$$N_W = \frac{1}{2} \rho S b \sqrt{V_X^2 + V_Y^2} \left(C_{N_\beta} \frac{V_Y}{\sqrt{V_X^2 + V_Y^2}} + C_{N_R} \frac{b}{2} \frac{R}{\sqrt{V_X^2 + V_Y^2}} \right) \quad (6)$$

and since

$$N_W = I_{zz} \ddot{\psi}_w \quad (7)$$

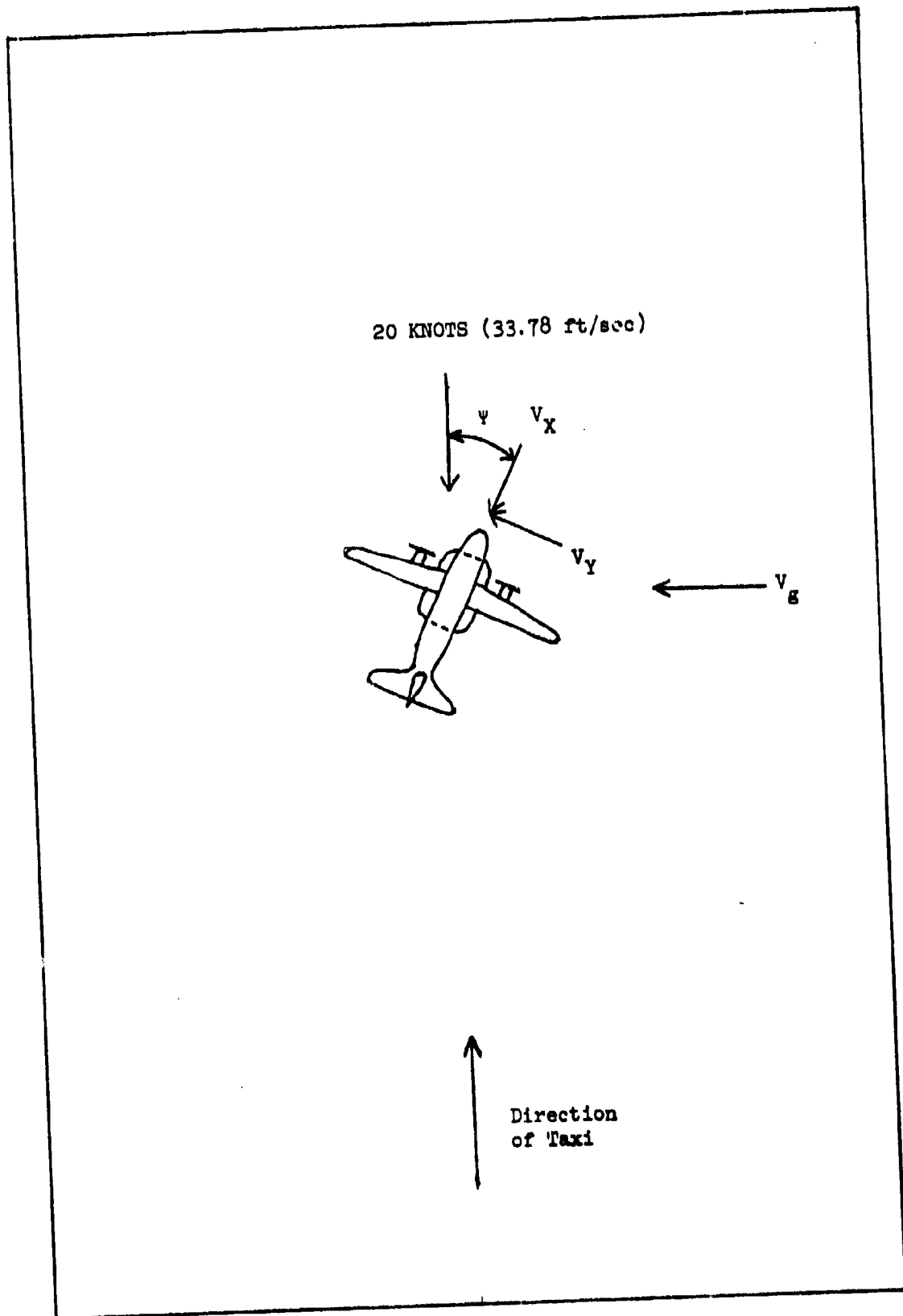


Fig. 5 Wind Effect on Taxiing ACLS Aircraft

and

$$R = \dot{\Psi}_w \quad (8)$$

(assuming zero roll and pitch), then

$$I_{zz} \ddot{\Psi}_w = K_1 V_Y \sqrt{V_X^2 + V_Y^2} + K_2 \sqrt{V_X^2 + V_Y^2} \dot{\Psi}_w \quad (9)$$

where $K_1 = \frac{1}{2} \rho S b C_{N\beta}$ and $K_2 = \frac{1}{4} \rho S b^2 C_{N_R}$.

From the geometry of the problem in Fig. 5,

$$\begin{aligned} V_X &= 33.78 \cos \Psi_w + V_g \sin \Psi_w \\ V_Y &= -33.78 \sin \Psi_w + V_g \cos \Psi_w \end{aligned} \quad (10)$$

Assuming that the heading angle will be kept small by the pilot, the small angle approximations can be applied and (10) becomes

$$\begin{aligned} V_X &= 33.78 + V_g \Psi_w \\ V_Y &= -33.78 \Psi_w + V_g \end{aligned} \quad (11)$$

It is desired to linearize equation (9) by a Taylor Series expansion. The operating point is defined as $V_{g0} = \Psi_{w0} = \dot{\Psi}_{w0} = \ddot{\Psi}_{w0} = 0$ and, as a result of (11), $V_{X0} = 33.78$ and $V_{Y0} = 0$. When equation (11) is substituted into (9), the result is of the form

$$I_{zz} \ddot{\Psi}_w = f(\dot{\Psi}_w, V_X, V_Y) = g(\dot{\Psi}_w, \Psi_w, V_g) \quad (12)$$

The Taylor Series expansion is

$$I_{zz} \ddot{\psi}_w = g(\dot{\psi}_{w0}, \psi_{w0}, v_{g0}) + \left. \frac{\partial g}{\partial \dot{\psi}_w} \right|_{\dot{\psi}_{w0}, \psi_{w0}, v_{g0}} (\dot{\psi}_w - \dot{\psi}_{w0}) + \left. \frac{\partial g}{\partial \psi_w} \right|_{\dot{\psi}_{w0}, \psi_{w0}, v_{g0}} (\psi_w - \psi_{w0}) + \left. \frac{\partial g}{\partial v_g} \right|_{\dot{\psi}_{w0}, \psi_{w0}, v_{g0}} (v_g - v_{g0}) + \text{H.O.T.} \quad (13)$$

and, by the Chain Rule,

$$\frac{\partial g}{\partial \dot{\psi}_w} = -\frac{\partial f}{\partial \dot{\psi}_w} \quad (14)$$

$$\frac{\partial g}{\partial \dot{\psi}_w} = \frac{\partial f}{\partial v_x} \frac{\partial v_x}{\partial \dot{\psi}_w} + \frac{\partial f}{\partial v_y} \frac{\partial v_y}{\partial \dot{\psi}_w} \quad (15)$$

$$\frac{\partial g}{\partial v_g} = \frac{\partial f}{\partial v_x} \frac{\partial v_x}{\partial v_g} + \frac{\partial f}{\partial v_y} \frac{\partial v_y}{\partial v_g} \quad (16)$$

At the operating point: $\frac{\partial f}{\partial \dot{\psi}_w} = 33.78 K_2$, $\frac{\partial f}{\partial v_x} = 0$, $\frac{\partial f}{\partial v_y} = 33.78 K_1$,

$\frac{\partial v_y}{\partial \dot{\psi}_w} = -33.78$, and $\frac{\partial v_y}{\partial v_g} = 1$, so $\frac{\partial g}{\partial \dot{\psi}_w} = 33.78 K_2$, $\frac{\partial g}{\partial \psi_w} = -(33.78)^2 K_1$,

and $\frac{\partial g}{\partial v_g} = 33.78 K_1$. Ignoring the higher order terms (H.O.T.), the

Taylor Series expansion about the operating point becomes

$$I_{zz} \ddot{\psi}_w = 33.78 K_2 \dot{\psi}_w - (33.78)^2 K_1 \psi_w + 33.78 K_1 v_g \quad (17)$$

When equation (17) is put into transfer function form and the parameter values from Fig. 6 are substituted, the result is

$$\frac{\psi_w}{V_g} = \frac{0.0007518}{s^2 + 0.0756s + 0.0254} \quad (18)$$

The aircraft acts as a second order filter, with a damping factor of 0.24 and a natural frequency of 0.16 radian per second. These numbers agree with the damping factor and natural frequency of the Dutch Roll mode for the same stability derivatives, which serves as a good check on the mathematics. The block diagram of the plant model, with numerical values inserted, can be seen in Fig. 7.

Engines: 2 x GE/T64-14
 2 x UCAL ST 6-73 (for ACLS)

Propellers: Ham. Std. 63-E60-15, 3 bladed, 14.5 ft. diam.

Wing Area: 945 sq. ft.

Wing Span: 96 ft.

\bar{c} : 10.3 ft.

Weights: Max. Takeoff 41,000 lb. (structural limit)
 Max. Landing 39,100 lb. (structural limit)

Low Speed Stability Derivatives (Ref. 12)

$$C_{N_R} = -0.22$$

$$C_{N_\beta} = 0.105$$

Inertia (41,000 pound A/C, 41.5% \bar{c})

$$I_{zz} = 508642.0 \text{ slugs ft}^2$$

Sea Level Air Density

$$\rho = 0.00237690 \text{ slugs/ft}^3$$

Fig. 6 Relevant Data for the XC-8A Model

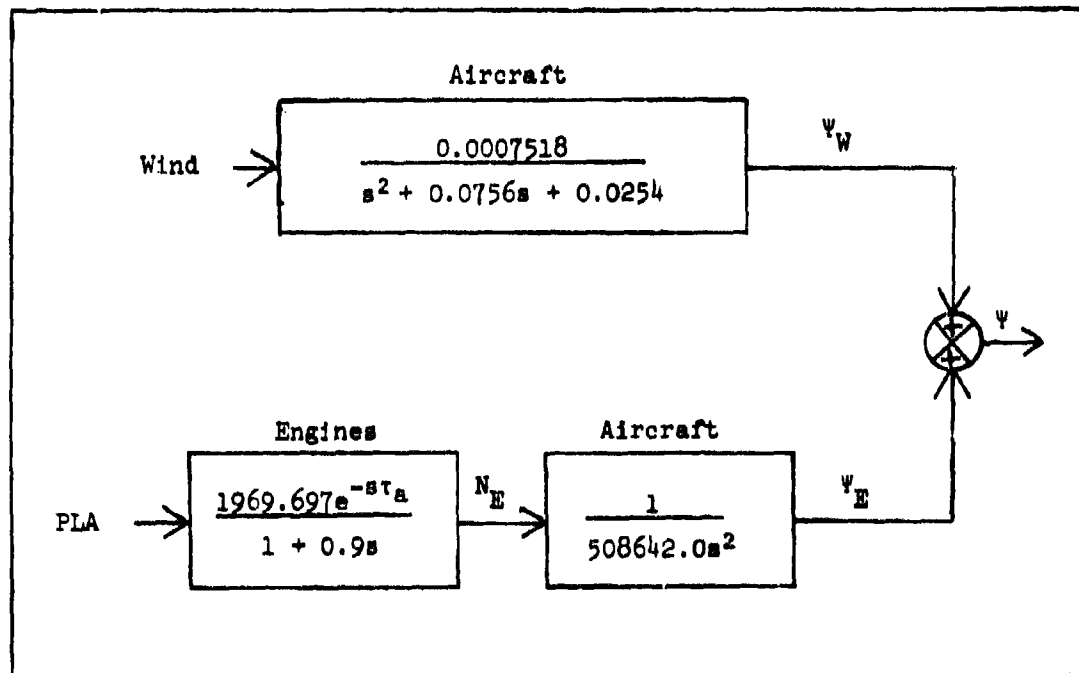


Fig. 7 Block Diagram of the Plant Model

III. The Wind Model

The wind model accounted for the only disturbance to the plant and was used to determine the effectiveness of the controller. Many different wind models were found in a literature search, among them the well-known vonKarman and Dryden wind models, but they were all functions of the aircraft speed. These models all assume the aircraft to be flying through a gust field which is frozen in time and do not apply very well to a taxiing aircraft, where the gust effect is from a combination of temporal and spatial fluctuations. Since a model for this was not available, and there was not sufficient time to collect data and analyze it, the wind was approximated as a band limited white noise, with a bandwidth of one radian per second. Band limited white noise is defined to be a noise with a constant power spectral density (PSD) over a finite range, as seen in Fig. 8. The exact cutoff frequency was not critical as long as it was high enough, since the noise was cut off at a much lower frequency as a result of filtering by the aircraft. This lower cutoff frequency was based on the assumption that no structural vibrations were to be modeled.

The wind was assumed to be blowing across the taxiway and consisted of the gusting effect only. The steady component of crosswind was not considered important to the problem as the pilot could sense it and apply a steady correction. However, it does affect the dynamics of the aircraft response by changing the coefficients in equations (13) and (18). As the steady component of wind increases, the gust effect on the aircraft decreases and the aircraft response becomes overdamped.

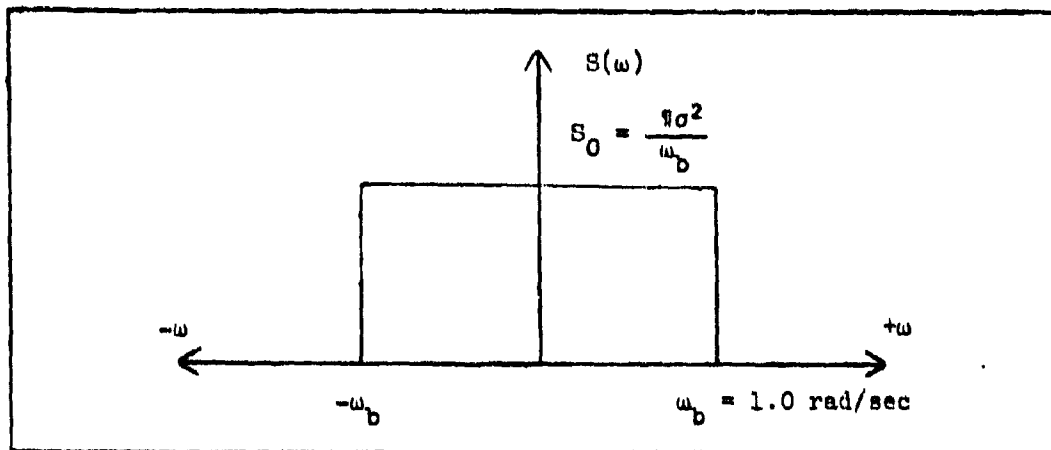


Fig. 8 Power Spectral Density of the Wind Model

Since this is an improvement over the lightly damped case, it was decided to eliminate the steady component of crosswind and design for the worst case. Thus, a mean of zero was selected for the wind gusts. The determination of the variance presented a more difficult problem. Since the aircraft was restricted from flying when the wind gusts exceeded a certain level, the intensity of the maximum gusts encountered was under human control. Assuming that the average gusts encountered would be ten knots, or \pm five knots about the mean, a standard deviation of five knots (8.45 feet per second) was selected for the wind, and the resulting power spectral density can be seen in Fig. 8. The calculations for this figure can be found in Appendix D.

IV. The Pilot ModelBackground

In order to analyze the heading control problem and then to design a control system to correct it, it was necessary to have a model for the pilot in the inner control loop of Fig. 1. Extensive documentation was found on the subject of pilot modeling, especially in references 13, 14, 15, and 16; and the bibliography in reference 16 provided a good source for a literature search. The model selected was the most widely accepted one in the field of control systems engineering, the Crossover Model. Since no deterministic method was found to write down a mathematical model for the human pilot, many engineering judgments had to be made in the selection process. The design and final analysis of the design were based on these judgments, which could not be validated by experiments with human pilots, due to lack of time and equipment.

The Crossover Model was derived from a quasi-linear representation of the non-linear, time-varying human pilot. The pilot can be represented over a wide range of frequencies by a transfer function plus a remnant. One form of the transfer function is (Ref. 16)

$$Y_P = K_P e^{-j\omega\tau} \left(\frac{T_L j\omega + 1}{T_I j\omega + 1} \right) \left(\frac{T_K j\omega + 1}{T'_K j\omega + 1} \right) \left\{ \frac{1}{(T_N j\omega + 1) \left[\left(\frac{j\omega}{\omega_N} \right)^2 + \left(\frac{2\xi_N}{\omega_N} \right) j\omega + 1 \right]} \right\} \quad (19)$$

where

K_P

= gain

$e^{-j\omega\tau}$

= fixed time-delay due to conduction time of various subsystem elements

$$\frac{T_L j\omega + 1}{T_I j\omega + 1} = \text{equalization characteristic; } T_L \text{ and } T_I \text{ values depend on form of controlled element}$$

$$\frac{T_K j\omega + 1}{T'_K j\omega + 1} = \text{terms which are used to describe very low frequency phase data}$$

and the term in brackets accounts for neuromuscular system elements. This is called the precision model and accounts for the major sub-systems in the behavior of the pilot. The variables can change from one person to the next and can even change for the same person at a single task as fatigue, boredom, motivation, and other human factors change.

The remnant is a term used to account for the difference between the output of the human pilot and the output of the model. It is represented by a power spectral density of a noise injected into the system at the pilot's output, and is mostly caused by non-linear, time-varying pilot behavior. The remnant term has been refined over the years but is still difficult to model. In this project, the remnant was not considered important at the frequencies of interest (about one to five radians per second).

The Crossover Model

The Crossover Model, as discussed here, applies to the compensatory tracking task, as seen in block diagram form in Fig. 7. In the compensatory task, the pilot receives a visual signal, equivalent to the difference between the forcing function and the output of the controlled element, and attempts to minimize this error signal. For the Crossover

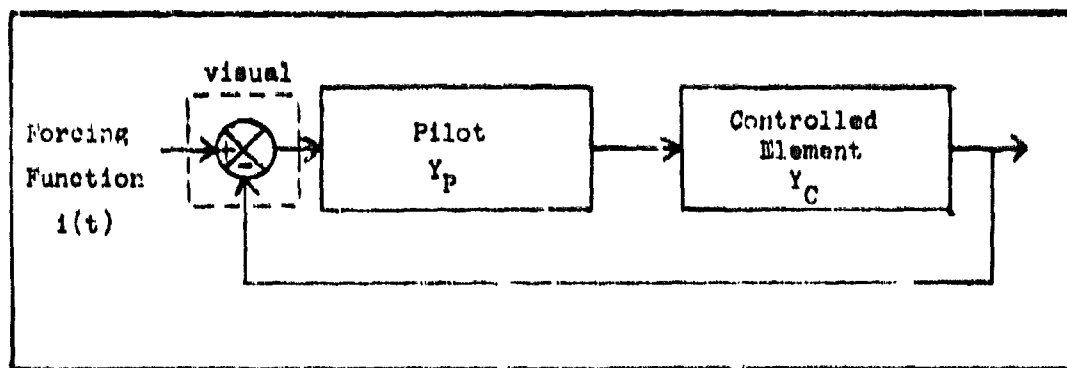


Fig. 9 The Compensatory Tracking Task

Model to be valid, the forcing function must be a random appearing input and the signal to the pilot must be visual. The effects of other pilot cues, such as motion, have been studied elsewhere (Ref. 18).

By experimental observation, the characteristics of the open loop transfer function of the compensatory system have been found to be similar for many different controlled elements. The open loop log-magnitude-versus-log-frequency (Bode) diagrams all have a straight line with a slope of minus twenty decibels (db) per decade in the region where the log magnitude crosses the zero db point. This is where the term "Crossover Model" originates. In other words, in the crossover region of frequency, the open loop transfer function is

$$Y_P Y_C = \frac{\omega_c^{-\tau s}}{s} \quad (20)$$

where ω_c is the crossover frequency and τ is the time delay due to both the pilot and the controlled element. It is obvious that the Crossover Model of the pilot is dependent on the form of the controlled element.

When the controlled element transfer function is known, the model for the pilot in the crossover region can be found from

$$Y_P = \frac{\omega_C^{-\tau_0 s}}{s Y_C} \quad (21)$$

where τ_0 is the time-delay associated with the pilot and any time-delays in the controlled element are not considered. This is easily done mathematically, but the pilot is not capable of efficiently becoming a second order derivative or higher. When he is asked to do so, his opinion of the controlled element seriously deteriorates. This opinion can be objectively rated on a scale from one to ten, called the Cooper-Harper Scale, which is well known to test pilots and aircraft design engineers as a basis for rating the handling qualities of aircraft (Fig. 10).

The pilot's time delay is dependent on the controlled element and on the forcing function bandwidth. This time delay is difficult to evaluate deterministically as it can be improved with training and varies with different people. However, it can be predicted with reasonable accuracy by (Ref. 13)

$$\tau_0 = \tau_0(Y_C) - \Delta\tau_0(\omega_1) \quad (22)$$

where τ_0 depends upon the controlled element and $\Delta\tau_0$ depends upon the forcing function bandwidth, ω_1 . The term $\Delta\tau_0$ is approximately $0.08 \omega_1$.

Pilot Rating	Demands on the Pilot	Aircraft C Characteristics
1	Pilot compensation not a factor for desired performance	Excellent Highly desirable
2	Pilot compensation not a factor for desired performance	Good Negligible deficiencies
3	Minimal pilot compensation required for desired performance	Fair - Some mildly unpleasant deficiencies
4	Desired performance requires moderate pilot compensation	Minor but annoying deficiencies
5	Adequate performance requires considerable pilot compensation	Moderately objectionable deficiencies
6	Adequate performance requires extensive pilot compensation	Very objectionable but tolerable deficiencies
7	Adequate performance not attainable with maximum tolerable pilot compensation. Controllability in question	Major deficiencies
8	Considerable pilot compensation is required for control	Major deficiencies
9	Intense pilot compensation is required to retain control	Major deficiencies
10	Control will be lost during some portion of required operation	Major deficiencies

Fig. 10 Cooper-Harper Handling Qualities Rating Scale

The crossover frequency is another subjective variable. It is estimated as (Ref. 13)

$$\omega_o = \omega_{co}(Y_C) + \Delta\omega_o(\omega_1) \quad (23)$$

To a first approximation, $\Delta\omega_c$ is zero for the forms of controlled elements found in aircraft, and ω_{co} can be found from the condition for a neutrally stable system at the crossover frequency, with no input. The equation is

$$\tau\omega_{co} = \frac{1}{2} \quad (24)$$

where τ is the sum of τ_0 and the controlled element time-lag, if there is one.

The ACLS Pilot Model

As seen in Fig. 5, the controlled element for the ACLS aircraft is

$$Y_C = \frac{0.0043 e^{-s\tau_a}}{s^2 (s + 1.111)} \quad (25)$$

This is a very difficult element for the pilot to control. He has to generate a transfer function of the form

$$Y_P = K_P e^{-s\tau_0} s(s + 1.111) \quad (26)$$

in the crossover region. This means that the acceleration channel of the pilot is activated, causing his zero input time-delay (τ_0) to be about 0.8 second (Ref. 16:26) and the Cooper-Harper rating to be extremely high (about nine or ten, Ref. 16:37). The pilot rating alone is sufficient reason to reject the controlled element as undesirable. Since it is only a subjective measurement, the system was analyzed from the Crossover Model theory.

The lowest value of the controlled element time-delay was 0.2 second. Adding this to the τ_0 value of 0.8 second and using equation (24), the crossover frequency was found to be 1.57 radians per second. The crossover frequencies for the other controlled element time-delays of 0.4, 0.6, 0.8, and 1.0 seconds were 1.31, 1.12, 0.98, and 0.87 radians per second, respectively. According to reference one, a realistic value of crossover frequency for handling qualities considerations is about 2.0 ± 0.5 radians per second. Thus, the crossover frequency of the system is lower than desired. Also, the lower crossover frequency causes a higher system rms error as the error is inversely proportional to the square of the crossover frequency (Ref. 16:15).

V. Control System Design

Design Philosophy

The control system design was based on the idea that the form of the controlled element determines the pilot's describing function. Also, it was desired to reduce the engine time-delay as much as possible. A general formula for the pilot's describing function in the crossover region is

$$Y_P = K_P e^{-s\tau_e} \frac{T_L s + 1}{T_I s + 1} \quad (27)$$

where T_L and T_I are the amounts of lead and lag that the pilot must generate to compensate for the controlled element dynamics. The lead (T_L) is the quantity which has the most effect on the pilot's opinion of the system. A reasonable maximum for T_L is five seconds and a graph showing the effect of lead generation on the pilot opinion rating is seen in Fig. 11. The pilot rating scale referred to is the one shown in Fig. 10.

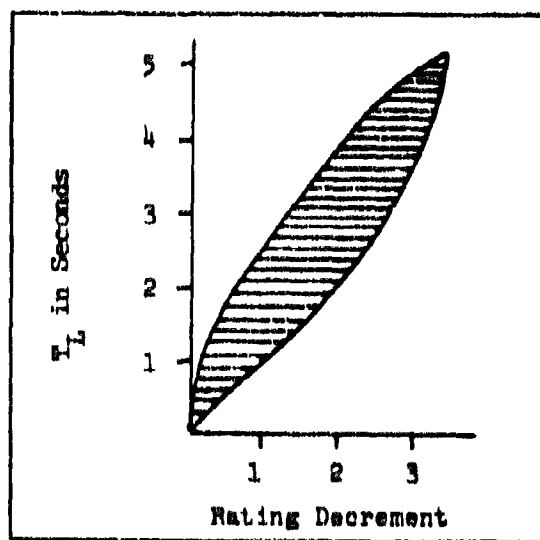


Fig. 11 Rating Decrement Due to Pilot Lead as Inferred from Handling Qualities Tests (Ref. 14:247)
(Open curve due to uncertainty of T_L)

According to Ref. 1, the best handling qualities are obtained when the value of T_L is less than about 1.5 seconds. It was decided to make the value of T_L for this design study equal to one second. As will be seen, this criterion had to be relaxed somewhat for stability reasons. For the pilot lead to be one second, the controlled element was required to have a factor of $s+1$ in the denominator, at the cross-over frequency. Assuming that the controlled element can be configured to

$$Y_C = \frac{K_C}{s(s+1)} \quad (28)$$

then the pilot describing function would be

$$Y_P = K_P e^{-N\tau_0} (s+1) \quad (29)$$

in the crossover region. The pilot's lag term was not presented in equation (29) because it was assumed that the ideal controlled element would have no lead term in the numerator. This lead term is the usual cause of the pilot's adopting a lag. For a controlled element of the form of equation (28), the value of the pilot's pure time-delay with zero input (τ_0) is approximately 0.33 second (Ref. 15). (Other values of time-delay, ranging from 0.16 second to 0.50 second, were found in the literature.) The objective of the control system design, then, was to closely approximate $K_C/s(s+1)$ in the crossover region.

The first step in the classical control theory design procedure was to change the controlled element into a feedback control system. From a study of the original system, it was determined that the

quantities available for feedback were the heading and the heading rate. The heading rate was easier to detect by using an available piece of aircraft hardware, the yaw rate gyro. With the yaw rate (heading rate) fed back to the input of the engines, the second step consisted of inserting a cascade compensator into the plant ahead of the engines. The resulting block diagram for the controlled system is seen in Fig. 12.

Design Method

The block diagram of Fig. 12 shows a block containing a $1/s$ (an integrator) outside of the control loop. This integrator contributes the s term in the denominator of equation (28), the desired transfer function of the controlled element. Thus, the objective in designing the compensation control loop (CCL) was to make it assume the closed loop transfer function

$$Y_{CCL} = \frac{K_0}{s+1} \quad (30)$$

The method for the design of the compensator for the feedback control system came from reference 22. The principle was to equalize the system as if the time-delay was not there and then to compensate for the time-delay. The time-delay was reduced by adding lead compensation to the system, with the zeros of the lead compensator outside of the system bandpass.

The first step taken was to draw the Root Locus of the CCL with yaw rate feedback and no compensation added. In Appendix A, an explanation is given of how to draw the Root Locus for a feedback control system with time-delay. The Root Locus plots for values of

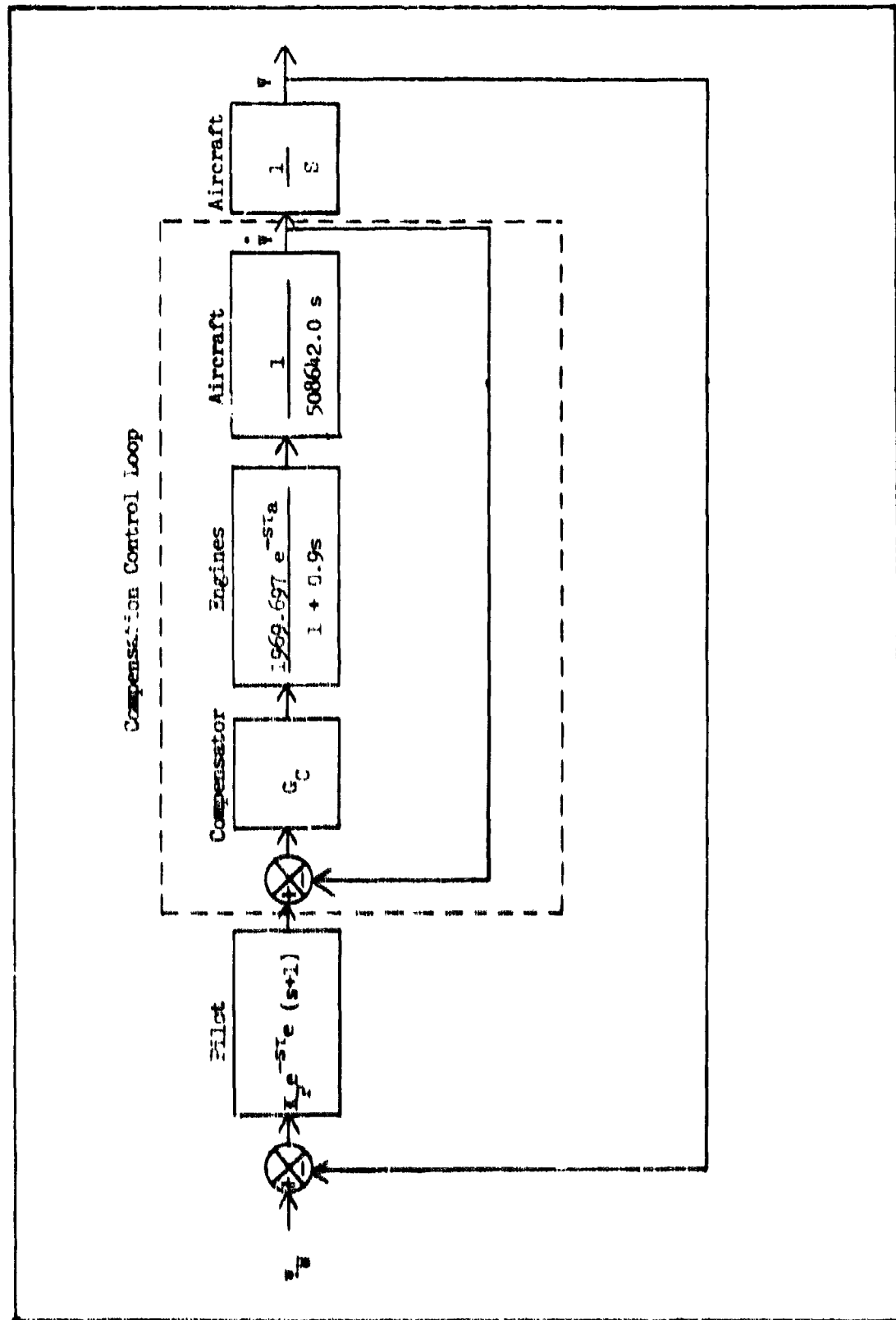


Fig. 12 Block Diagram of the Heading Control Loop with Compensator Added

τ_a equal to 0.2, 0.4, 0.6, 0.8, and 1.0 seconds can be seen in Figures B.1 through B.5 in Appendix B. From the plots, it could be seen that it was impossible to select a gain which would put one dominant root at -1. If one root was put at -1, then another root would be more dominant and almost at the origin.

Therefore, the first procedure in the design was to reconfigure the Root Locus so that one root could be selected at -1 and the other roots would be less dominant. This was done with a compensator of the form

$$G_C = K_A \frac{(s + 1.111)}{(s + 11.111)} \quad (31)$$

where K_A was the amplification factor and the pole was chosen to be ten times the zero for mathematical simplicity. The Root Locus plots for the system with this lead compensator added, for the various values of τ_a , are drawn in Figures B.6 through B.10 in Appendix B. From each of these plots, it was possible to select one root at -1, with the other roots being less dominant. For the $\tau_a = 1.0$ second case, the second root was very close to the first at -1, but this was corrected in the second design step.

The second step, designing a multi-order lead compensator to reduce the pure time-delay of the engine response, was more difficult than the first. The transfer function for the compensator, called the time delay compensator (TDC) was

$$G_{TDC} = K_{TDC} \left[\frac{(s + z)}{(s + p)} \right]^n \quad (32)$$

where K_{TDC} was the gain constant, n was the order (number of poles and zeros), and z and p were the approximate locations of the zeros and poles, respectively. Each pole was set equal to ten times the zero to keep its effect negligible. A pole was used with each zero in order to keep the system realizable. The phase lead contribution of the compensator was approximately $n \tan^{-1} \frac{\omega}{z}$ and this phase angle had to compensate for the phase lag of the engine time-delay. The two were set equal at the crossover frequency to yield

$$n \tan^{-1} \left(\frac{\omega}{z} \right) = \omega \tau_m \quad (33)$$

with the restriction that the zero(s) should lie outside of the crossover frequency. Reference 22 suggests a limit on the number (n) of zeros to keep the amplitude response of the system respectably low for higher frequencies. The number of zeros was set at two in this case because the system had two poles near the lower frequencies of interest. By using the value of 0.33 second for the pilot's zero input time-delay and assuming that the engine time-delay would be reduced to zero, the crossover frequency found from equation (24) was 4.76 radians per second. Using this value for the crossover frequency in equation (33), and by setting n equal to two, the approximate locations of the poles and zeros were found. As the value of τ_m increased, it was assumed that the crossover frequency would decrease because of inability to eliminate all of the phase lag due to τ_m . The assumed values of crossover frequency, order of the compensator, and selected locations of the poles and zeros for the five τ_m values can be seen in Table I. As can be seen, it was necessary to decrease the crossover frequency to the

Table I
Time Delay Compensator Parameter Values

Parameter τ_a	Assumed ω_c	Zeros	Poles
0.2	4.76	9.2 9.3	92.0 93.0
0.4	2.3	4.5 4.6	45.0 46.0
0.6	2.1	2.8 2.9	28.0 29.0
0.8	1.7	2.0 2.1	20.0 21.0
1.0	1.5	1.6 1.7	16.0 17.0

minimum acceptable as the value of τ_a increased, to keep π larger than ω_0 .

With the entire compensation system designed, except for the amplifier gains, the next step was to draw the Root locus plots for each system so that the sensitivity, or open loop gain, could be selected. The Root locus plots for the five systems are drawn in Figures B.11 through B.15 in Appendix B. From these, the sensitivity that caused the position of the dominant root to be at -1 was selected. This sensitivity, K , is actually the product $K_A K_{TPC}$ (0.004304). Using this sensitivity, a closed loop Bode plot of the CCL was drawn. This was compared to the Bode plot of a transfer function equal to $T_{I,2} + 1 / T_{I,1} + 1$ to determine the amount of lead and lag that the plot would have to generate to compensate for the system. Finally, the total system was checked for stability by adding the frequency response

curves of the pilot model, the CCL, and the integrator. In two cases, for τ_a equal to 0.8 and 1.0, it was necessary to lower the sensitivity of the CCL to make the total system stable. Since each of the values of engine time delay required a different design analysis, they will be discussed separately.

The CCL closed loop Bode plot for τ_a equal to 0.2 second is seen in Fig. 13. The gain used was 1018.29 because that gain caused the dominant root to lie at -1. The log magnitude plot closely resembles

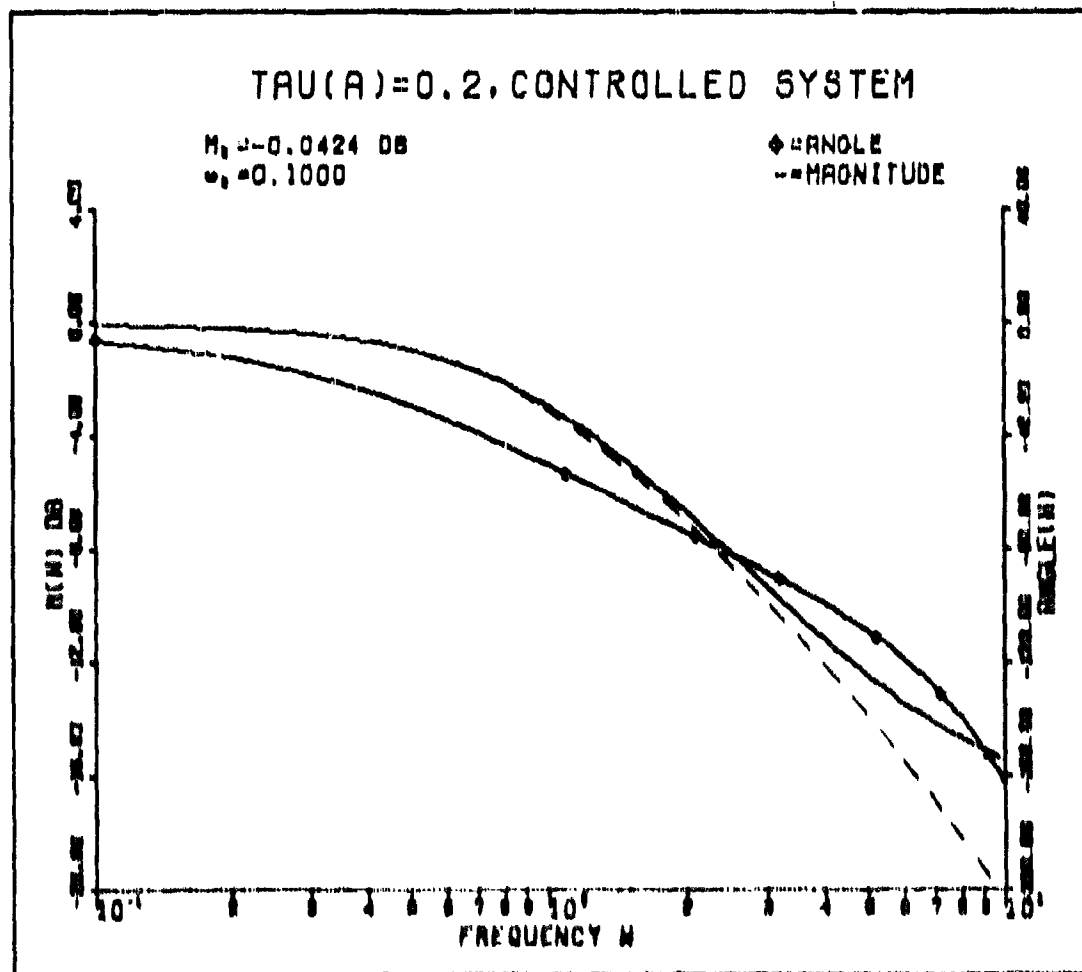


Fig. 13 Closed Loop Bode Plot of CCL, $\tau_a = 0.2$ second
 (broken line is equivalent transfer function log magnitude)

a plot of the transfer function $1/s+1$, which is drawn as a broken line in Fig. 13. The two log magnitude curves are similar up to $\omega = 4.0$. Since the pilot attempts to cancel the dynamics of the CCL in the crossover region, his transfer function is

$$Y_P = K_P e^{-sT_0} (s+1) \quad (34)$$

which is exactly as desired. The pilot gain (K_P) is the gain needed to raise the total system open loop log magnitude curve so that it crosses the zero db line at the crossover frequency. The crossover frequency was found from the condition for neutral stability with zero input. At the crossover frequency of $\omega = 3.6$, the pilot's phase angle (assuming the zero input pilot time-delay was 0.33 second) was 5° , the CCL phase angle was -95° , and the integrator phase angle was -90° . The pilot's gain was not equal to the crossover frequency in this and the following cases.

The CCL closed loop Bode plot for $T_M = 0.6$ second is seen in Fig. 14. The gain used was 1065.05 and this caused the dominant root to lie at -1 . The log magnitude plot alone resembles a plot of the transfer function $0.33s+1/s+1$, which is drawn as a broken line in Fig. 14. The two log magnitude curves are similar up to $\omega = 4.0$. The pilot's transfer function in this case is

$$Y_P = K_P e^{-sT_0} \frac{s+1}{0.33s+1} \quad (35)$$

The pilot now has to generate a lag of 0.33 second in addition to a lead of one second. The crossover frequency was found to be 3.25 radians per second. At this frequency, the pilot's phase angle was -15° , the CCL phase angle was -75° , and the integrator phase angle was -90° .

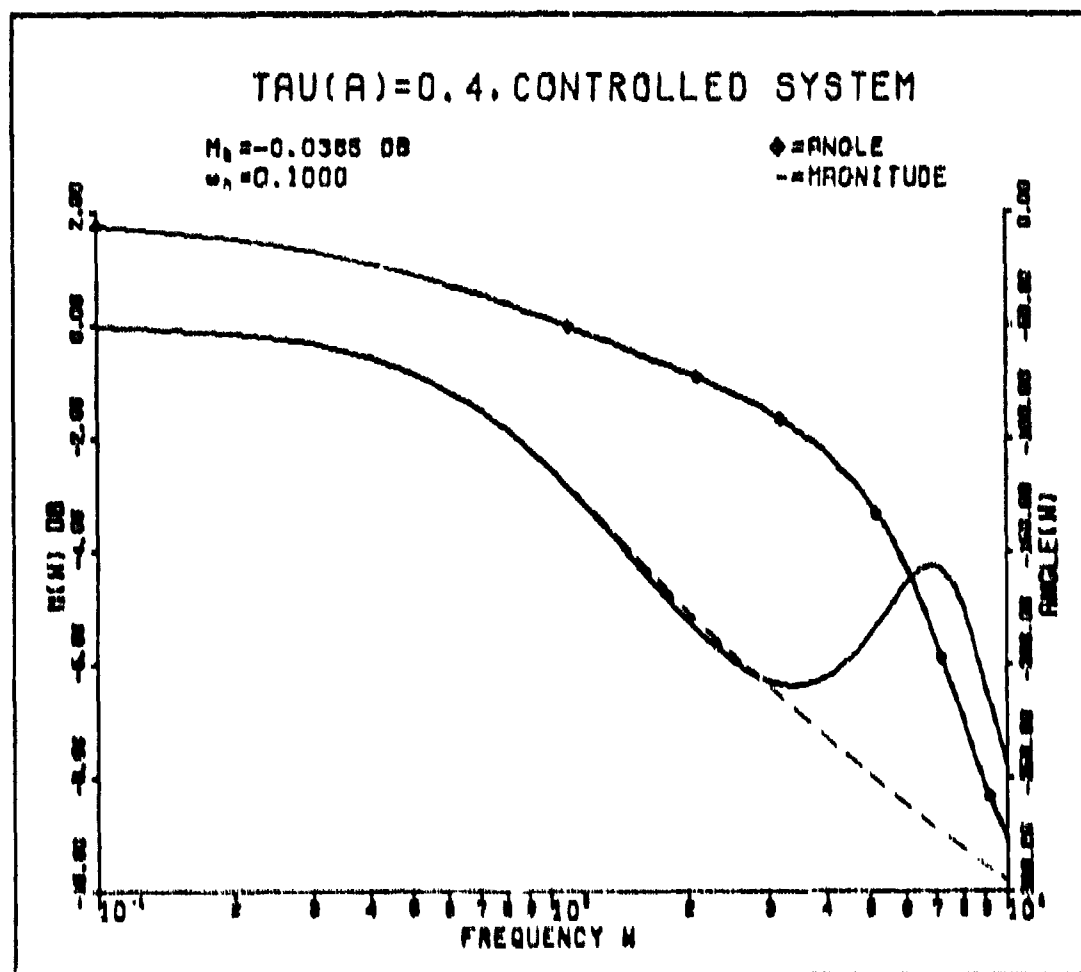


Fig. 14 Closed Loop Bode Plot of CCL, $\tau_n = 0.4$ Second
 (Broken line is equivalent transfer function
 log magnitude)

The CCL closed loop Bode plot for $\tau_n = 0.6$ second is seen in Fig. 15. The gain used in this case was 1226.62, causing the dominant root to lie at -1. This log magnitude plot resembles a plot of the transfer function $0.67s+1/s+1$, which is drawn as a broken line in Fig. 15, up to $\omega = 2.1$. The pilot's transfer function for this case is

$$Y_p = K_p e^{-s\tau_n} \frac{s+1}{0.67s+1} \quad (36)$$

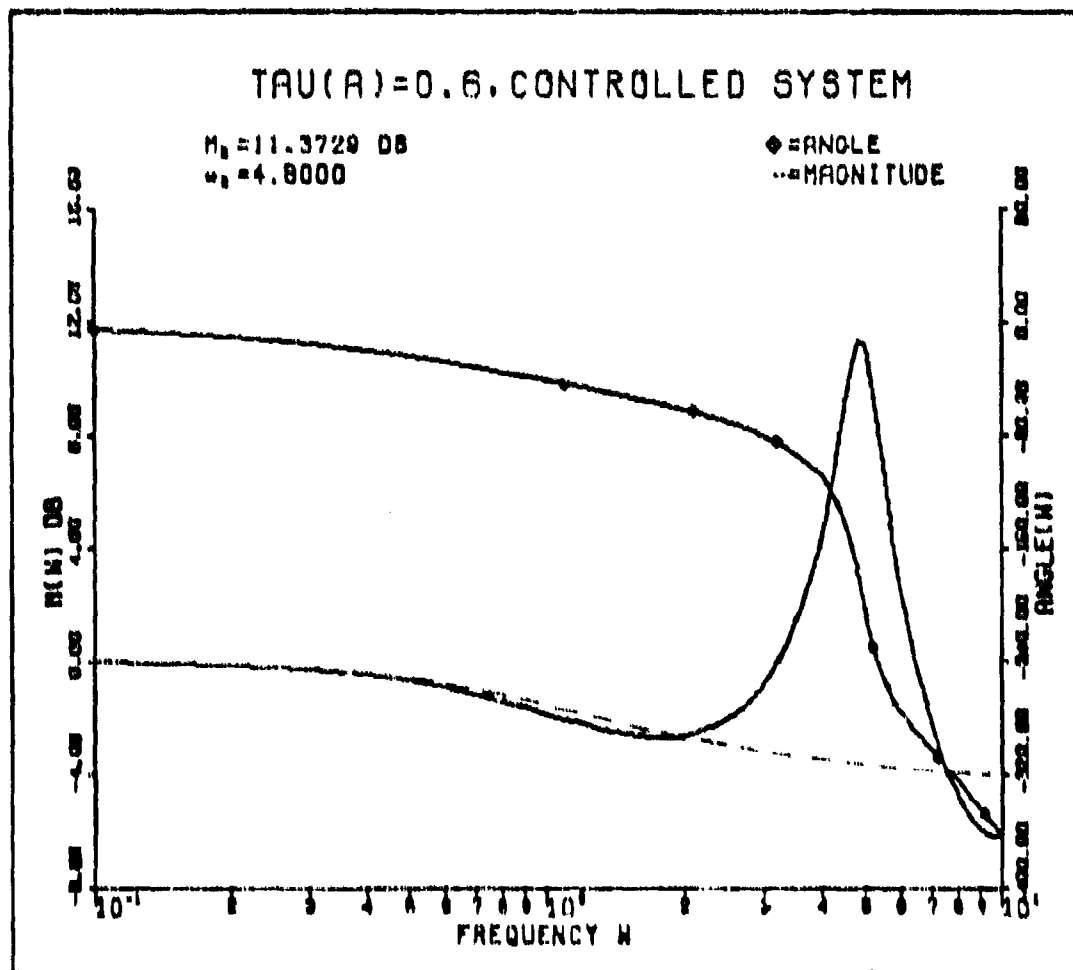


Fig. 15 Closed Loop Bode Plot of CCL, $\tau_A = 0.6$ Second
 (Broken line is equivalent transfer function
 log magnitude)

The pilot now has to generate a lead of one second and a lag of 0.67 second. The crossover frequency and pilot gain were found to be 2.0 radians per second. At this frequency, the pilot's phase angle was -28° , the CCL phase angle was -62° , and the integrator phase angle was -90° .

The CCL closed loop Bode plot for $\tau_A = 0.8$ second is seen in Fig. 16. The gain used was 735.44 and was the gain required to place

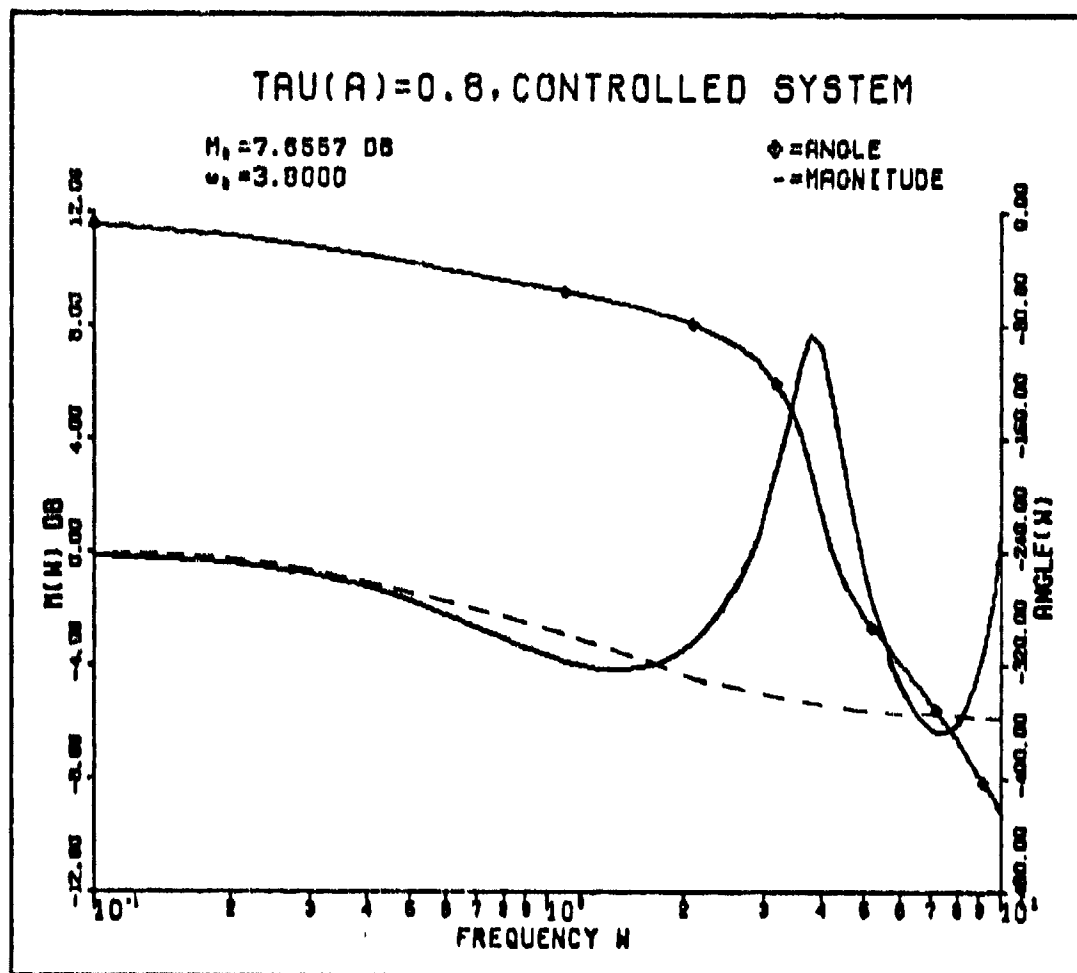


Fig. 16 Closed Loop Bode Plot of CCL, $\tau_A = 0.8$ Second
 (Broken line is equivalent transfer function
 log magnitude)

the dominant root at -0.6 . A higher value of gain caused the system to be unstable by giving it a negative gain margin, so it was decided to require the pilot to generate a little more lead. With the gain value used, the gain margin was 1.13 db at 1.9 radians per second, with the pilot time-delay set at 0.2 second as explained in Chapter VI. The log magnitude plot closely resembles a plot of the transfer function $s+1/1.67s+1$, which is drawn as a broken line in the figure, up to $\omega = 1.8$. The pilot's transfer function is now

$$Y_P = K_P e^{-sT_e} \frac{1.67s+1}{s+1} \quad (37)$$

The increase in the pilot lead over the three previous cases was undesirable, but should not seriously degrade the pilot rating, and is still a significant improvement over the uncompensated system. The crossover frequency was found to be 1.7 radians per second, where the pilot's phase angle was -20° , the CCL phase angle was -70° , and the integrator phase angle was -90° .

The CCL closed loop Bode plot for $\tau_a = 1.0$ second is seen in Fig. 17. The gain used was 476.74, because higher values of gain caused instability in the system by causing the gain margin to be negative. With the value of gain used the gain margin was 0.30 db at $\omega = 1.7$ radians per second and the dominant root was positioned at -0.5 . The log magnitude plot closely resembles a plot of the transfer function $0.9s+1/2s+1$, which is drawn as a broken line in Fig. 17, up to $\omega = 1.5$. The pilot's transfer function is now

$$Y_P = K_P e^{-sT_e} \frac{2s+1}{0.9s+1} \quad (38)$$

The pilot is required to generate a lead of two seconds, which is undesirable, but the lead cannot be reduced if the system is to remain stable. The amount of lead required should not be a problem to the pilot and is still an improvement over the uncompensated system. The crossover frequency was found to be 1.5 radians per second, where the pilot's phase angle was -10° , the CCL phase angle was -80° , and the integrator phase angle was -90° .

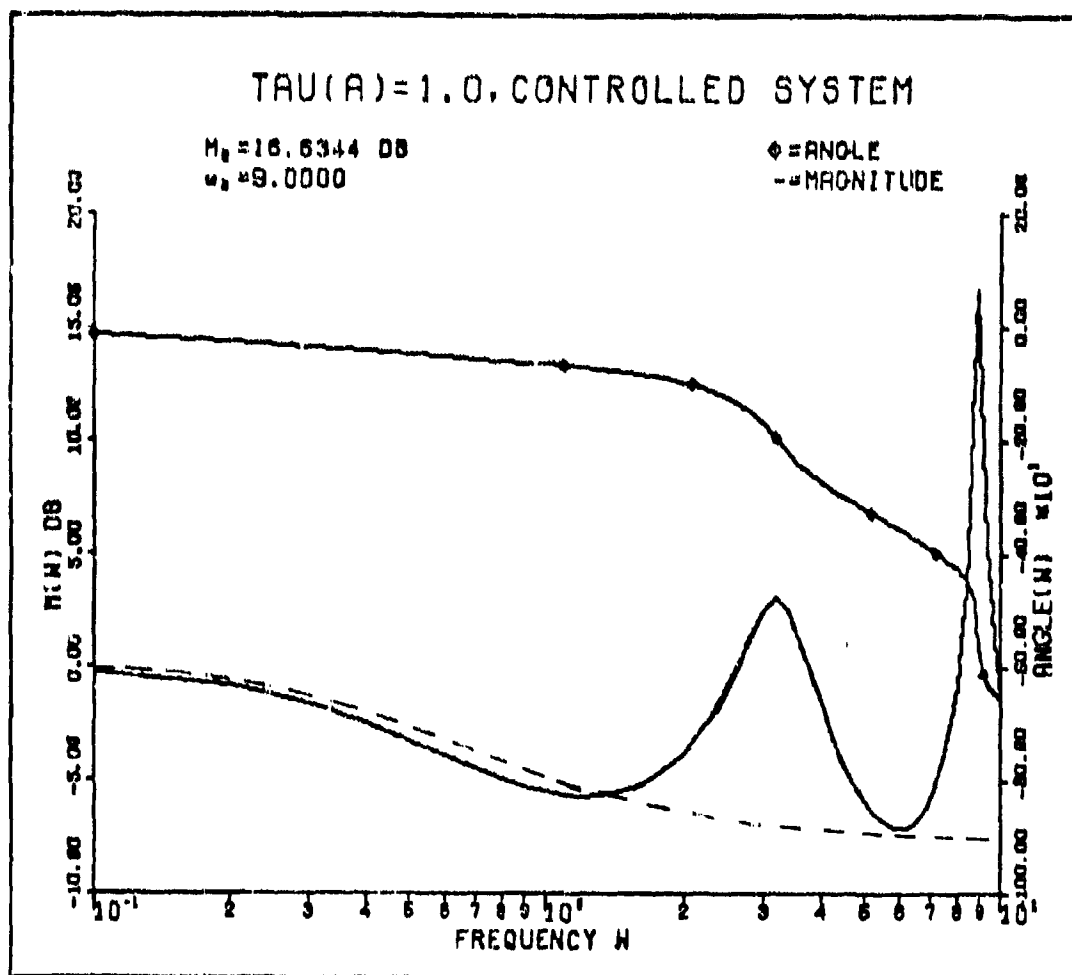


Fig. 17 Closed Loop Bode Plot of CCL, $\tau_a = 1.0$ Second
 (Broken line is equivalent transfer function
 log magnitude)

A summary of the data discussed in all five cases is presented in Table II. As the engine time-delay was increased, the system performance could not be kept as high as desirable, but it was still a great improvement over the system without the compensator added. The improvement was mainly because the pilot had only to generate a small amount of lead rather than an acceleration form of dynamics.

Table II

Required Pilot Parameters for the Compensated Systems

Pilot Parameter τ_a	K_P	T_L	T_I
0.2	3.60	1.00	0.00
0.4	2.25	1.00	0.33
0.6	2.00	1.00	0.67
0.8	1.70	1.67	1.00
1.0	1.50	2.00	0.90

VI. Simulation and Results

Simulation

The simulation was accomplished by using the CDC CYBER/74 digital computer at the Air Force Institute of Technology, Wright-Patterson AFB, Ohio, and the MIMIC programming language written by Mr. F. J. Sansom and Mr. H. F. Peterson at Wright-Patterson AFB, Ohio. A revision to the original program was made by Prof. C. W. Richard of the Mathematics Department at AFIT, which enables one to obtain plots of the computed data. MIMIC is a programming technique by which analog type simulations can be performed on the digital computer, using a fourth order Runge-Kutta integration routine. The step size can be left to vary so that the local relative error is kept below 5×10^{-6} , or it can be bounded by DTMAX and DTMIN. Each MIMIC program allows the use of up to five user written subroutines, written in Fortran language. This feature was very useful as the time delay function in the MIMIC language used an excessive amount of central processor time, which caused the program to run for about eight times the amount of time that the system would be actually operating. A time delay subroutine was written in Fortran language, specifically for this simulation, where the integration step size was fixed, and the program ran for about one third of the actual system operation time. The result was a considerable savings in time and money.

Two separate MIMIC programs were written, one for the uncompensated system, and one for the compensated system. These programs can be seen in Appendix C and an explanation of the programming technique can be seen in Ref. 3.

Wind Gust Simulation. The representation for the wind was previously described as a band limited white noise. This noise was simulated in the program by passing a train of pulses, whose width was 0.2 second, through a first order filter. The amplitude of the pulses was a gaussian distributed random variable, obtained from the normal random number generator in the MIMIC program. This generator was called every 0.2 second, causing the pulse amplitude to change at 0.2 second intervals. The method of representing a band limited white noise by a pulse train is described in Appendix D. The integration step size was set at 0.01 second as a compromise between computation time and accuracy and, therefore, Shannon's Sampling Theorem (Ref. 9) was satisfied. This theorem states that the sampling frequency should be at least twice the pulse frequency in an information system. The pulses were passed through a first order filter to make certain that the power spectral density (PSD) had a bandwidth of one radian per second. If $S(in)$ is the PSD of the input to the filter and $S(out)$ is the output PSD, then according to Ref. 17,

$$S(out) = |H(j\omega)|^2 S(in) \quad (39)$$

where $H(j\omega)$ is the system transfer function. A filter with the transfer function $1.54/(j\omega+1.54)$ attenuates the PSD by three db at $\omega = 1.0$, so the bandwidth of the filter is one radian per second.

Pilot Simulation. The pilot model used was the simple Crossover Model with no low frequency phase data terms or neuromuscular terms, as explained in Chapter VII. The crossover frequency and the resulting

pilot gain were calculated from the neutral stability criterion, using the zero input pilot time delay. According to the literature, the phase margin that occurs in the use of the Crossover Model results from a decrease in the pilot time-delay. The only analytical means found to reduce this was by equation (22), where the time-delay decrease was due to the forcing function bandwidth. In this case, the bandwidth of the disturbance was too small (about 0.2 radian per second) to have any effect on the pilot time-delay. However, the delay could also be reduced by such intangibles as motivation, training, and skill. For purposes of the simulation, it was assumed that, for the uncompensated system, the pilot time-delay would be reduced from 0.8 second to 0.6 second, and for the compensated system, from 0.33 second to 0.2 second. These values are comparable to values of time-delay found by experiment in References 13 and 16.

Error Analysis. The operation of the system was analyzed by computing the mean square error as defined in Ref. 20. If e is the difference between the output and the input in a control system, the mean square error can be defined as

$$\overline{e^2} = \frac{1}{T} \int_0^T e^2 dt \quad (40)$$

where T is the elapsed time. This computation was performed as part of the MIMIC program. Ten runs were made for each value of engine time-delay, each run having a different random noise input, and the runs were made for both the uncompensated and the compensated systems. The average of the mean square error was calculated for each set of ten runs so that a wide statistical spread would be obtained.

Simulation Results

Two main results were obtained from the simulation. Plots were drawn of the input heading disturbance and output heading versus time for both the uncompensated and the compensated system, at each value of engine time-delay. On each of the ten plots, shown in Figures 18 through 27, the input and output angles are scaled on the y-axis and time is scaled on the x-axis. The corresponding uncompensated and compensated system response plots for each value of engine time-delay show that the pilot model can follow the input disturbance more closely with the compensator added. An explanation of the evident oscillation of the output is presented in Chapter VII. The plots were all drawn for the same random input heading disturbance.

The second result obtained was the collection and averaging of the mean square error data. Ten runs, each with a different random input, were made for each system at each value of engine time-delay. The mean square error at 100 seconds was averaged over the ten runs for each case so that the uncompensated and compensated systems could be compared. The tabulation of the average mean square errors of the 100 second runs is seen in Table III. In all cases, the average mean square error for the compensated system was decreased by about 70% of the uncompensated system value.

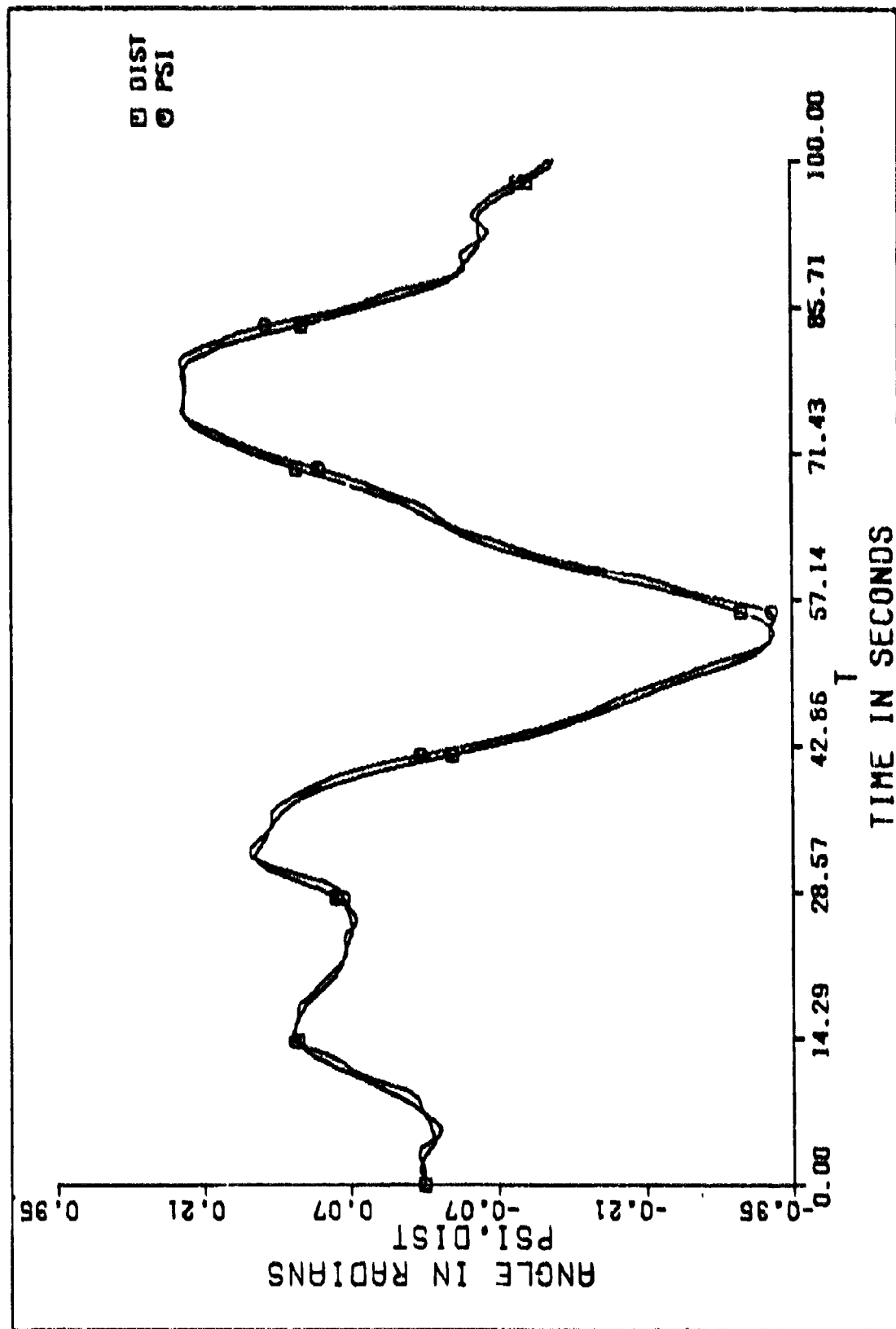


Fig. 18 Input and Output of Uncompensated System, $r_a = 0.2$ Second (DIST = Disturbance)

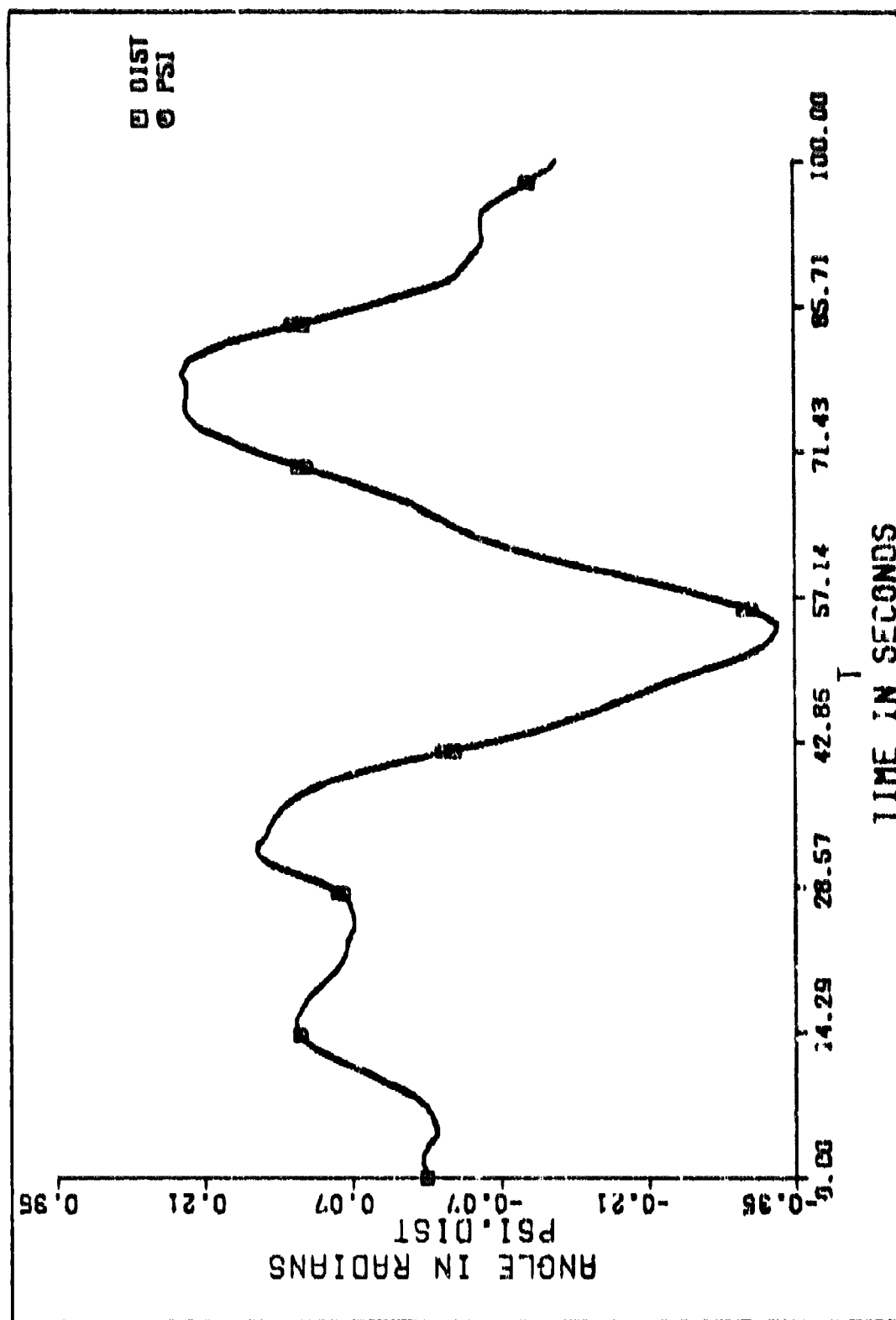


Fig. 19 Input and Output of Compensated System, $\tau_c = 0.2$ Second (DIST = Disturbance)

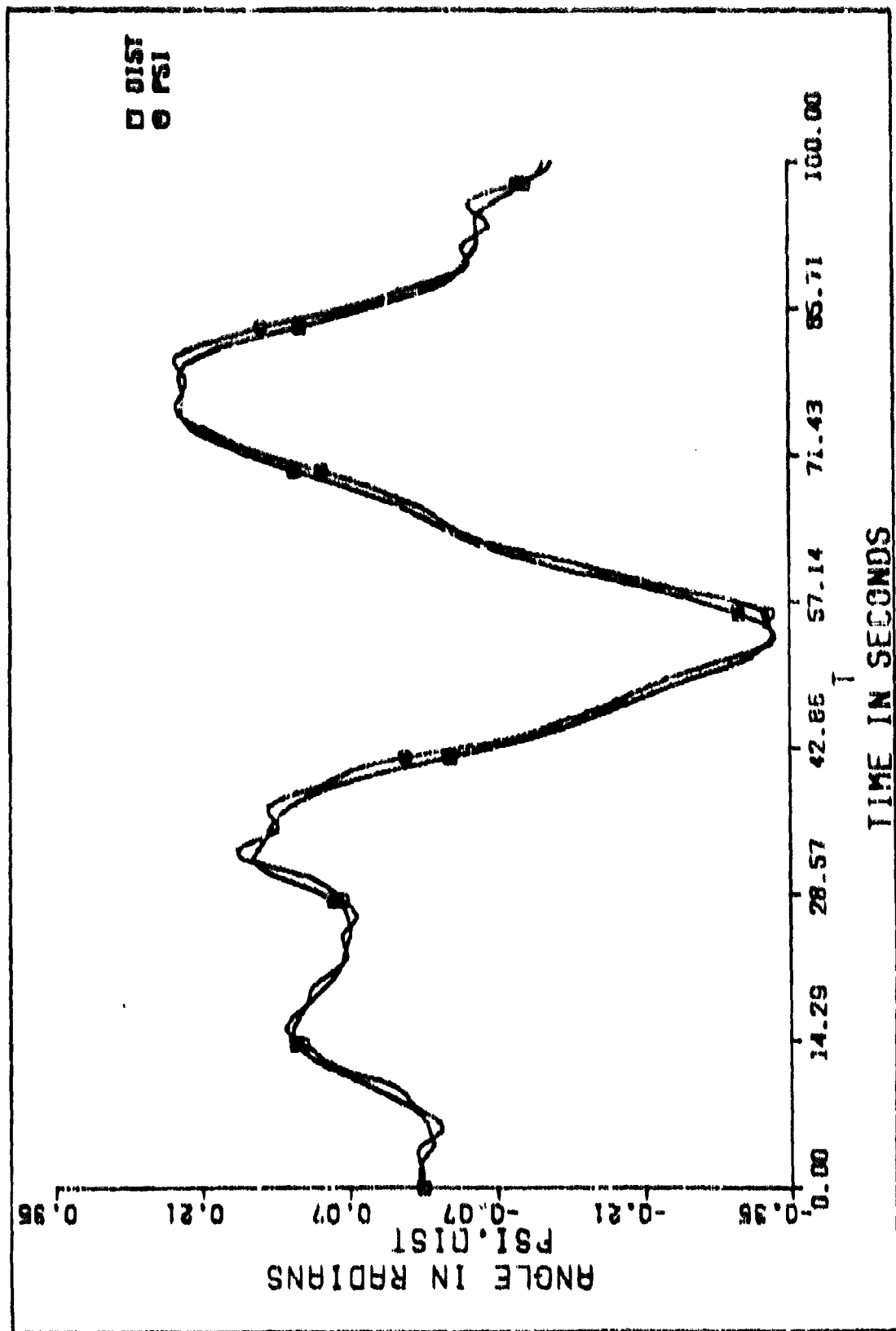


Fig. 20 Input and Output of Uncompensated System, $\tau_a = 0.4$ Second (DIST = Distance)

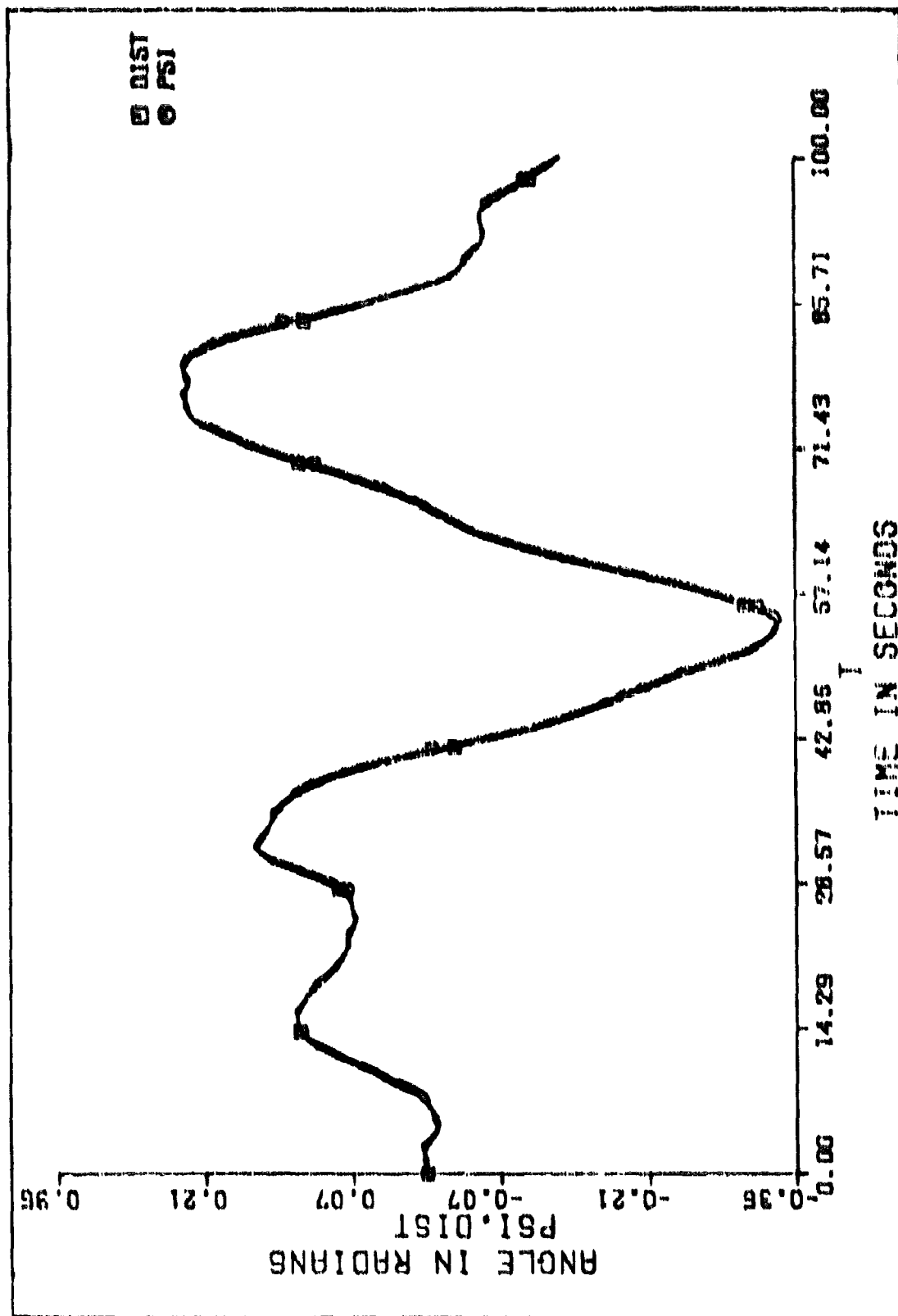


Fig. 21 Input and Output of Compensated System, $\tau_d = 0.4$ Second (DIST = Disturbance)

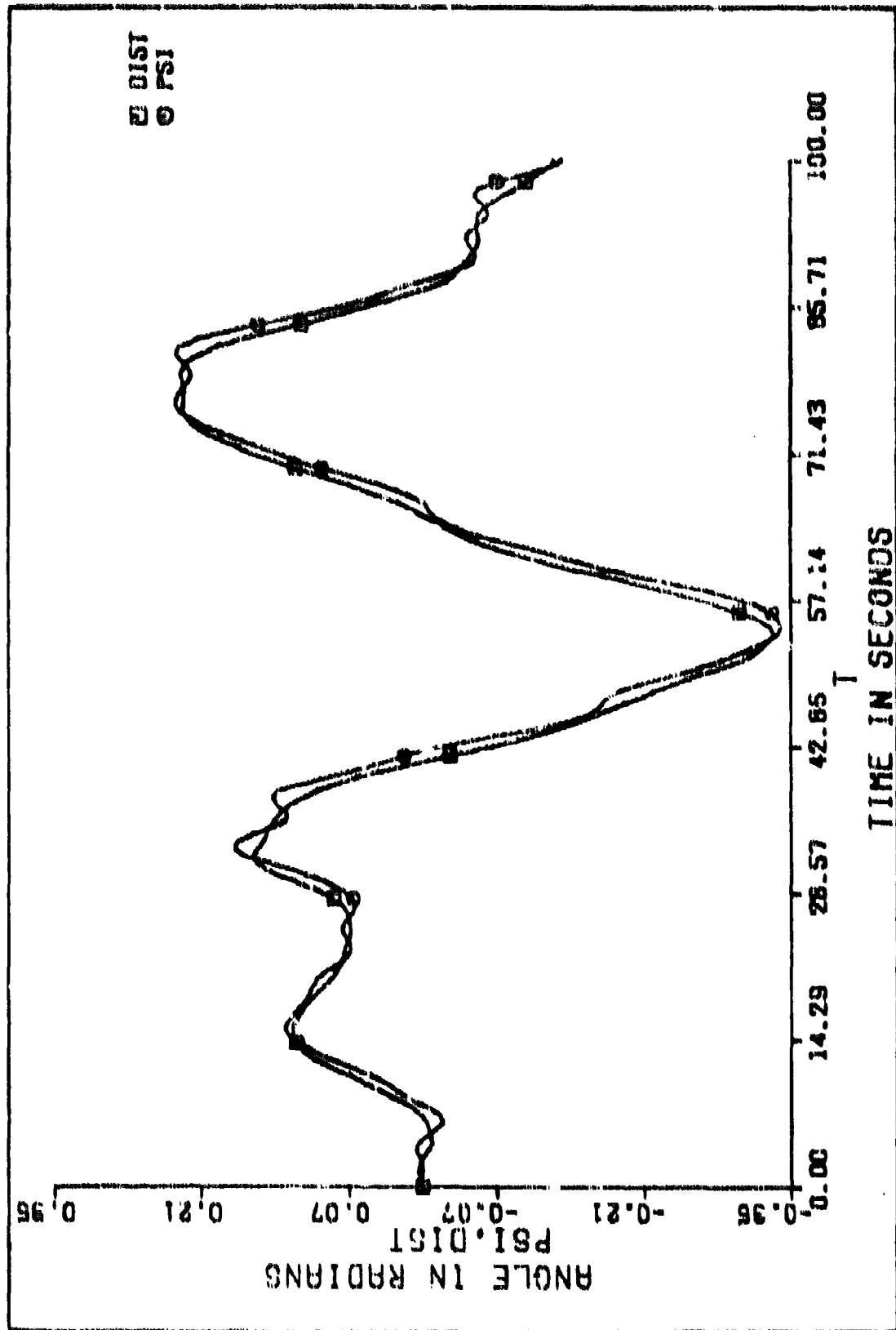


Fig. 22 Input and Output of Uncompensated System, $\tau_d = 0.6$ Second (DIST = Disturbance)

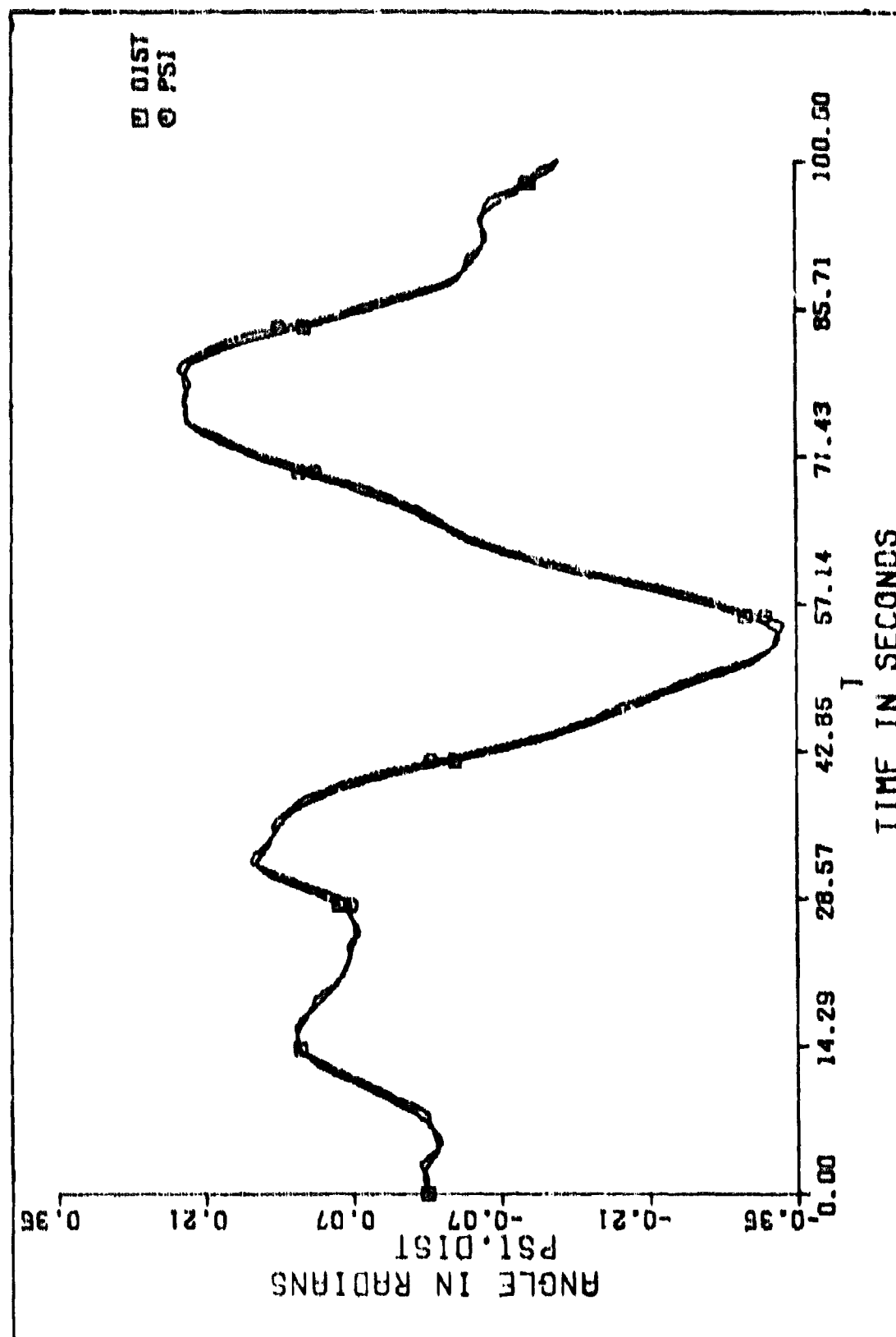


Fig. 23 Input and Output of Compensated System, $\tau_a = 0.6$ Second (DIST = Disturbance)

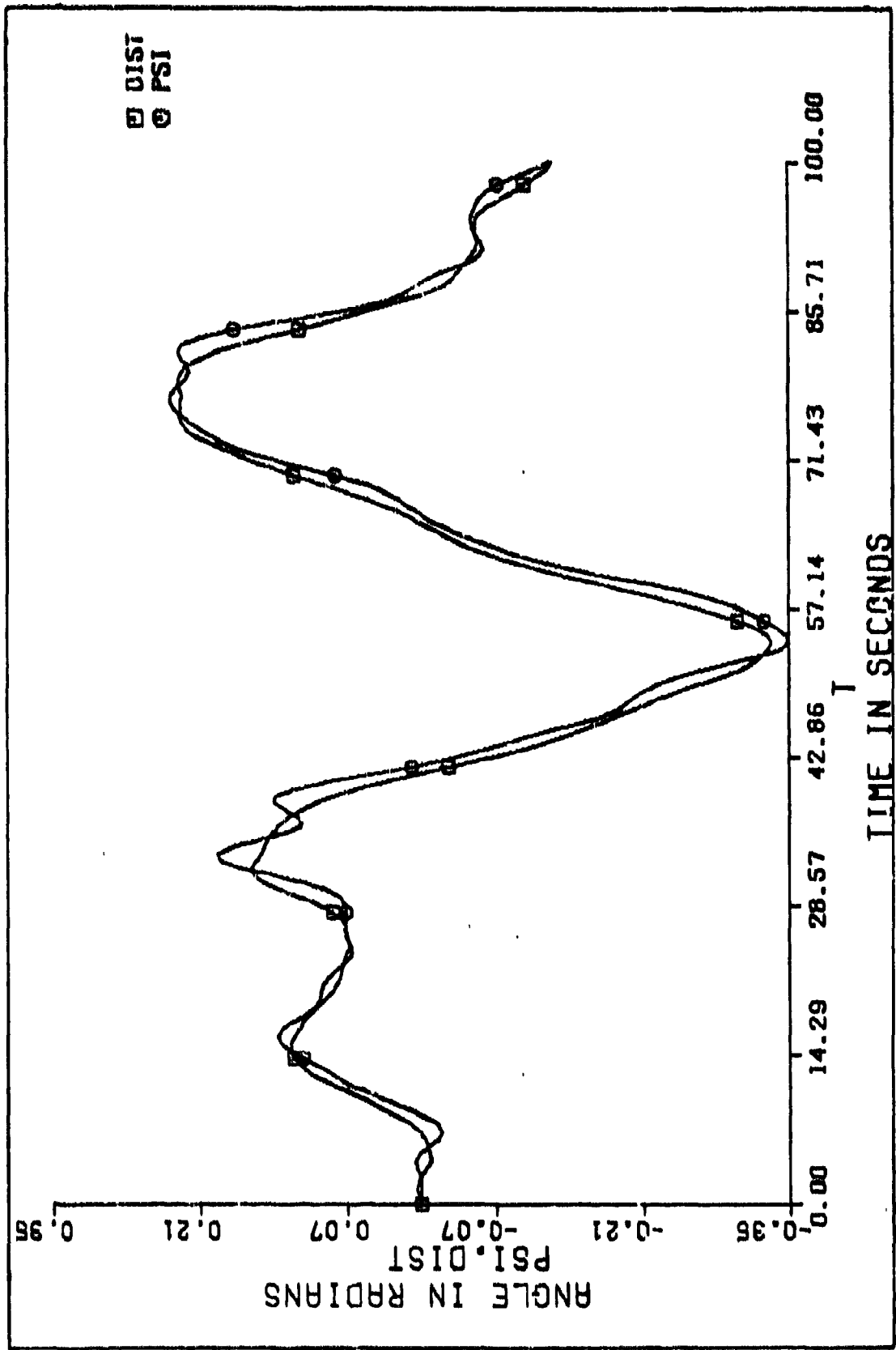


Fig. 24 Input and Output of Uncompensated System, $\tau_d = 0.8$ Second (DIST = Disturbance)

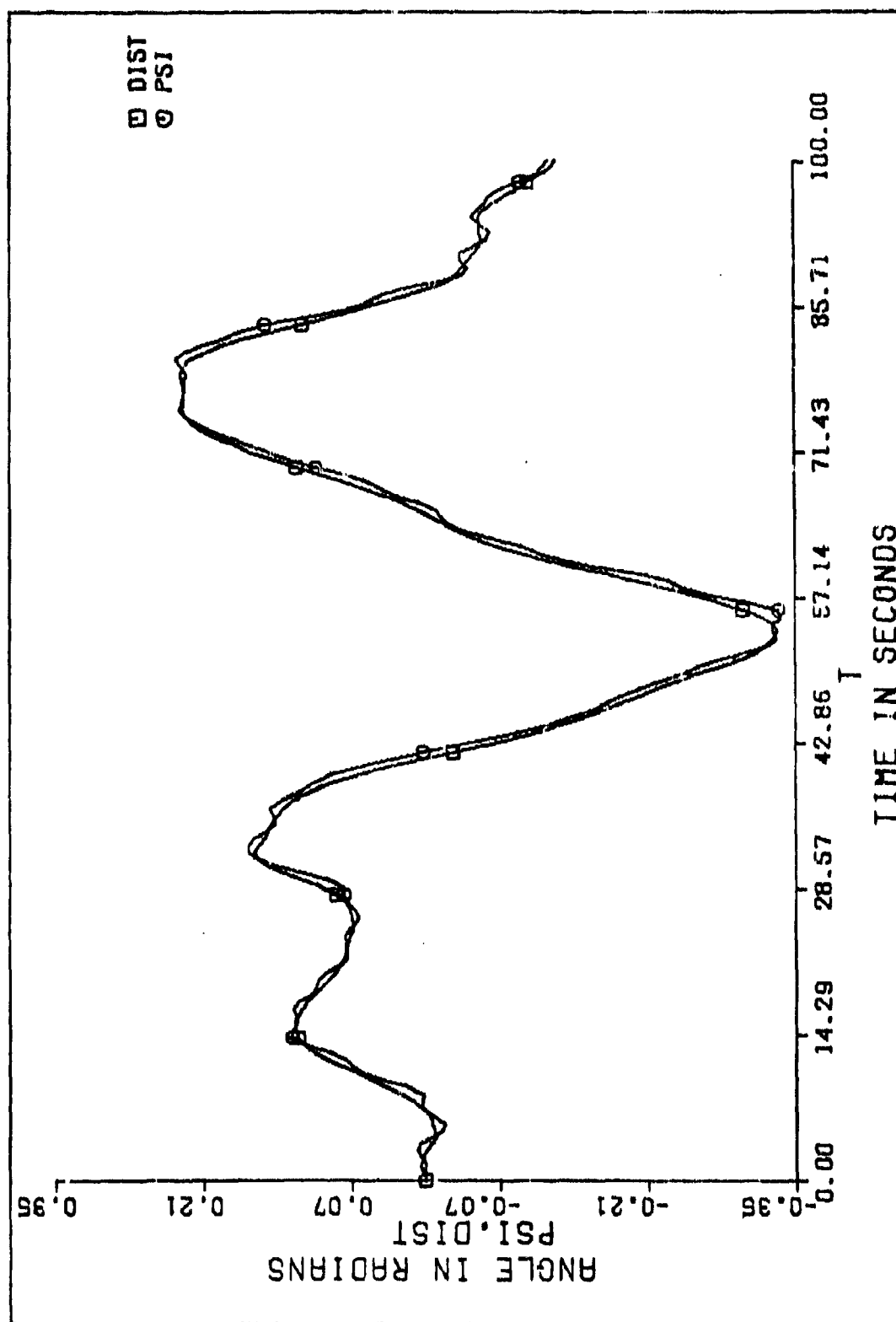


Fig. 25 Input and Output of Compensated System, $\tau_a = 0.8$ Second (DIST = Disturbance)

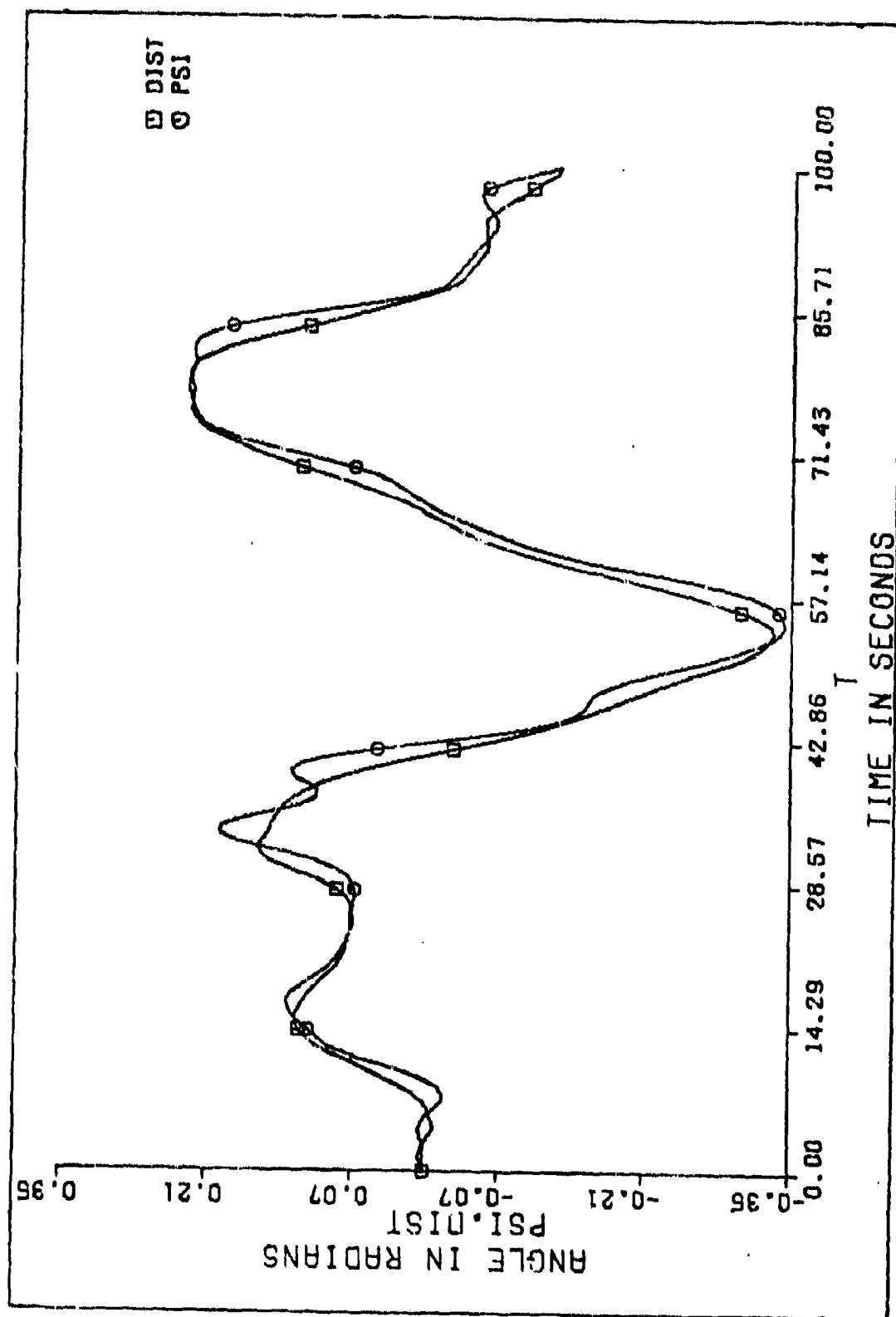


Fig. 26 Input and Output of Uncompensated System, $\tau_a = 1.0$ Second (DIST = Disturbance)

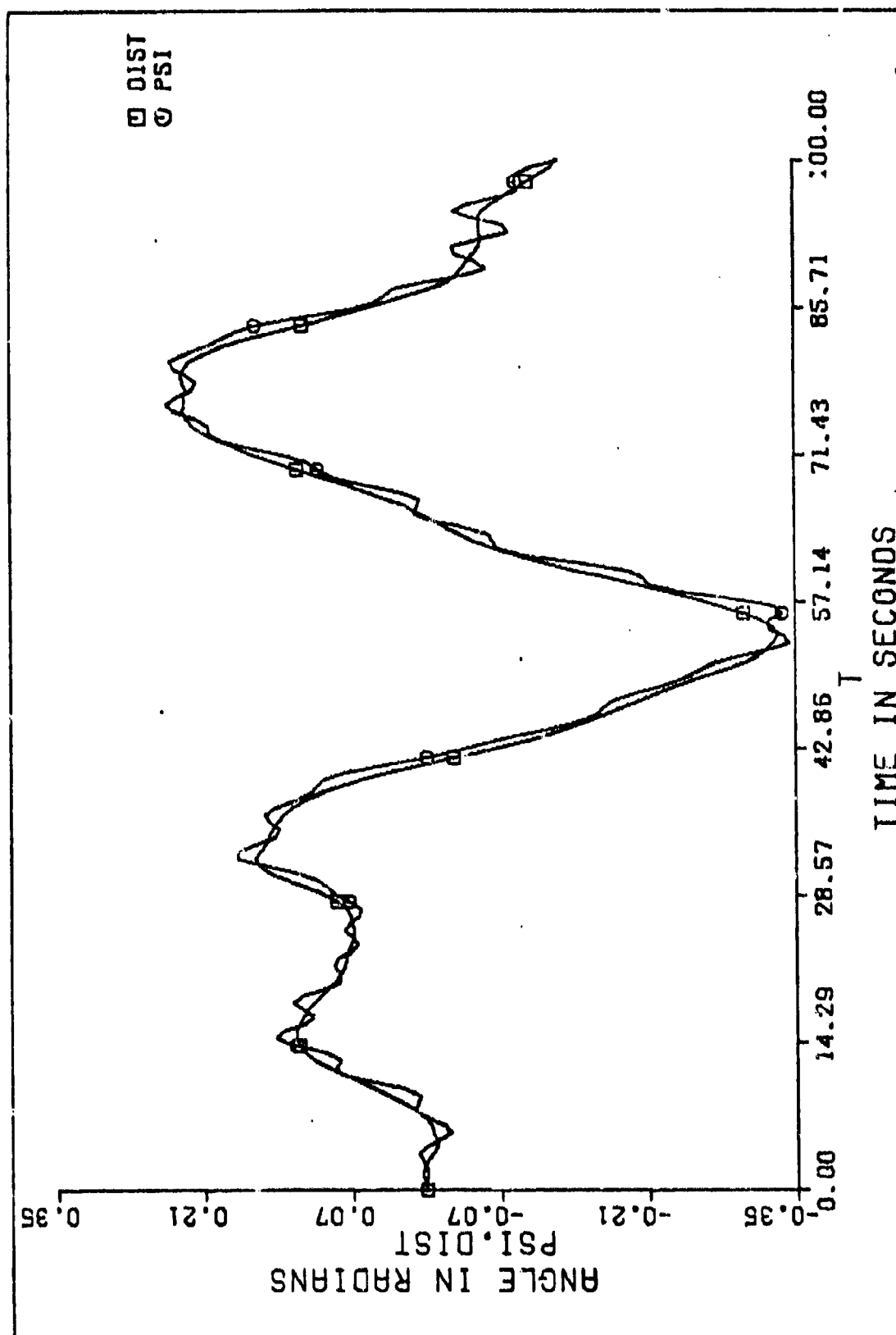


Fig. 27 Input and Output of Compensated System, $\tau_a = 1.0$ Second (DIST = Disturbance)

Table III
Average Mean Square Error Results

(All values $\times 10^{-5}$ radians²)

τ_a \ System	Uncompensated	Compensated
0.2	15.8602	2.6729
0.4	24.6697	7.3306
0.6	36.8200	9.8878
0.8	55.3387	15.4491
1.0	78.2099	27.6443

VII. Conclusions and Recommendations

Conclusions

Control Systems have been designed to improve the heading response of the taxiing ACLS aircraft to pilot input of differential thrust for five different values of engine time-delay. These designs were based on the Crossover Model for the pilot and were tested by using the same model, so they are dependent on the model's accuracy. However, the Crossover Model has been in use for almost ten years and nothing was found in the literature to dispute it.

In the graphs showing the simulation input and output versus time, some high frequency oscillation is evident. This oscillation, it is believed, would be eliminated by a human pilot due to the high frequency filtering action of his neuromuscular reactions. This filtering is modeled by the neuromuscular terms in equation (19), which were not used in this project. The use of the neuromuscular terms requires an in depth study of physiology, and that was considered beyond the scope of this thesis. However, according to Ref. 13, the neuromuscular frequencies are usually in the region of from 10 to 15 radians per second.

The average mean square error values are all reduced by about 70% with the addition of the compensator. The average mean square error for the compensated system with an engine time-delay of 0.8 second is about the same as the error for the uncompensated system with a time-delay of 0.2 second. Similarly, the error for the compensated system with a delay of one second compares with that of the

uncompensated system with a delay of 0.4 second. Whether the compensated system mean square errors are small enough can only be determined by experiments with human pilots.

Even without the improvement in average mean square error, subjectively speaking, a great improvement has been obtained. With the uncompensated system, the pilot had to generate an acceleration term in the crossover region in order to satisfy the Crossover Model. That is, the pilot model had to become

$$Y_p = K_p e^{-sT} s(s+1.111) \quad (41)$$

which is very difficult for the human pilot and leads to a high pilot opinion rating, which is unfavorable, and a large pilot time-delay. The compensator allowed the pilot to adopt the form of a simple first order lead with a time constant of from one to two seconds, depending on the engine time-delay. This results in a low pilot opinion rating, which is an indication of good handling qualities, and a small pilot time-delay (about 0.2 second).

Recommendations

An experiment using the analog computer and a visual display should be set up so that the control design can be tested with human pilots in the loop. This would check the accuracy of the pilot model used and would reveal what improvement is possible with the control systems that have been designed.

When attempting to model the aircraft engines, a need was found for information on dynamic modeling of aircraft engines of various

types. An excellent subject for a research topic would be the dynamic modeling of both turboprop and turbojet engines.

The possibility exists that the ACLS will be installed on aircraft with more than two engines in the future. A study could be performed on the best method of differential thrust control for those type of aircraft. For example, it may be better to use only the two outboard engines or the two inboard engines rather than all of them.

Bibliography

1. Ashkenas, I. L. A Study of Conventional Airplane Handling Qualities Requirements, Part I Roll Handling Qualities. AFFDL-TR-65-138. Wright-Patterson Air Force Base, Ohio: Research and Technology Division, Air Force Systems Command, November 1965.
2. Blakelock, J. H. Automatic Control of Aircraft and Missiles. New York: John Wiley and Sons, Inc., 1965.
3. CDC Publication 44610400. MIMIC Digital Simulation Language (Revision E). Sunnyvale, California: Control Data Corporation, 1972.
4. Chu, Y. "Feedback Control Systems with Dead-Time Lag or Distributed Lag by Root-Locus Method." AIIE Transactions, Vol. 71, Part II: pp. 291-296 (November 1952).
5. Coles, A. V. Air Cushion Landing System CC-115 Aircraft. AFFDL-TR-72-4, Part I. Wright-Patterson Air Force Base, Ohio: Air Force Flight Dynamics Laboratory, Air Force Systems Command, May 1972.
6. Currie, D. P. "Dynamic and Static Performance of the 63 E 60-25 Propeller System for the Dehavilland DHC-5 Aircraft." Hamilton Standard Technical Memo, CD 535 (March 1972).
7. D'Azzo, J. J. and C. H. Houpis. Feedback Control System Analysis and Synthesis (2nd Ed.). New York: McGraw-Hill Book Co., 1966.
8. Franklin, James A. Turbulence and Lateral-Directional Flying Qualities. NASA-CR-1718. Washington, D. C.: National Aeronautics and Space Administration, April 1971.
9. Javid, M. and E. Brenner. Analysis, Transmission, and Filtering of Signals. New York: McGraw-Hill Book Co. Inc., 1963.
10. Kurylowich, G. "Approach, Landing, and Taxiing Simulation of an Aircraft Equipped with an ACLS." Proceedings of the AFSC 1973 Science and Engineering Symposium Held at Kirtland Air Force Base, New Mexico, Vol. I. Washington D. C.: Air Force Systems Command, October 1973.
11. Kurylowich G. "A Digital Computer Flight Simulation of an ACLS Vehicle." Proceedings of the First Conference on Air Cushion Landing Systems. Tullahoma, Tennessee: University of Tennessee Space Institute, 1973.

12. Kurylowich G. "ACLS Equations of Motion-Table-Top Simulation." Unpublished. Wright-Patterson Air Force Base, Ohio: Air Force Flight Dynamics Laboratory, January 1974.
13. McRuer, D. T., et al. Human Pilot Dynamics in Compensatory Systems. AFFDL-TR-65-15. Wright-Patterson Air Force Base, Ohio: Research and Technology Division, Air Force Systems Command, July 1965.
14. McRuer, D. T. and H. R. Jax. "A Review of Quasi-Linear Pilot Models." IEEE Transactions on Human Factors in Electronics, Vol. HFE-8: pp. 231-249 (September 1967).
15. McRuer, D. T., et al. New Approaches to Human-Pilot/Vehicle Dynamic Analysis. AFFDL-TR-67-150. Wright-Patterson Air Force Base, Ohio: Air Force Flight Dynamics Laboratory, Air Force Systems Command, February 1968.
16. McRuer, D. T. and E. S. Krendel. Mathematical Models of Human Pilot Behavior. AGARD-AG-188. London, England: North Atlantic Treaty Organization, January 1974.
17. Papoulis, A. Probability, Random Variables, and Stochastic Processes. New York: McGraw-Hill Book Co., 1965.
18. Salmon, E. P. and J. T. Gallagher. "Identification of Pilot Dynamics with and without Motion Cues." Proceedings of the Sixth Annual Conference on Manual Control. Wright-Patterson Air Force Base, Ohio: Air Force Flight Dynamics Laboratory, April 1970.
19. Stapleford, R. L., et al. Measurement of Pilot Describing Functions in Single-Controller Multiloop Tasks. NASA-CR-1238. Washington, D. C.: National Aeronautics and Space Administration, January 1969.
20. Truxal, J. G. Control System Synthesis. New York: McGraw-Hill Book Co., Inc., 1955.
21. Weir, D. H. and D. T. McRuer. Pilot Dynamics for Instrument Approach Tasks: Full Panel Multiloop and Flight Director Operations. NASA-CR-2019. Washington, D. C.: National Aeronautics and Space Administration, May 1972.
22. White, S. A. "Simplified Procedure for Classical Controller Design for Linear Closed-Loop System with Transport Delay." IEEE Transactions on Automatic Control, Vol. AC-16: pp. 374-375 (August 1971).

Appendix A

Root Locus Plots for Control Systems with Time-Lag

An essential part of the design was the use of root locus plots of control systems with time-lag. These plots can be easily obtained from the ROOTL program in the library of AFITPROGRAMS on the CDC CYBER/74 digital computer at AFIT. The principle behind plotting the root locus for control systems with time-lag was found in Ref. 4.

If $G(s)$ is the open loop transfer function for a control system, then the root locus is obtained from the characteristic equation, which is

$$G(s) = -1 \quad (A-1)$$

This complex equation may be split in two parts so that the magnitude of $G(s)$ is equal to one and the angle of $G(s)$ is equal to ± 180 degrees (for the principle plane). The root locus is a plot of the angle condition and the gain values on the locus are found from the magnitude condition.

If the open loop transfer function has a time-lag equal to T , then the characteristic equation is

$$G(s) e^{-Ts} = -1 \quad (A-2)$$

Now, the angle condition becomes

$$\angle G(s) - \omega T = \pm n\pi, \quad n=1, 2, 3, \dots \quad (A-3)$$

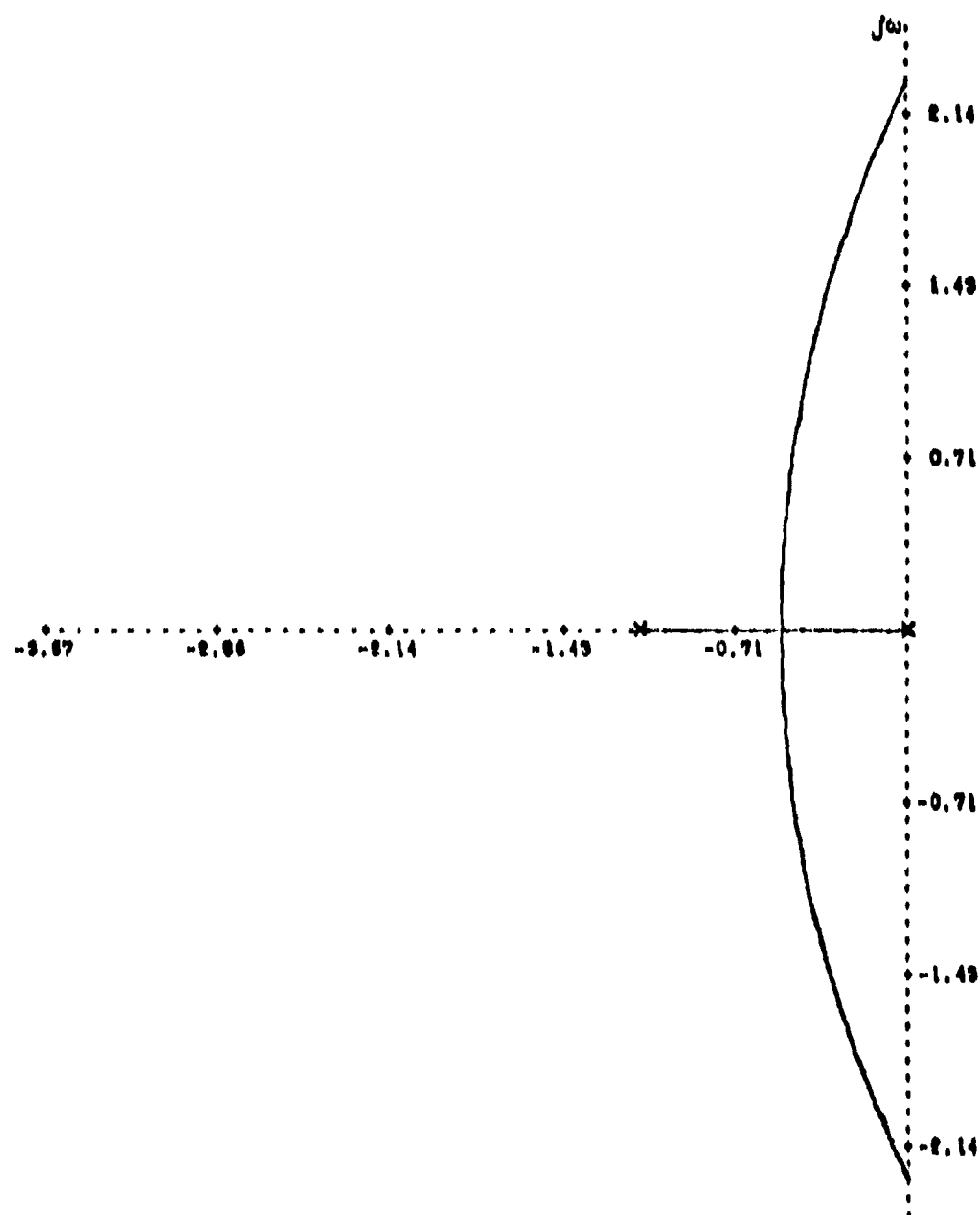
In order to draw the root locus, a family of root loci are drawn for various angles of $G(s)$ and a second family is drawn on the same s -plane of various angles of $-sT$. The loci for angles of $G(s)$ are difficult to construct, but the loci for $-sT$ angles are simply horizontal lines, crossing the $j\omega$ axis at right angles. Points are now plotted of the intersection of the two families of loci where the intersecting loci values total ± 180 degrees. When the points are all joined, the result is the root locus for the time-lag system. The gain values can be determined from the magnitude condition as in the case without time-lag. The magnitude equation becomes

$$\left| G(s) e^{-Ts} \right| = 1 \quad (A-4)$$

When a control system has a time-lag, there are an infinite number of roots of the characteristic equation. The root locus contains an infinite number of branches when the s -plane is extended to infinity. This results from the repetition of the angle loci of $-sT$ in the above construction procedure. The infinite number of branches lie in horizontal bands as seen on the root loci in Appendix B. When the time-lag increases, the bands become closer together.

Appendix B

Root Locus Plots Used for the Design

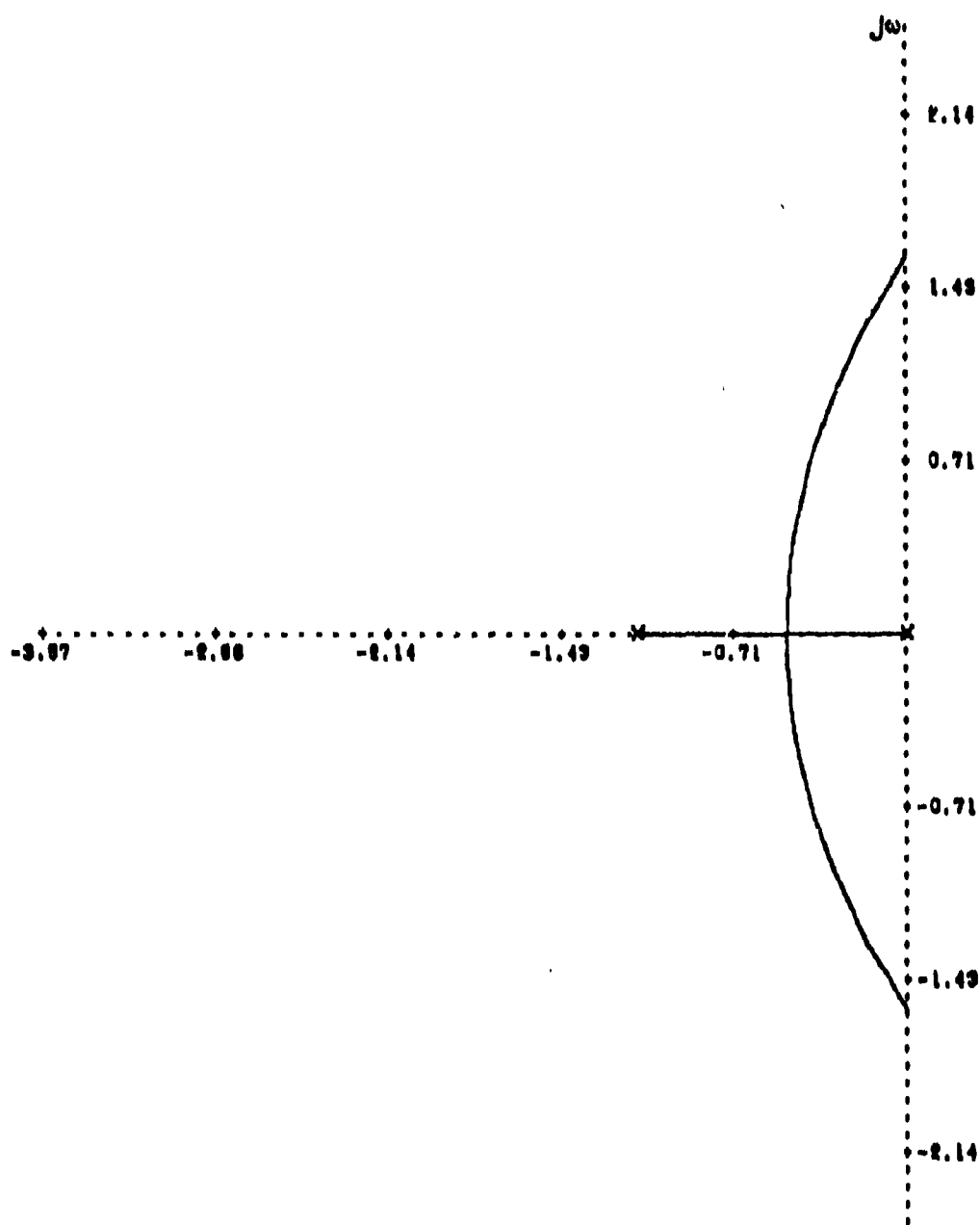
YAW RATE FEEDBACK, $\tau_u = 0.2$ 

SCALE - 0.7142 UNITS/INCH

$$G(s)H(s) = \frac{K + 0.2s}{s(s + 1.11)}$$

Fig. B.1 Root Locus Plot for Yaw Rate Feedback, $\tau_u = 0.2$ Second

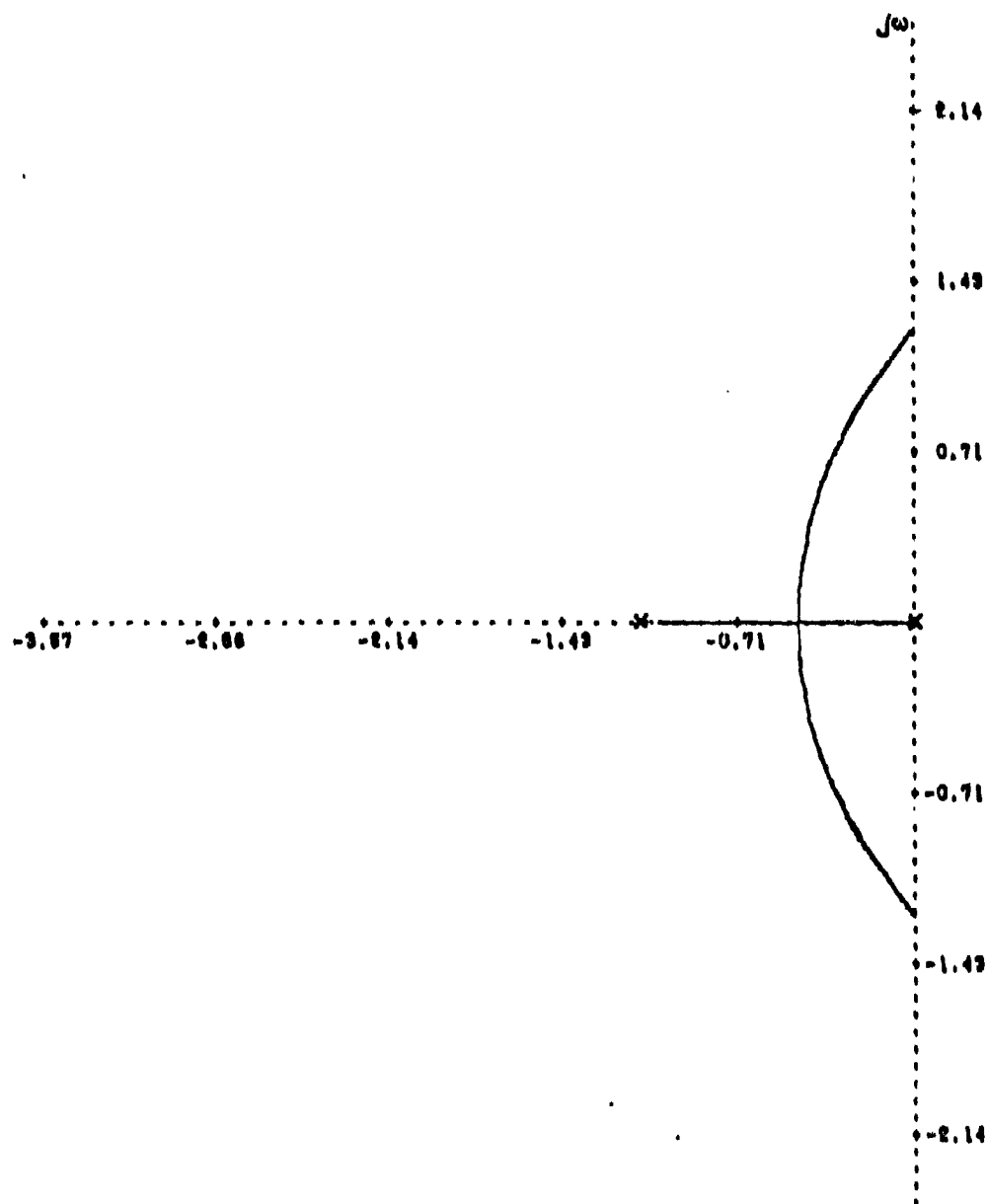
YAW RATE FEEDBACK, $\tau_u = 0.4$



SCALE - 0.7149 UNITS/INCH

$$G(s)H(s) = \frac{K + 0.48}{s(s + 1.11)}$$

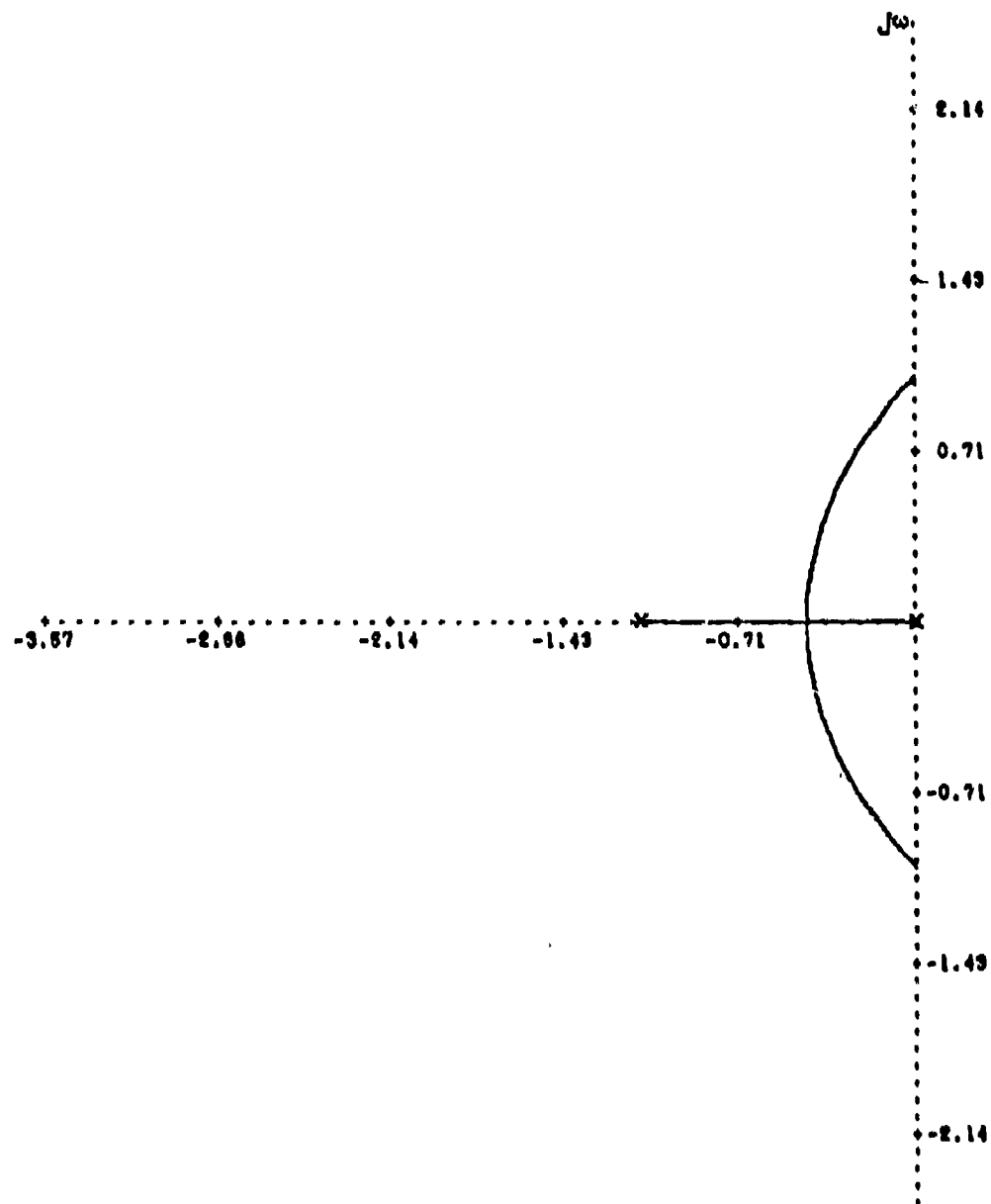
Fig. B.2 Root Locus Plot for Yaw Rate Feedback, $\tau_u = 0.4$ Second

YAW RATE FEEDBACK, $\tau_u = 0.6$ 

SCALE - 0.7143 UNITS/INCH

$$O(S)H(S) = \frac{K e^{-0.88}}{S(S+1.111)}$$

Fig. B.3 Root Locus Plot for Yaw Rate Feedback, $\tau_u = 0.6$ Second

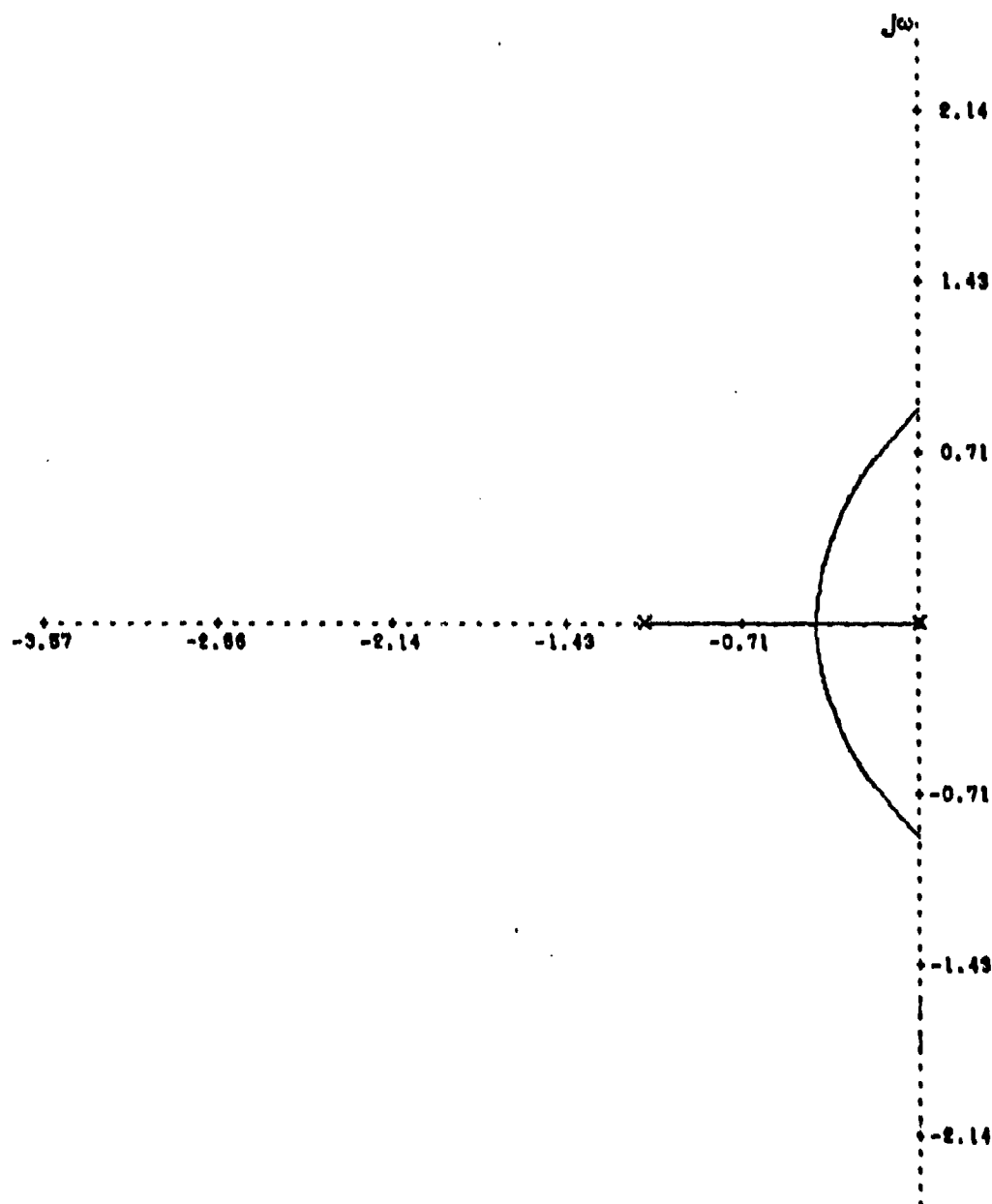
YAW RATE FEEDBACK, $\tau_u = 0.8$ 

SCALE - 0.7143 UNITS/INCH

$$G(s)H(s) = \frac{K + 0.88}{s(s + 1.111)}$$

Fig. B.4 Root Locus Plot for Yaw Rate Feedback, $\tau_u = 0.8$ Second

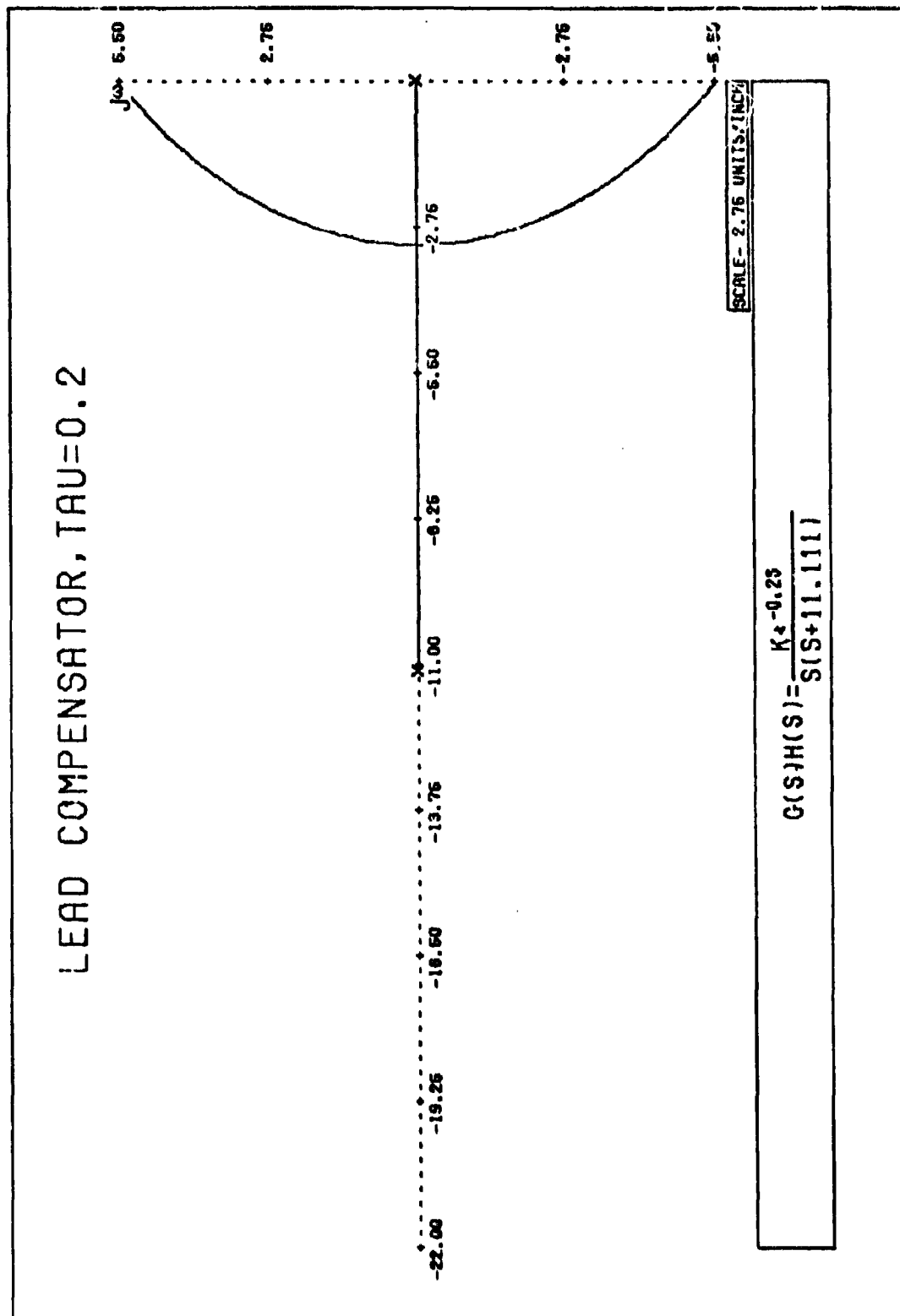
YAW RATE FEEDBACK, $\tau_u = 1.0$

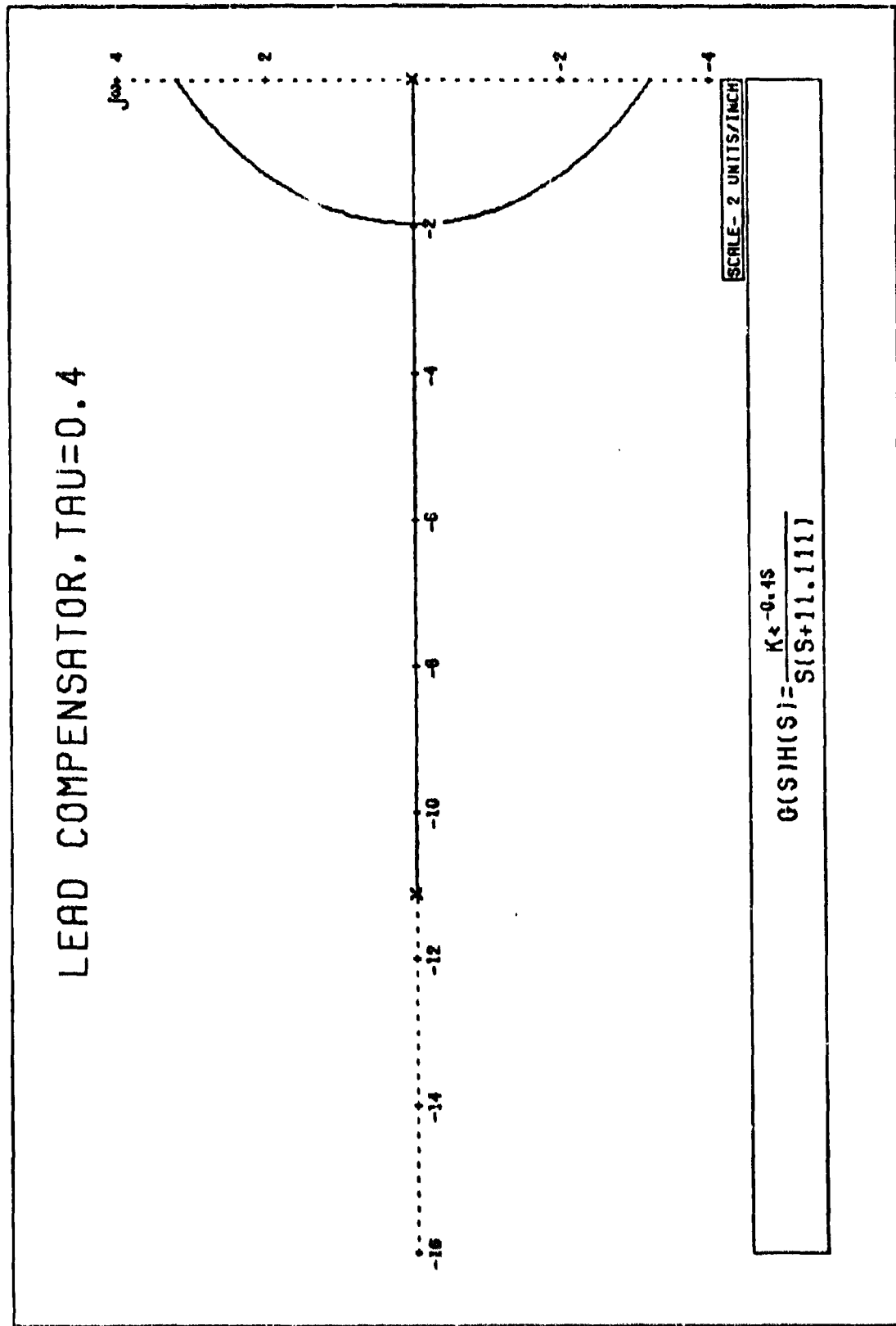


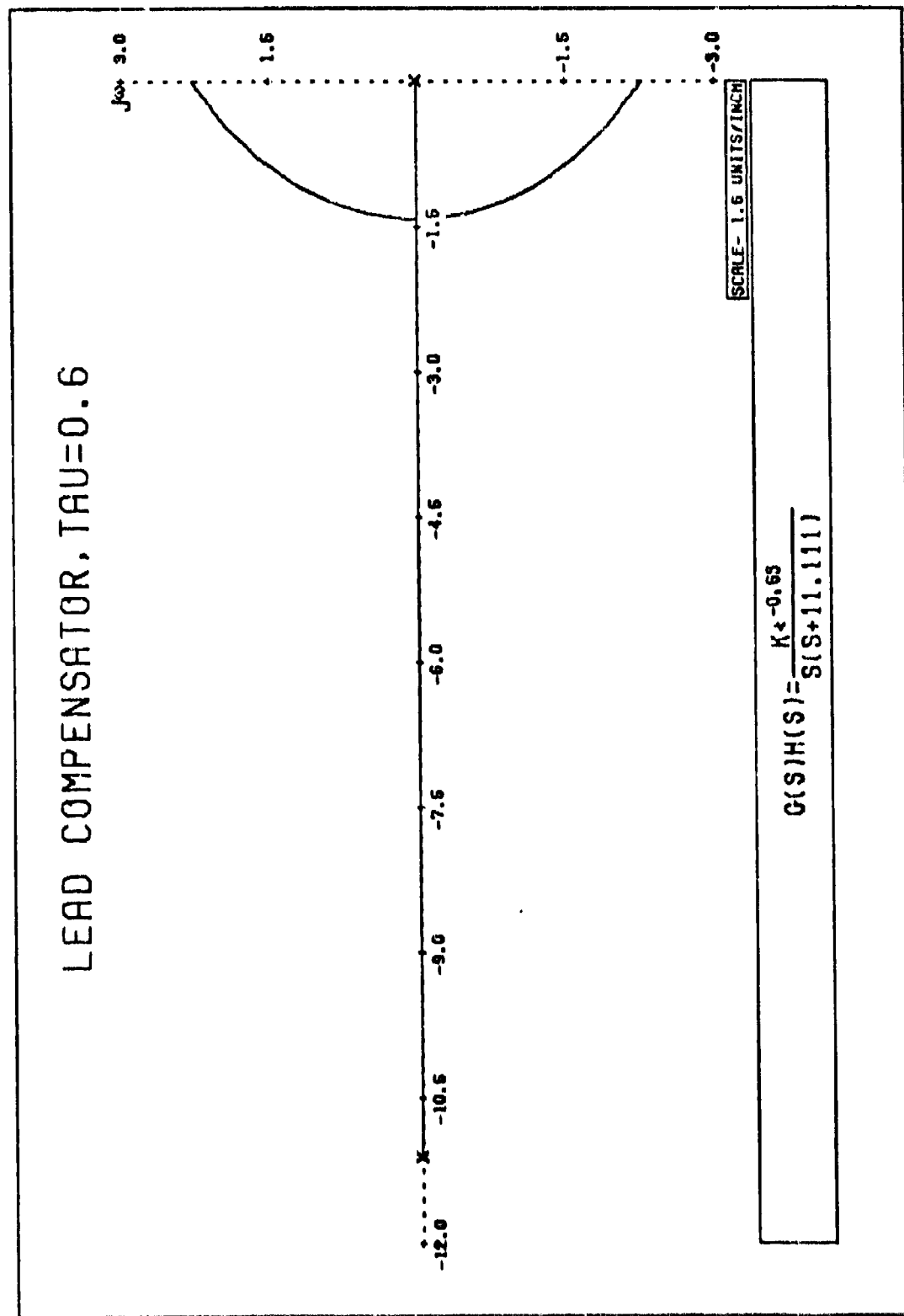
SCALE - 0.7143 UNITS/INCH

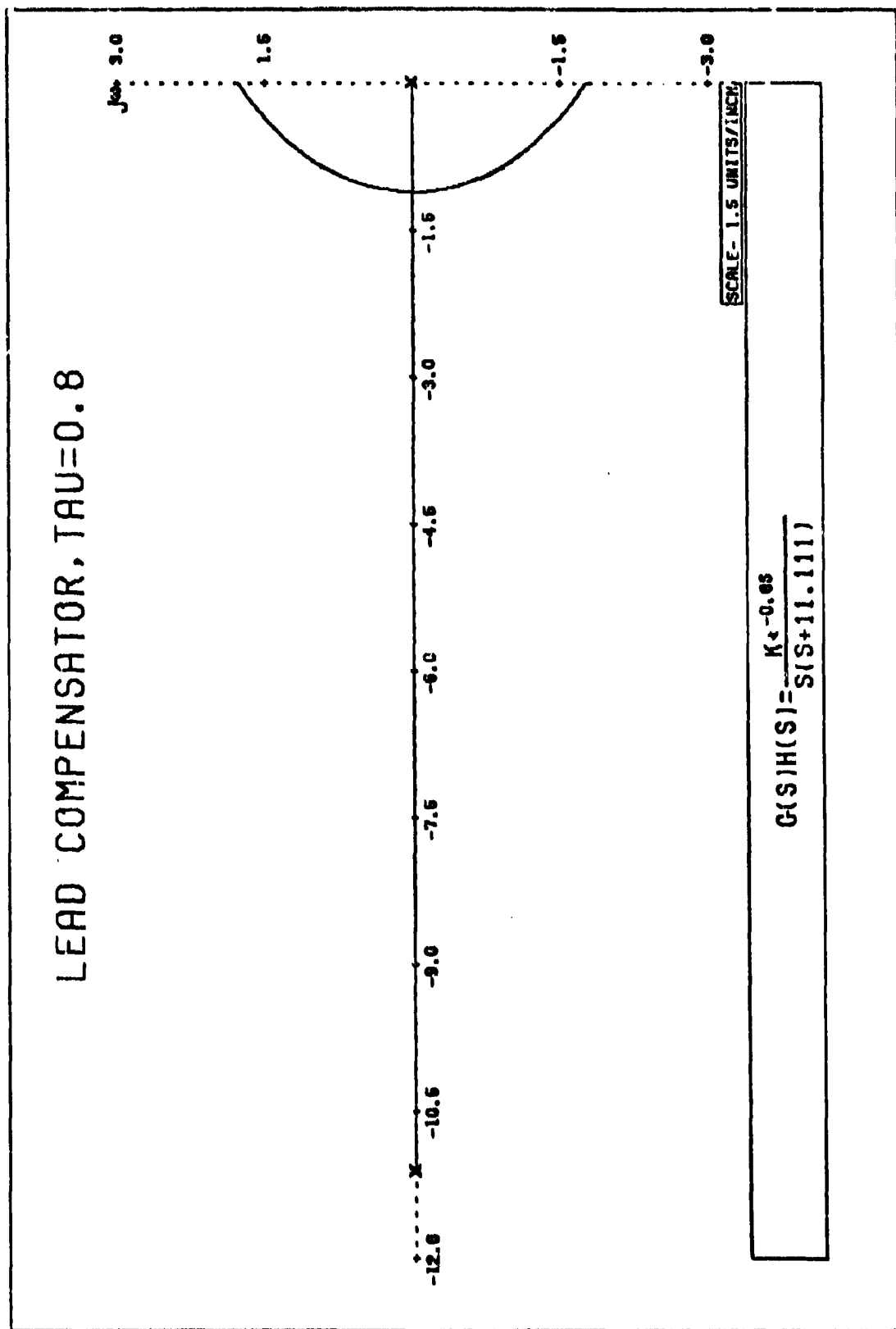
$$O(S)H(S) = \frac{K + 18}{S(S + 1.111)}$$

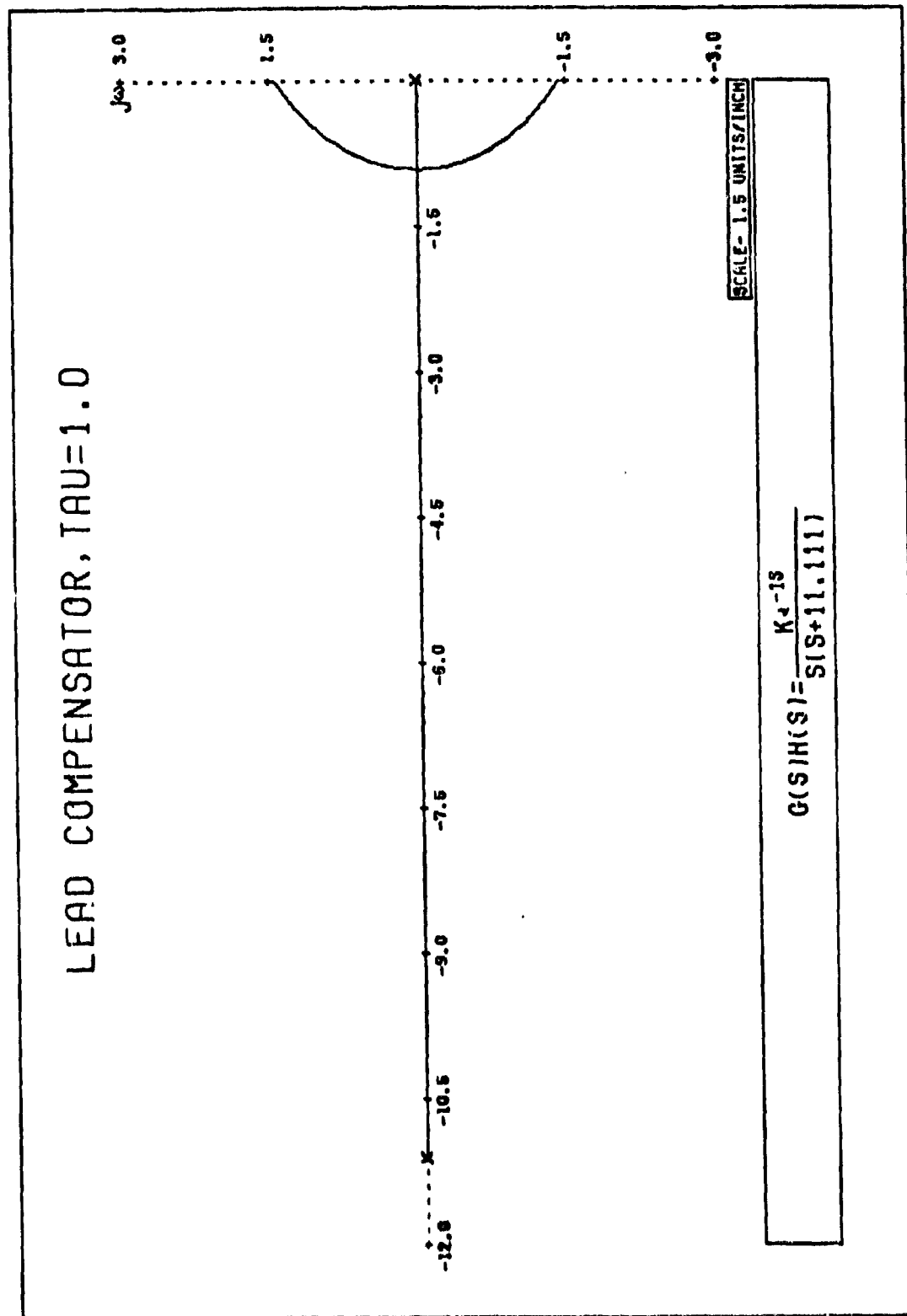
Fig. B.5 Root Locus Plot for Yaw Rate Feedback, $\tau_u = 1.0$ Second

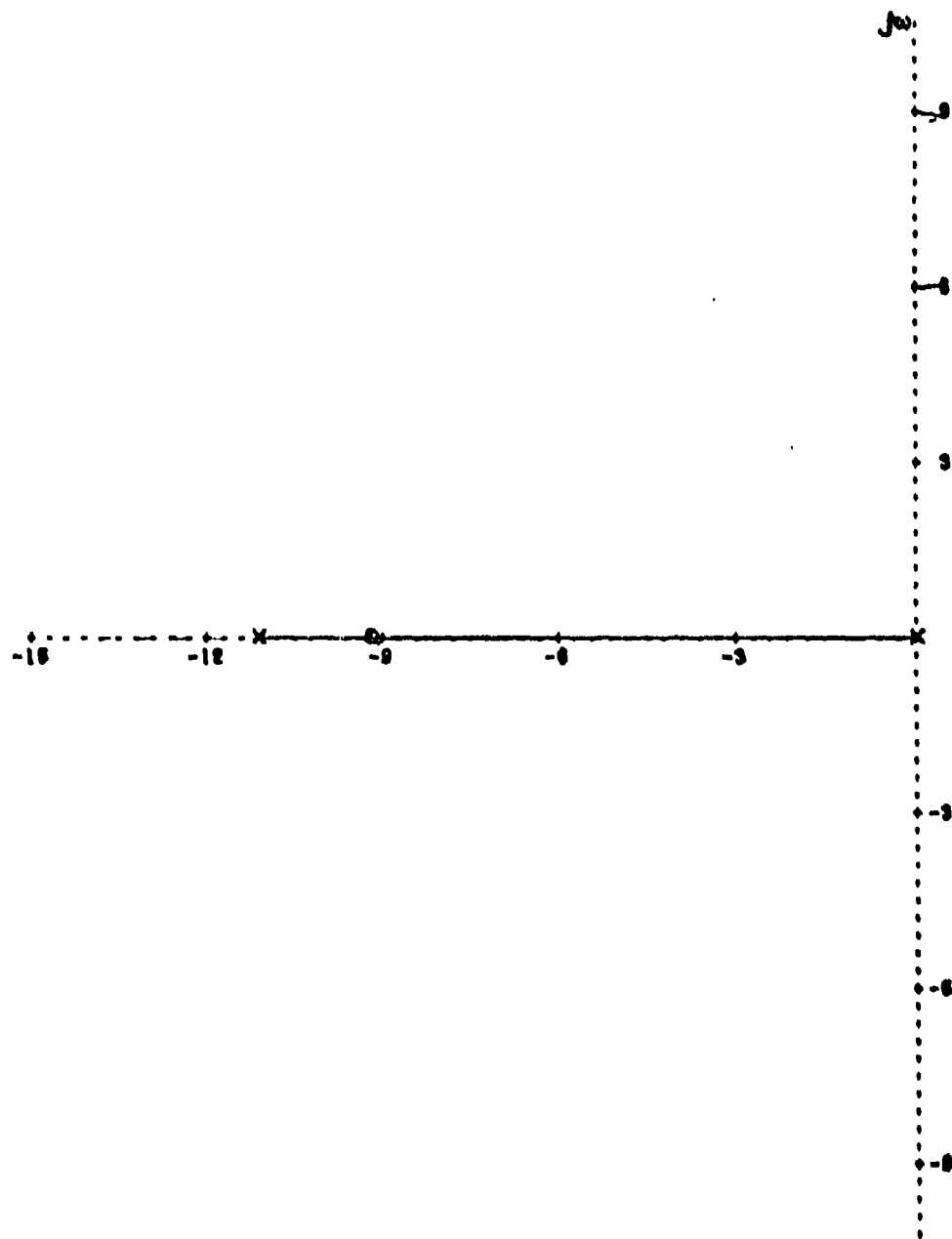
Fig. B.6 Root Locus Plot for Lead Compensator, $\tau_a = 0.2$ Second

Fig. B.7 Root Locus Plot for Lead Compensator, $\tau_a = 0.4$ Second

Fig. B.8 Root Locus Plot for Lead Compensator, $\tau_a = 0.6$ Second

Fig. B.9 Root Locus Plot for Lead Compensator, $\tau_a = 0.8$ Second

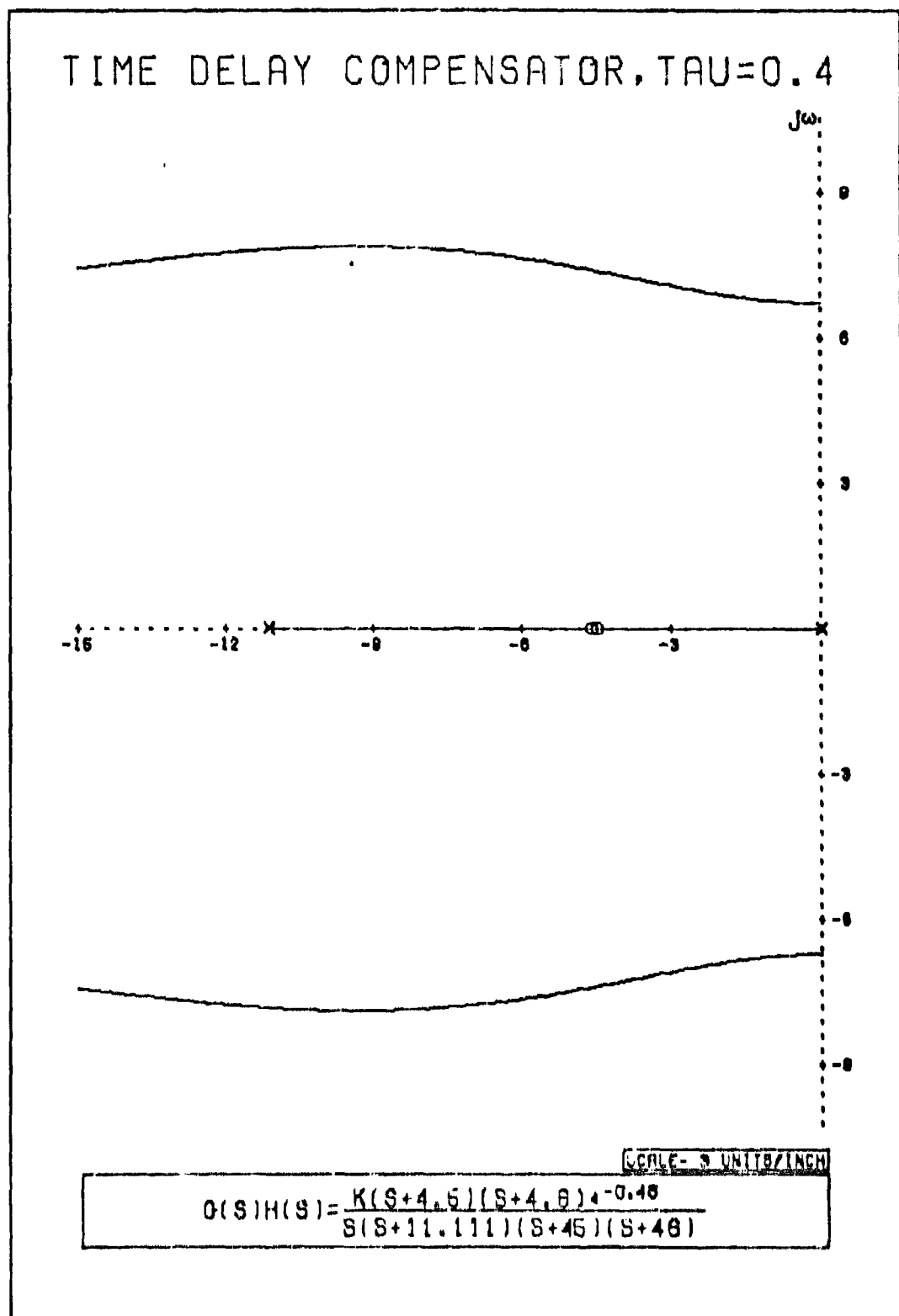
Fig. B.10 Root Locus Plot for Lead Compensator, $\tau_a = 1.0$ Second

TIME DELAY COMPENSATOR, $\tau_d = 0.2$ 

SCALE - 1 UNIT/INCH

$$G(s)H(s) = \frac{K(s+9.2)(s+9.3)e^{-0.2s}}{s(s+11.111)(s+92)(s+93)}$$

Fig. B.11 Root Locus Plot for Time-Delay Compensator, $\tau_d = 0.2$ Second

Fig. B.12 Root locus Plot for Time-Delay Compensator, $\tau_u = 0.4$ Second

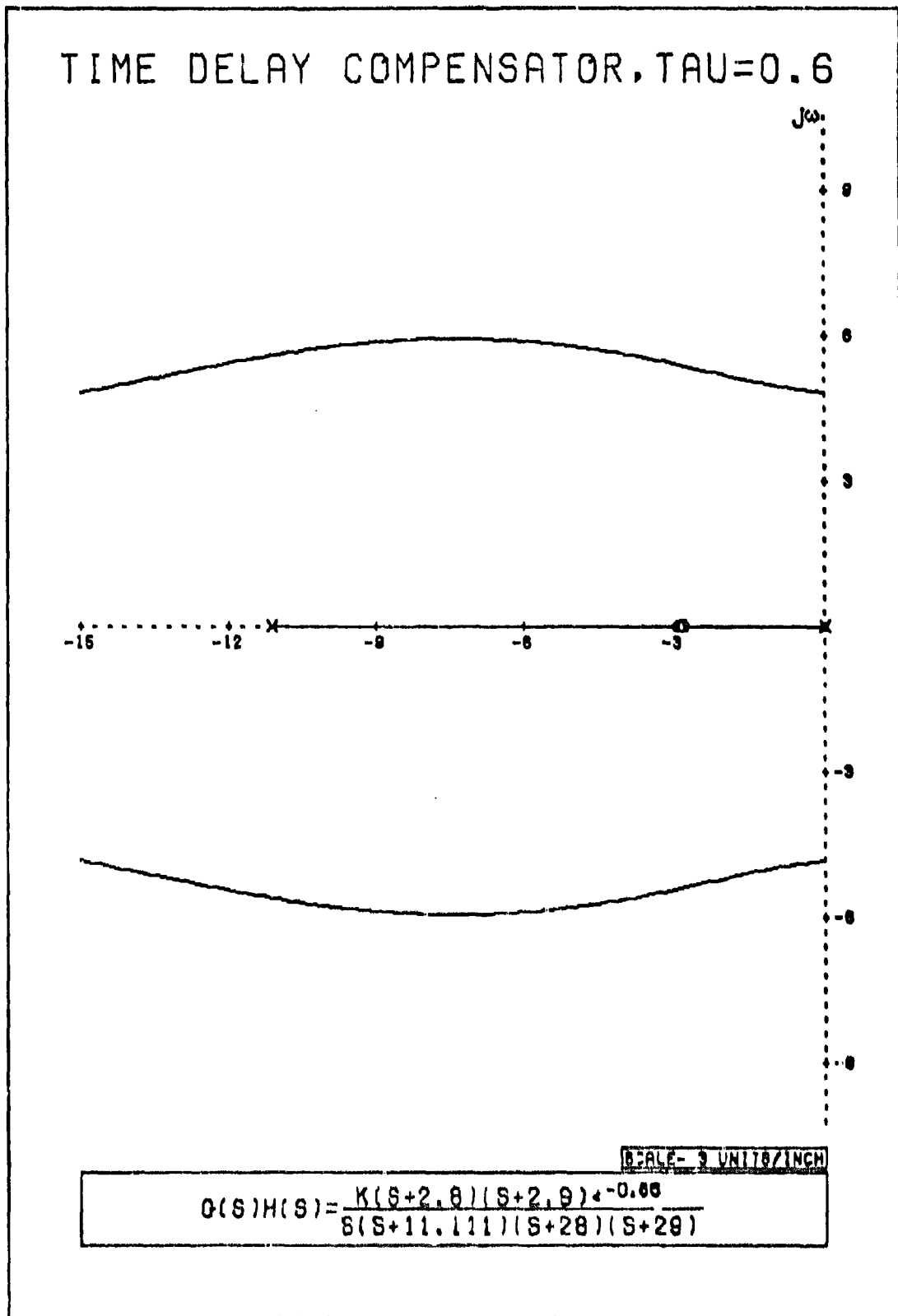


Fig. B.13 Root Locus Plot for Time-Delay Compensator, $\tau_u = 0.6$ Second

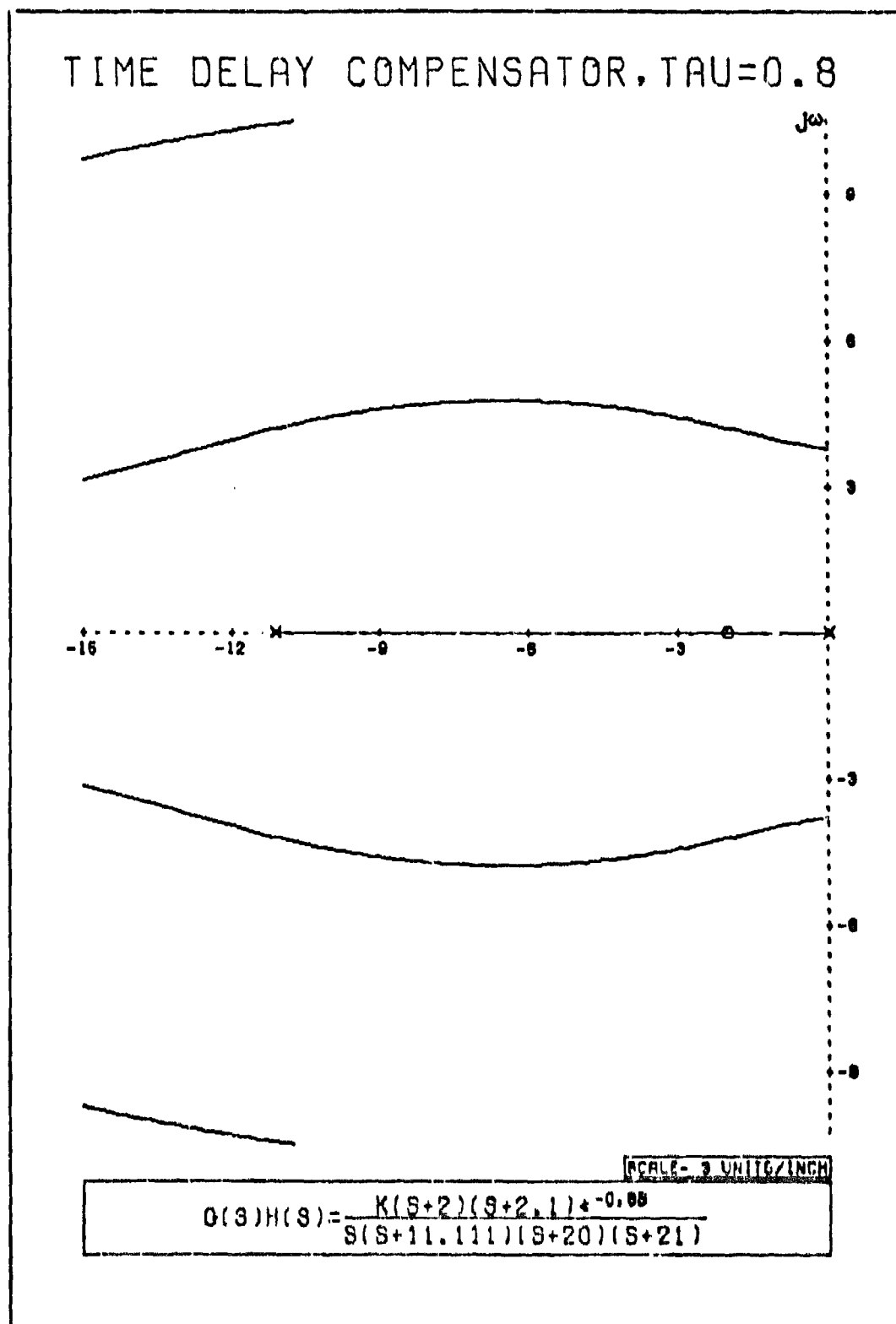
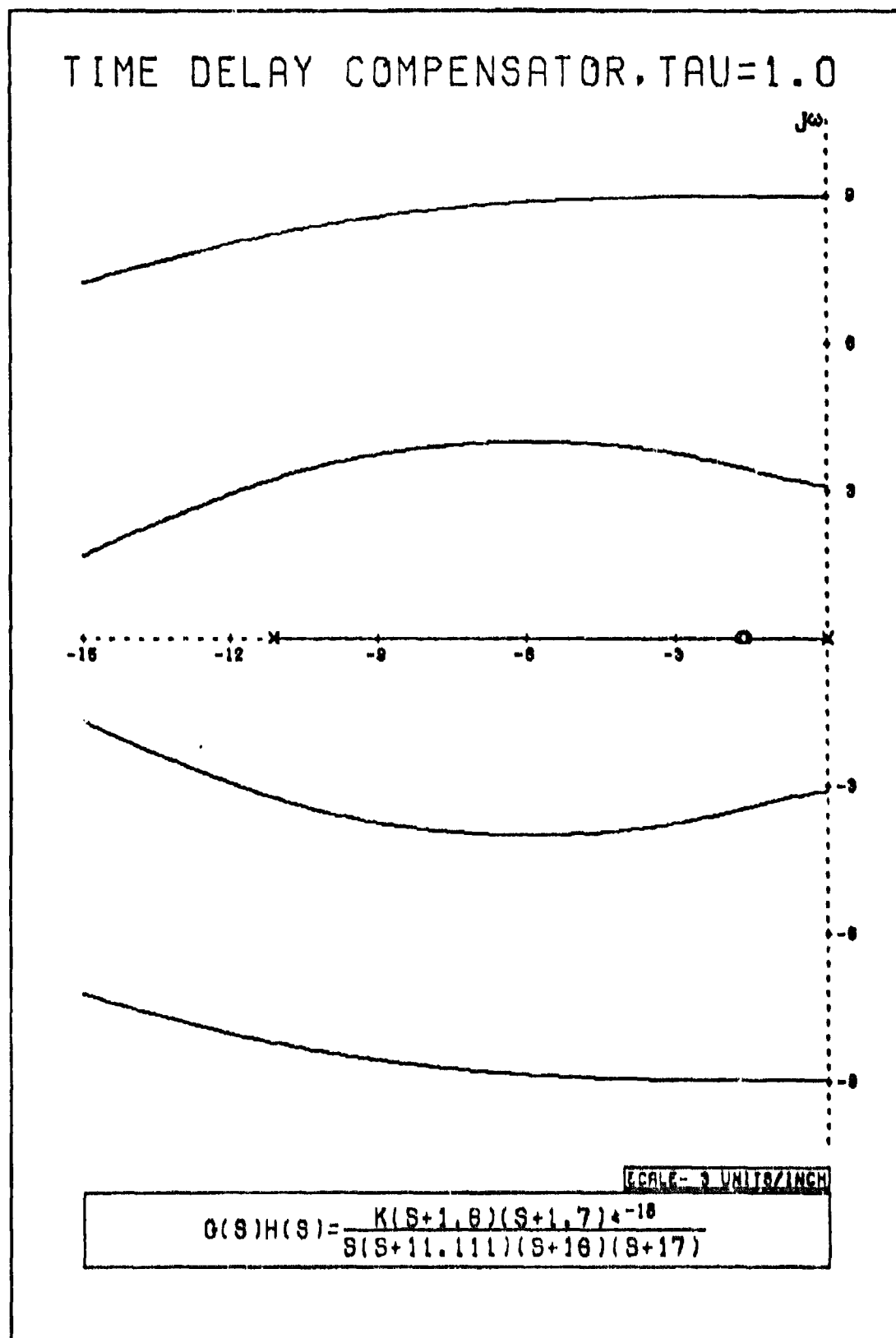


Fig. B.14 Root Locus Plot for Time-Delay Compensator, $\tau = 0.8$ Second

Fig. B.15 Root Locus Plot for Time-Delay Compensator, $\tau_d = 1.0$ Second

Appendix C

MIMIC Simulation Program

```

***MIMIC SOURCE-LANGUAGE PROGRAM***
LIST
.
.
. UNCOMPENSATED SYSTEM
.
.
. CONSTANTS
.
.      CON(DAMP,START)
.
. CROSSOVER PARAMETERS
.
.      PAR(WC,TAUA,TAUE)
.
.
. HEADING DISTURBANCE MODEL
.
.
. PULSE GENERATOR (RESETS THE PULSE AMPLITUDE TO
.   A NEW GAUSSIAN NUMBER EVERY .2 SECOND
.
.      FAKE   = SR5(START)
.      DEL    = SR1(T)
.      YES    = FSW(DEL,FALSE,TRUE,FALSE)
.      PULSE  = RNG(0.,23.6)
.
. FILTER TO SIMULATE WIND CUTOFF
.   AT 1 RAD/SEC ON POWER SPECTRAL DENSITY
.
.      WIND   = INT(1.54*(PULSE-WIND),0.)
.
. AIRCRAFT TRANSFER FUNCTION - HEADING/WIND
.
.      DISTO  = INT(DAMP*WIND-.0768*DISTO-.0256*DIST,0.)
.      DIST   = INT(DISTO,. )
.
.
. CROSSOVER MODEL
.
.
.      ERROR  = DIST-PSI
.      ERROR1 = WC*INT(ERROR,0.)
.      TAU    = TAUA+TAUE
.      PSI    = SR2(ERROR1,TAU)
.
.
. AVERAGE MEAN SQUARED ERROR ANALYSIS
.
.
.      SERROR = INT(ERROR*ERROR,0.)
.      MSERR  = SERROR/T

```



```

. FINISH
.
.      FIN(T,100.)
.
. PRINT INTERVAL
.
.      DT      = .1
.
. INTEGRATION STEP SIZE
.
.      DTMIN   = .01
.      DTMAX   = DTMIN
.
. OUTPUT
.
.      HOR(TIME,PULSE,DIST,PSI,ERROR,MSERR)
.      OUT(T,PULSE,DIST,PSI,ERROR,MSERR)
.
. PLOTTING INFORMATION
.
. PLOT ONLINE(SC)
.
.      PLO(T,DIST,PSI)
.      SCA(1.,.007,.007)
.      ZER(C.,50.,50.)
.      TTX(TIME IN SECONDS)
.      TTY(ANGLE IN RADIANS)
.      OPT(1.40,1.,1.,2.,1.,1.,)
.
. END
.
.      END

```

FUNCTION SR1(A)

*
 * FUNCTION SUBPROGRAM SETS SR1 EQUAL TO ZERO
 * WHEN SUBROUTINE FIRST CALLED ON A TIME EQUAL TO
 5 * A MULTIPLE OF 0.2 SECONDS
 *

COMMON/SWITCH/IOUT,IPAR,DUMMY(17)
 IF(IPAR.NE.1)GO TO 1
 L=0
 10 1 CONTINUE
 SR1=10.
 IF(A-C.LT.0.001.AND.L.NE.0)RETURN
 X=A/.2+.0001
 NX=X
 15 Y=X-NX
 IF(Y.LE.0.0001) SR1=0.
 L=L+1
 C=A
 RETURN
 20 END

FUNCTION SR2(XIN,DELAY)

*
 *
 * FUNCTION TO DELAY XIN (TOTAL TIME DELAY)
 5 *
 *

DIMENSION XSTOR(640)
 COMMON/SWITCH/IOUT,IPAR,DUMMY(17)
 INTEGER OUT
 LOGICAL TEST
 10 IF(IPAR.NE.1)GO TO 101
 IN=0
 OUT=0
 TEST=.FALSE.
 15 DO100 I=1,640
 100 XSTOR(I)=0.0
 101 CONTINUE
 IF(IOUT.EQ.1)TEST=.TRUE.
 IF(TEST)10,1
 20 1 NUM=400*(DELAY+.00001)
 SR2=0.0
 RETURN
 10 CONTINUE
 IF(IOUT.EQ.1)GO TO 20
 IN=IN+1
 IN1=IN
 SR2=XSTOR(IN1)
 OUT=NUM-IN1
 IF(OUT.EQ.0)IN=0
 25 20 XSTOR(IN1)=XIN
 RETURN
 30 END

FUNCTION SR5(A)

*
*
* FUNCTION TO INITIALIZE GAUSSIAN DISTRIBUTION
*
*

5

DATA N/0/
IF(N.NE.0)GO TO 1
CALL RANSET(A)
1 N=1
SR5=0.
RETURN
END

10

```

***MIMIC SOURCE-LANGUAGE PROGRAM***
LIST
.
. COMPENSATED SYSTEM
.
. CONSTANTS
.
.      CON(DAMP,START)
.
. PILOT PARAMETERS
.
.      PAR(KSUBP,TAUE,TSUOL,TSUBI)
.
. AIRCRAFT AND COMPENSATOR PARAMETERS
.
.      PAR(K,TAU1,Z1,P1,Z2,P2)
.
. HEADING DISTURBANCE MODEL
.
. PULSE GENERATOR (RESETS THE PULSE AMPLITUDE TO
.   A NEW GAUSSIAN NUMBER EVERY .2 SECOND
.
.      FAKE   = SRG(START)
.      DEL    = SR1(T)
.      YES    = PSW(DEL,FALSE,TRUE,FALSE)
. YES      PULSE = RNG(0.,231.8)
.
. FILTER TO SIMULATE WIND CUTOFF
.   AT 1 RAD/SEC ON POWER SPECTRAL DENSITY
.
.      WIND   = INT(1.54*(PULSE-WIND),J.)
.
. AIRCRAFT TRANSFER FUNCTION - HEADING/WIND
.
.      DISTD  = INT(DAMP*WIND-.0768*DISTD-.0256*DIST,0.)
.      DIST   = INT(DISTD,0.)
.
. ACLS INNER LOOP MODEL
.
. PILOT OBSERVES HEADING AND DISTURBANCE
.
.      PILOTI = DIST-PSI
.
. CROSSOVER PILOT MODEL (YP)
.
. KSUBP IS THE PILOT GAIN
.
.      PIL1   = KSUBP*PILOTI

```

```

. PILOT DYNAMICS
. (IF TSUBI IS 0., THEN PIL2=TSUBL*DER(T,PIL1,0.))+PIL1
.
.   LAG      = 1./TSUBI
.   NOLAG    = FSW(TSUBI,FALSE,TRUE,FALSE)
.   YESLAG   = NOT(NOLAG)
.   NOLAG    PIL2 = TSUBL*DER(T,PIL1,0.))+PIL1
.   YESLAG   PIL2 = LAG*(TSUBL*PIL1+INT(PIL1-PIL2,0.))
.
. PILOT TIME DELAY
.
.   PILOTO = SR2(PIL2,TAUE)
.
. YAW RATE FEEDBACK
.
.   PLA1    = PILOTO-PSID
.
. COMPENSATOR
.
. COMPENSATION CONTROL LOOP SENSITIVITY=K
.
.   PLA2    = K*PLA1
.
. LEAD COMPENSATOR  $S+Z1/S+P1$ 
.
.   PLA3    = PLA2+INT(71*PLA2-P1*PLA3,0.)
.
. LEAD COMPENSATOR  $S+Z2/S+P2$ 
.
.   PLA     = PLA3+INT(Z2*PLA3-P2*PLA,0.)
.
. LEAD COMPENSATOR,  $(S+1.1111)/(S+11.111)$  CHANGES
.   ENGINE DENOMINATOR FROM  $(S+1.1111)$  TO  $(S+11.111)$ 
.
. ENGINE DYNAMICS
.
.   NT      = INT(PLA-11.111*NT,0.)
.
. ENGINE TIME DELAY
.
.   N       = SR3(NT,TAUA)
.
. AIRCRAFT DYNAMICS
.
.   PSID    = INT(N,0.)
.   PSI     = INT(PSID,0.)
.
. AVERAGE MEAN SQUARED ERROR ANALYSIS
.
.   ERROR   = INT(PILOTI*PILOTI,0.)
.   MSERR   = ERROR/T

```

```

. FINISH
.
.           FIN(T,100.)
.
. PRINT INTERVAL
.
.       DT       = .1
.
. INTEGRATION STEP SIZE
.
.       DTMIN    = .01
.       DTMAX    = DTMIN
.
. OUTPUT
.
.           HDR(TIME,PULSE,DIST,PSI,PSID,MSERR)
.           OUT(T,PULSE,DIST,PSI,PSID,MSERR)
.
. PLOTTING INFORMATION
.
. PLOT ONLINE(SC)
.
.           PLO(T,DIST,PSI)
.           ZER(0.,50.,90.)
.           SCA(1.,.007,.007)
.           TTX(TIME IN SECONDS)
.           TTY(ANGLE IN RADIANS)
.           OPT(1.4,1.,1.,2.,1.,1.)
.
. END
.
.           END

```

FUNCTION SR1(A)

*
 * FUNCTION SUBPROGRAM SETS SR1 EQUAL TO ZERO
 * WHEN SUBROUTINE FIRST CALLED ON A TIME EQUAL TO
 * A MULTIPLE OF 0.2 SECONDS
 *

```

5      COMMON/SWITCH/IOUT,IPAR,DUMMY(17)
      IF (IPAR.NE.1) GO TO 1
      L=0
10     1 CONTINUE
      SR1=10.
      IF (A-C.LT.0.001.AND.L.NE. ) RETURN
      X=A/.2+.0001
      NX=X
15     Y=X-NX
      IF (Y.LE.0.0001) SR1=0.
      L=1
      C=A
      RETURN
20     END
  
```

FUNCTION SR2(XIN,DELAY)

*
 *
 * FUNCTION TO DELAY XIN (PILOT TIME DELAY)
 *
 *

```

5      DIMENSION XSTOR(135)
      COMMON/SWITCH/IOUT,IPAR,DUMMY(17)
      INTEGER OUT
      LOGICAL TEST
10     IF (IPAR.NE.1) GO TO 101
      IN=0
      OUT=0
      TEST=.FALSE.
15     DO 100 I=1,135
100    XSTOR(I)=0.0
101    CONTINUE
      IF (IOUT.EQ.1) TEST=.TRUE.
      IF (TEST) 10,1
20     1 NUM=400*(DELAY+.01001)
      SR2=0.0
      RETURN
10    CONTINUE
      IF (IOUT.EQ.1) GO TO 20
      IN=IN+1
      IN1=IN
      SR2=XSTOR(IN1)
      OUT=NUM-IN1
      IF (OUT.EQ.0) IN=0
25     20 XSTOR(IN1)=XIN
      RETURN
30     END
  
```

FUNCTION SR3(XIN,DELAY)

```

*
*
* FUNCTION TO DELAY XIN (ENGINE TIME DELAY)
5
*
*
* DIMENSION XSTOR(400)
* COMMON/SWITCH/IOUT,IPAR,DUMMY(17)
* INTEGER IOUT
10 * LOGICAL TEST
* IF(IPAR.NE.1)GO TO 101
* IN=0
* OUT=0
* TEST=.FALSE.
15 * DO100 I=1,400
100 * XSTOR(I)=0.0
101 * CONTINUE
* IF(IOUT.EQ.1)TEST=.TRUE.
* IF (TEST)10,1
20 * 1 NUM=400*(DELAY+.00001)
* SR3=0.0
* RETURN
10 * CONTINUE
* IF(IOUT.EQ.1) GO TO 20
25 * IN=IN+1
* IN1=IN
* SR3=XSTOR(IN1)
* OUT=NUM-IN1
* IF(OUT.EQ.0)IN=0
30 * 20 XSTOR(IN1)=XIN
* RETURN
* END

```

FUNCTION SR5(A)

```

*
*
* FUNCTION TO INITIALIZE GAUSSIAN DISTRIBUTION
5
*
*
* DATA N/0/
* IF(N.NE.0)GO TO 1
* CALL RANSET(A)
10 * 1 N=1
* SR5=0.
* RETURN
* END

```


Appendix D

Pulse Representation of Band Limited White Noise

Band limited white noise has a power spectral density which is flat up to the cutoff frequency and then is zero at higher frequencies as in Fig. D.1. When the mean of the Gaussian distribution for the

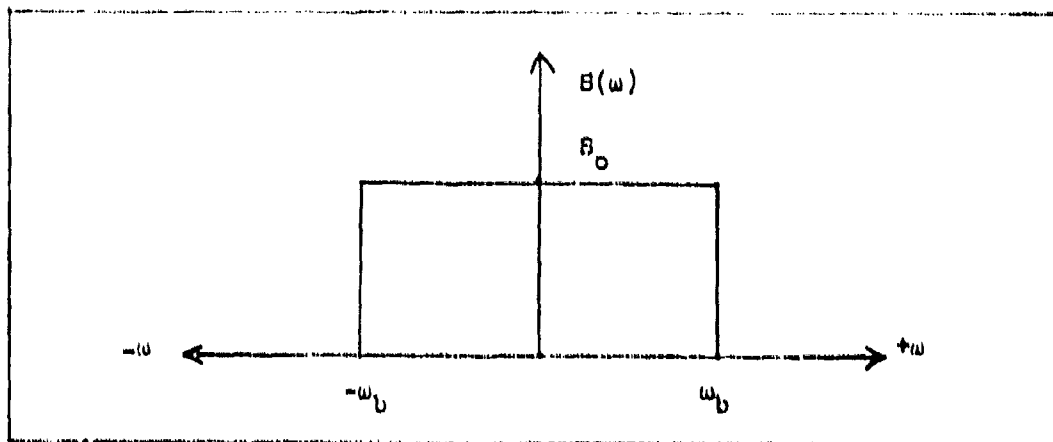


Fig. D.1 Power Spectral Density of Band Limited White Noise

noise is zero, the variance can be found from the autocorrelation $R(0)$, which is equal to the area under the power spectral density curve from $\omega = -\infty$ to $\omega = +\infty$, divided by 2π . The following equation expresses this (Ref. 171338):

$$R(0) = \sigma^2 = \frac{1}{2\pi} \int_{-\infty}^{\infty} B(\omega) d\omega \quad (D-1)$$

where σ is the variance of the Gaussian distribution. The value of B_0 in Fig. D.1 can be calculated from the relationship in equation (D-1) and is

$$B_0 = \frac{\pi \sigma^2}{\omega_b} \quad (D-2)$$

The band limited white noise is represented by a series of pulses, whose amplitude is a Gaussian distribution with mean equal to zero, and standard deviation equal to σ_p , and whose width is T . This pulse train is shown in Fig. D.2. The autocorrelation of these pulses appears as in Fig. D.3.

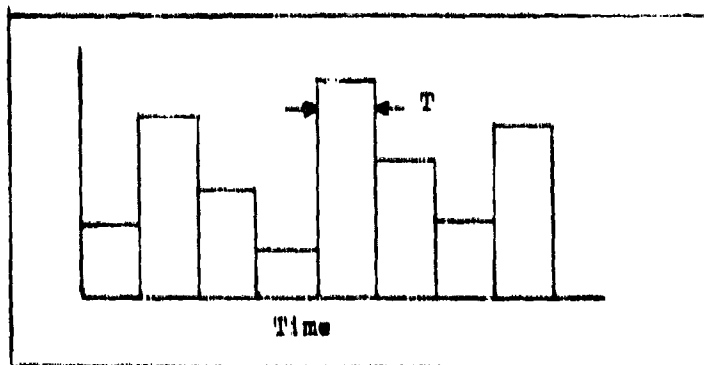


Fig. D.2 Pulse Train

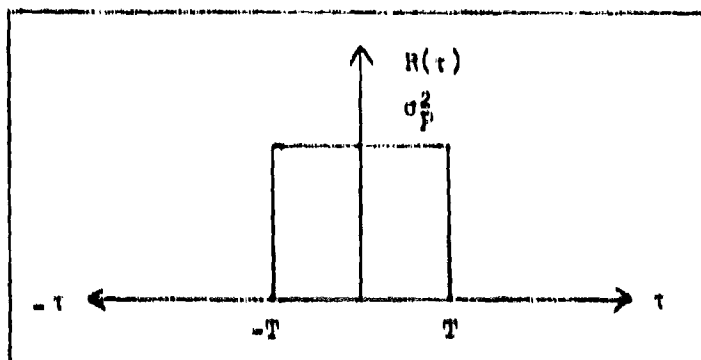


Fig. D.3 Autocorrelation of a Pulse Train

The power spectral density of a process is equal to the Fourier Transform of its autocorrelation. This is expressed as

$$R(\omega) = \int_{-\infty}^{\infty} e^{-j\omega\tau} R(\tau) d\tau \quad (D-3)$$

Therefore, the power spectral density of the pulse train is

$$\begin{aligned}
 S(\omega) &= \int_{-T}^T e^{-j\omega\tau} \sigma_p^2 d\tau \\
 &= 2\sigma_p^2 T \frac{\sin \omega T}{\omega T}
 \end{aligned}
 \tag{D-4}$$

which, when plotted, looks like Fig. D.4. If the pulse width is kept small, the center part of the curve will be kept flat. The pulse train can then be passed through a first order filter to cut off the power spectral density curve beyond the flat portion. The result is a close approximation to the ideal band limited white noise.

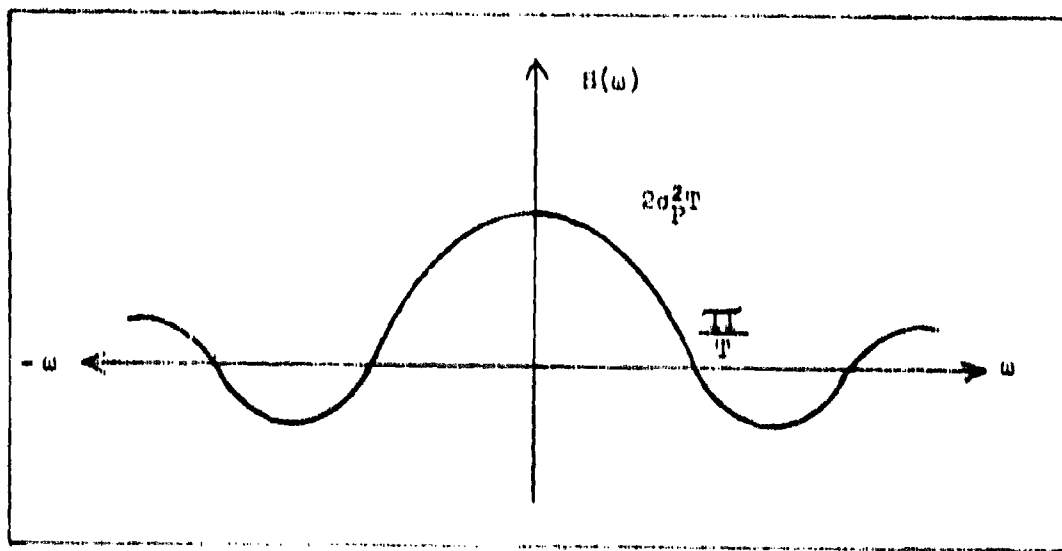


Fig. D.4 Power Spectral Density of a Pulse Train

Vita

Matthew A. Husson III was born in New York City on 29 October 1942. He graduated from Red Bank Catholic High School in Red Bank, New Jersey in 1960 and then interrupted his education for one year, while working in the engine room of an oil tanker. He then attended Newark College of Engineering in Newark, New Jersey, from where he received a Bachelor of Science degree in Electrical Engineering in 1966, along with a regular commission in the United States Air Force. He graduated from Air Force pilot training at Webb AFB, Texas in 1967, and served for one year in the Republic of Vietnam, flying the F-100. He was then assigned to England for four years, where he flew the F-100 and the F-111 aircraft. After returning from England, he was assigned to the Air Force Institute of Technology.

Permanent address: 167 Buttonwood Drive
Fair Haven, New Jersey 07701

This thesis was typed by Mrs. Patty Shumaker.